University of Alberta

Laminar Mixing of a Yield Stress Fluid Using Helical Ribbon Impellers

by

Stephen J. Curran ©

A thesis submitted to the faculty of graduate studies and research in
partial fulfilment of the requirements for the degree of

Master of Science
in
Chemical Engineering

Department of Chemical and Materials Engineering

Edmonton, Alberta
Fall 1998

National Library
of Canada

Acquisitions and
Bibliographic Services

395 Wellington Street
Ottawa ON K1A 0N4
Canada

Bibliothèque nationale
du Canada

Acquisitions et
services bibliographiques

395, rue Wellington
Ottawa ON K1A 0N4
Canada

Your file Votre référence

Our file Notre référence

The author has granted a non-exclusive licence allowing the National Library of Canada to reproduce, loan, distribute or sell copies of this thesis in microform, paper or electronic formats.

L'auteur a accordé une licence non exclusive permettant à la Bibliothèque nationale du Canada de reproduire, prêter, distribuer ou vendre des copies de cette thèse sous la forme de microfiche/film, de reproduction sur papier ou sur format électronique.

The author retains ownership of the copyright in this thesis. Neither the thesis nor substantial extracts from it may be printed or otherwise reproduced without the author's permission.

L'auteur conserve la propriété du droit d'auteur qui protège cette thèse. Ni la thèse ni des extraits substantiels de celle-ci ne doivent être imprimés ou autrement reproduits sans son autorisation.

0-612-34349-9

Canadä

University of Alberta

Library Release Form

Name of Author: Stephen J. Curran

Title of Thesis: Laminar Mixing of a Yield Stress Fluid Using Helical Ribbon Impellers

Degree: Master of Science

Year this Degree Granted: 1998

Permission is hereby granted to the University of Alberta Library to reproduce single copies of this thesis and to lend or sell such copies for private, scholarly, or scientific research purposes only.

The author reserves all other publication and other rights in association with the copyright in the thesis, and except as herein before provided, neither the thesis nor any substantial portion thereof may be printed or otherwise reproduced without the author's prior written permission.

S Curran

Stephen J. Curran
23 Harrison Hey,
Huyton-with-Roby,
Liverpool, L36 5YR
United Kingdom.

Date: 5 August, 1998

University of Alberta

Faculty of Graduate Studies and Research

The undersigned certify that they have read, and recommend to the Faculty of Graduate Studies and Research, a thesis entitled **Laminar Mixing of a Yield Stress Fluid Using Helical Ribbon Impellers** submitted by **Stephen J. Curran** in partial fulfilment of the requirements for the degree of Master of Science in Chemical Engineering.

Bob Hayes
Dr. R. E. Hayes, Supervisor

Kresta
Dr. S. M. Kresta

F.E. Hicks
Dr. F. E. Hicks

Date: 5 August, 1998

Abstract

Mixing studies have been carried out using aqueous Carbopol 940 solutions in a vessel equipped with single and double flight helical ribbon impellers. The rheology of these solutions has been well characterised using steady and dynamic viscometric measurements. The solutions possess yield stress and are shear thinning and are best described by the Herschel-Bulkley rheological equation.

Power consumption studies in the mixer have been performed using torque measurements. Circulation and mixing time studies have been carried out using a thermal technique. These studies have been based on three impeller rotational speeds, two levels of fluid viscosity and upward and downward pumping of the impellers. It has been found that power requirements for the double ribbon impeller are slightly greater than for the single ribbon impeller. The most efficient mixing is achieved using the double ribbon impeller for both levels of fluid viscosity. The most inefficient mixing has been found when using the single ribbon impeller in downward pumping mode for high viscosity solutions.

The quantitative results that have been obtained from mixing trials using the thermal method have been confirmed qualitatively using a flow visualisation technique by video analysis.

To Michael, Patricia and Carmel

Acknowledgements

The completion of this thesis is closure to 30 very memorable months at the University of Alberta. The list of people who have made an impact on my life in this time is enormous and in this short paragraph I can only mention those who have made a special contribution.

First and foremost, I am indebted to my supervisor, Dr. Robert Hayes for giving me the opportunity to study in Canada. His patience, wisdom and knowledge will long be remembered. I am also indebted to Dr. Yadollah Maham whose continual optimism and love of life is a lesson for us all. I acknowledge and appreciate the efforts of Artin Afacan with the experimental set-up and Dr. Michael Williams for his invaluable advice in matters of rheology.

Special thanks to my colleagues Christopher Cox and Kurt Schmidt for nights of trainspotting, l'ambiance and artificial peace. Thanks also to Shane Lodewyk and Ed Shields, to category d and my long time "buddy", John Carvell.

The generous support of the University of Alberta is gratefully acknowledged.

Finally, I would like to thank my family, Michael, Patricia and Carmel, whose love and support has brought me where I am today.

Table of Contents

Page

1. Introduction 1

2. Literature Review 5

2.1 Laminar Mixing 6

2.2 Power Consumption 6

2.2.1 Dimensional Analysis 24

2.2.2 Couette Flow Analogy 36

2.2.2.1 Shear Rates in the Mixing Vessel 39

2.2.3 Drag Force Based Analogy 47

2.2.4 Discussion of Power Consumption Correlations 51

2.3 Methods to Study Mixing 54

2.4 Mixing Time 56

2.5 Circulation Time 63

2.6 Conclusions on Circulation and Mixing Times 66

2.7 Carbopol: Chemistry and Physical Behaviour 68

3. Experimental Procedure 75

3.1 Preparation of Carbopol Solutions 75

3.1.1 Sample Preparation for Rheological Studies 77

3.1.2 Steady State Rheological Tests 78

3.1.3 Dynamic Rheological Tests 84

3.2 Mixing Trials 85

Page

3.2.1 Equipment 85

3.2.2 Mixing by Thermal Method 92

4. Results and Discussion 97

4.1 Rheological Characterisation 97

4.2 Power Consumption Analysis 106

4.2.1 Newtonian Polyethylene Glycol Solutions 106

4.2.2 Non-Newtonian Carbopol Solutions 111

4.2.2.1 The Shear Rate Constant, k_s 111

4.3.1 Mixing Trials by Thermal Technique 126

4.3.1.1 Circulation Time 126

4.3.1.2 Mixing Time 134

4.3.2 Mixing Assessment from Flow Visualisation 141

5. Conclusions 144

6. Recommendations 147

7. References 148

Appendix A1 Sample Titration Calculation for 1.48wt% Carbopol 159

Appendix B1 Shear Stress-Shear Rate Data for 1.48wt% Carbopol Solutions 162

Appendix B2 Apparent Viscosity-Shear Rate for 1.48wt% Carbopol Solutions 163

Appendix B3 Least Squares Regression Data to fit the Herschel-Bulkley Equation 164

Appendix C1 Measured Torque and Power Data for 45wt% PEG Solution using HR1-B and DHR-1 167

Appendix D1 Measured Torque and Power Data for 1.48wt% Carbopol Solution using HR1-B and DHR-1 168

Appendix D2 Measured Torque and Power Data for 1.48wt% Carbopol Solution using HR1-B and DHR-1 169

Appendix E Mixing Trials by Thermal Method 170

Appendix G1 Flow Visualisation Experiment 205

Appendix G2 Flow Visualisation Experiment 208

Appendix G3 Flow Visualisation Experiment 211

Appendix G4 Flow Visualisation Experiment 214

List of Tables

Table Page

2.2.1 Power Consumption Data for Helical Ribbon Impellers 35

2.2.2 Correlations to Determine k_s from Literature 53

2.4.1 Mixing Time correaltions for Helical Ribbon Impellers (Ho & Kwong, 1973) 61

3.1 Shear Rate Data for Contraves Rheomat 115 Rotational Viscometer 81

3.2 Geometric Parametrs used for the Mixer in this Study 87

4.2.2.1 Calculated k_s Values from Correlations for Present Study at pH 2.79 and 11.5 115

4.3.1.1.1 Average values of Circulation Time, t_c, using 1.48wt% Carbopol 128

4.3.1.1.2 Average Values of k_c using 1.48wt% Carbopol 130

4.3.1.1.3 Values of Circulation number, Ci, for 1.48wt% Carbopol 133

4.3.1.2.1 Average Values of mixing time, t_m, for 1.48wt% Carbopol 137

4.3.1.2.2 Average values of k_m for 1.48wt% Carbopol 139

E Mixing trials by Thermal Method (Summary) 170

G1 Flow Visualisation Experiment 205

G2 Flow Visualisation Experiment 208

G3 Flow Visualisation Experiment 211

G4 Flow Visualisation Experiment 214

List of Figures

Figure Page

2.1.1 The Principle of Laminar Shear Mixing (Edwards, 1985) 8

2.1.2 Effect of Unidirectional Laminar Shear on Interfacial Area (Edwards, 1985) 10

2.1.3 Effect of Consecutive Shearing with Change in Direction (Edwards, 1985) 12

2.1.4 Velocity Profile and Flow Patterns in the Mixing Vessel (Chavan, 1983) 14

2.1.5 Distributive Mixing by Slicing and Rotating (Edwards, 1985) 15

2.1.5 General Characteristics of a Power Curve (Edwrads, 1985) 19

2.2.2 Two Dimensional Couette Flow (Cheng & Carreau, 1994) 23

2.6.1 Aqueous Linear Polymer and Microgel Structures (Ketz et. al., 1988) 71

2.6.2 Schematic of Carbopol Resin Molecule in Relaxed State 72

2.6.3 Hydrogen Bonding in Aqueous Carbopol Dispersions 73

2.6.4 Ionic-type Bonds from neutralisation with NaOH 74

3.1.1 Titration Curve for 1.48wt% Carbopol and Additions of 23wt% NaOH 79

3.1.2 Measured Data for 46.7wt% Polyethylene Glycol Solution in Contraves Rheomat 115 Viscometer before Calibration 82

3.1.3 Measured Data for 46.7wt% Polyethylene Glycol Solution in Contraves Rheomat 115 Viscometer after Calibration 83

3.2.1 Mixing Vessel 86

3.2.2 Single Ribbon Impeller, HR1-B 88

3.2.3 Double Ribbon Impeller, DHR-1 89

3.2.4 Coverplate of Mixing Vessel 91

3.2.5 Response of J-type Thermocouples used for Thermal Mixing Trials 93

3.2.6 Syringe Arrangement for Large Volume Injections 95

4.1.1 Shear Stress-Shear Rate Data from Steady State Tests on 1.48wt% Carbopol Solutions of Given pH 99

4.1.2 Variation of Apparent Viscosity with pH at the Given Sample Shear Rates, as Measured in a Contraves Rheomat 115 Rotational Viscometer using 1.48wt% Carbopol Solutions and 23wt% Aqueous NaOH 100

4.1.3 Varaiation of the Rheological Parameter, τ_y, with pH in the Herschel-Bulkley Equation (2.2.9) for 1.48wt% carbopol and 23wt% NaOH 102

4.1.4 Varaiation of the Rheological Parameter, K, with pH in the Herschel-Bulkley Equation (2.2.9) for 1.48wt% carbopol and 23wt% NaOH 103

4.1.5 Varaiation of the Rheological Parameter, n, with pH in the Herschel-Bulkley Equation (2.2.9) for 1.48wt% carbopol and 23wt% NaOH 104

4.1.6 Dynamic Viscosity Variation with pH for 1.48wt% Carbopol Solutions 105

4.2.1.1 Torque Measurements for HR1-B and DHR-1 in 45wt% Polyethylene Glycol Solution 107

4.2.1.2 Comparison of Measured Power Number and that Calculated from Correlations Given for 45wt% Polyethylene Glycol Solution using HR1-B Impeller Pumping Upwards 108

4.2.1.3 Comparison of Measured Power Number and that Calculated from Correlations Given for 45wt% Polyethylene Glycol Solution using DHR-1 Impeller Pumping Upwards 109

4.2.2.1 Torque Measurements for HR1-B and DHR-1 in 1.48wt% Carbopol Solution at pH at Given pH 114

4.2.2.2 Comparison of Apparent viscosity with Impeller Rotational Speed Using Different Correlations to Predict k_s for HR1-B Impeller Pumping Upwards in 1.48wt% Carbopol at pH 2.79 116

4.2.2.3 Comparison of Apparent viscosity with Impeller Rotational Speed Using Different Correlations to Predict k_s for DHR-1 Impeller Pumping Upwards in 1.48wt% Carbopol at pH 2.79 117

4.2.2.4 Comparison of Apparent viscosity with Impeller Rotational Speed Using Different Correlations to Predict k_s for HR1-B Impeller Pumping Upwards in 1.48wt% Carbopol at pH 11.5 118

4.2.2.5 Power Curve Comparisons using Measured Power Number and Predicted Reynolds Number from Various Correlations for HR1-B Impeller Pumping Upwards in 1.48wt% Carbopol at pH 2.79 119

4.2.2.6 Power Curves for Three Mixing Situations Based on the Herschel-Bulkley Analysis of of Rauline, (1998) 122

4.2.2.7 Variation of k_s with N for Herschel-Bulkley Fluids from the Analysis of Rauline, (1998) 123

4.2.2.8 Variation of Kp with N for Herschel-Bulkley Fluids from the Analysis of Rauline, (1998) 124

4.2.2.9 Power-Flow Correlation of Hall & Godfrey, (1970) and Reynolds Number Calculated using k_s from Equation (2.2.58) 125

4.3.1.1.1 HR1-B Pumping Upwards; 20rpm 1.48wt% Carbopol; pH 2.79 Estimation of Circulation Time, t_c 127

4.3.1.2.1 Progress of mixing in terms of arbitrary mixing index (I). The approach to the fully mixed condition is asymptotic and small errors in mixing index (δI) lead to large errors in mixing time. 135

4.3.1.2.2 HR1-B Pumping Upwards; 20rpm 1.48wt% Carbopol; pH 2.79 Estimation of Mixing Time, t_c 136

A2 Variation of pH with Volumetric Additions of 23wt% NaOH Based on Mole Balance Calculations 161

E1 : E32 Thermograms of Mixing Trials (Carbopol Solutions) 171

F1 : F2 Thermograms of Mixing Trials (PEG Solutions) 203

G1 Flow Visualisation 206

G2 Flow Visualisation 209

G3 Flow Visualisation 212

G4 Flow Visualisation 215

Nomenclature

A	area [m^2]
B	number of impeller blades
Bi	Bingham number
c	clearance of impeller blade from vessel wall [m]
c_θ	geometric constant in equation (2.2.67)
C_D	drag coefficient
Ci	dimensionless circulation number
d	impeller diameter [m]
D	vessel diameter [m]
e_m	mixer efficiency (equation 2.4.6)
f	correction factor in equation (2.2.30)
F	resisting force in equation (2.2.17) [N]
Fr	Froude number
g	acceleration due to gravity [ms^{-2}]
h	height of impeller [m]
H	height of fluid in the vessel [m]
HB	Herschel-Bulkley number
He	Hedstrom number
I	inertial force in equation (2.2.15) [N]
k_c	dimensionless circulation time
k_m	dimensionless mixing time

k_s	shear rate parameter in equation (2.2.6)
K	consistency (rheology parameter)
Kp	power constant
ℓ	blade length [m]
l	length of fluid element [m]
l'	streak length [m]
M	torque [Nm]
M_o	torque at zero impeller rotational speed [Nm]
n	power law index
N	impeller rotational speed [rps]
P	power [W]
Po	Power number
Q	pumping capcity
r	radius [m]
Re	Reynolds number
Re_{hb}	Herschel-Bulkley Reynolds number
s	ribbon pitch [m]
S	final surface area in equation (2.1.3)
S_o	initial surface area in equation (2.1.3)
t	time [s]
t_c	circulation time [s]
t_m	mixing time [s]

V	volume of fluid in vessel $[m^3]$
V_θ	velocity in θ-direction
w	width of impeller blade [m]
w	width of fluid element in equation (2.1.2) [m]
w'	width of streak in equation (2.1.2) [m]

Greek Symbols

α	fitting constant in equations (2.2.15) and (2.2.65)
β	fitting constant in equation (2.2.15)
ε	geometric parametr in equation (2.2.66); relative deviation from homogeneity in equation (2.4.1)
γ, $\dot{\gamma}$	shear rate $[s^{-1}]$
$\bar{\gamma}$, $\bar{\dot{\gamma}}$	average shear rate $[s^{-1}]$
μ	Newtonian viscosity [Pas]
η	viscosity [Pas]
η_a	apparent viscosity [Pas]
ρ	density $[kgm^{-3}]$
θ	temperature $[^0C]$
τ	shear stress [Pa]
τ_y	yield stress [Pa]

1. Introduction

Mixing is most commonly encountered in the process and allied industries, and much of the engineering knowledge of mixing phenomena has been developed from these industries. The success of many processes relies heavily on effective agitation and mixing of the process fluids. Mixing and agitation are not synonymous. A single phase homogeneous material can be agitated but cannot be mixed until a second material with one or more significantly different physical or chemical properties is added. Physical properties such as state of matter, temperature and viscosity are often encountered and typically, the most common objective of mixing is to achieve a desired degree of homogeneity of physical properties (Coulson et al., 1991). In addition, mixing is often also used to promote mass and heat transfer, especially for systems undergoing chemical reaction.

The diversity of mixing scenarios is huge and a unified approach to solving mixing problems is to use a design approach based on a classification of the phases that are present in the mixing vessel (Nienow, 1985). The diversity in part explains why the operation is a central one in the food, pharmaceutical, oil, polymer and paper industries, to name but a few. However, despite the extensive applications, tremendous problems are very often encountered with industrial mixing operations. This is largely due to a lack of understanding of the fundamentals of mixing. The design aspect is an important one in industry and many process designs are oversimplified. This is often because the physical and chemical complexity of the mixing operation is underestimated. Poor design, or even overdesign, is extremely costly on large scale production plants.

The damage resulting from poorly designed mixing operations has been reviewed (Smith, 1990). Typical problems encountered include unexpected shutdowns and loss of production time, mechanical failures, low yields in reactors and off specification final products amongst others. The mixing of high viscosity and rheologically complex fluids, as often found in the polymer and biotechnology sectors, is an area of greatest concern where industry losses run into billions of dollars. Mixing operations of this type are still generally considered to be inefficient, wasteful and unduly costly. Fundamental research in this area has been, and remains to be scarce but is likely to be invaluable to industries operating in this field.

The rheology of the process fluid is very important but is often overlooked. The three main types of impeller used in industrial mixing operations are propellers, paddles and Rushton turbines, and these solve about 95% of liquid mixing problems (McCabe et al., 1985). Because of this, they are often selected by industry without due consideration. In fact, these types of impeller are extremely ineffective when dealing with non-Newtonian fluids. The design and operation of these impellers can be very damaging to microstructure in polymer operations or to cell culture in biosystems. Furthermore, in shear thinning fluids, a cavern of low viscosity fluid quickly develops around these impellers and material outside the cavern remains relatively undisturbed (Bourne and Butler, 1969; Nienow and Elson, 1988). In such circumstances, power requirements are high and the mixing process remains inefficient when compared with Newtonian fluids (Metzner and Otto, 1957). In an attempt to overcome this problem, early work moved towards the use of multiple turbines, which had a closer clearance with the walls of the vessel (Metzner et. al., 1961).

In this way more of the fluid in this vessel would experience mixing and this method was demonstrated to be more power efficient. Calderbank and Moo-Young (1961) confirmed the importance of close clearance of the impeller with the vessel wall, showing that anchor impellers were more power efficient than turbines with non-Newtonian fluids. Anchors only produce radial currents however, which limits their mixing efficiency in high viscosity fluids. Various workers (Nagata (1957), Gray (1963), Parker (1964) and Bourne and Butler (1965)) have suggested that helical ribbon impellers were the most efficient for mixing high viscosity and non-Newtonian fluids. The reason is that they generate very effective three dimensional flow patterns, which results in intimate interaction of all fluid elements, and, coupled with close wall clearance, the entire fluid volume in the vessel is under agitation. This is true even at low impeller rotational speeds. In the last thirty years these types of impeller have been accepted as the optimum choice for mixing high viscosity and rheologically complex fluids, and their excellent efficiency at low rotational speeds make them ideal for polymer and bio-operations where low shear rates are desired.

Industry still tends to overlook the potential of helical ribbon impellers. Surprisingly few detailed studies on the mixing performance of these impellers with rheologically complex fluids are available in the literature, and without a proven track record there still seems to be some reluctance to employ them.

The research work presented in this thesis addresses the batch mixing of aqueous Carbopol 940 solutions using both single and double flight helical ribbon impellers under laminar flow conditions. The rheology of these fluids is established using both steady and dynamic viscometry and a Herschel-Bulkley rheological model. Mixing and circulation times are determined using a thermal technique. The results of the work are compared to previous work, and methods are presented on how the findings can be used in industrial processes. A lack of available data in the literature in this field makes the development of reliable scale up and scale down correlations difficult and this is an area of importance in industry. Correlations developed from this work provide data which may be used in this regard for similar systems.

The scope for mixing studies is vast, encompassing a whole host of physical and chemical scenarios. This work addresses one small area of this field and the findings strongly suggest that more studies are required.

A literature review of previous work using helical ribbon impellers is presented in Chapter 2. The important correlations that have been developed for studying mixing with these impellers, in both Newtonian and non-Newtonian fluids, are provided. Some of the more common methods used to study mixing performance are outlined in this chapter, and one section of the chapter is devoted exclusively to the chemical and physical behaviour of Carbopol solutions.

Experimental procedures used to determine both the rheology of the Carbopol solutions, and the mixing performance in the vessel, are described in Chapter 3. The results of this work, together with a discussion on their relationship to previous studies in the area, are presented in Chapter 4. Conclusions from this work are summarised in Chapter 5 and recommendations for future work are given in Chapter 6.

2. Literature Review

The majority of published research work related to fluid mixing addresses the turbulent mixing of low viscosity Newtonian fluids. This is not surprising, as most mixing operations fall into this category. Turbulent mixing is a much faster process than mixing in the laminar regime and is therefore very desirable, however, situations arise which necessitate mixing under laminar flow conditions. Examples include cases where the fluid is highly viscous, as is frequently encountered in polymer operations, or where one or more of the mixture components is shear sensitive. The configuration of a laminar mixing vessel is governed by three characteristic parameters: mixing time, power consumption and mixer efficiency (Patterson et al., 1979). Power consumption is well understood but the information on mixing time and mixer efficiency still remains limited (Godfrey, 1985). Power consumption correlations have been well developed for Newtonian fluids and more recently, have been extended to non-Newtonian fluids.

The prediction of mixing time and mixer efficiency is much less developed owing to a lack of scientific knowledge of the nature of the mixing process or the effect of non-Newtonian properties on mixer performance. However, from empirical data, correlations have been suggested to overcome this lack of knowledge, primarily for the purposes of industrial mixer design. The mixer efficiency is cause for real concern, largely because of the impossibility of finding a usable definition of the (thermodynamically) perfect mixing process (Patterson et al., 1979). Some attempts have been made to develop efficiency parameters based on both published empirical data for mixing times, and dimensional analyses related to power consumption (Ottino and Macosko, 1979), (Patterson et al., 1979). No unique approach is available to solve batch mixing problems completely and modern thought is to use computational fluid dynamics to obtain approximate solutions. This technique is quicker and cheaper than traditional experimental work, although the validity of the results must always be questioned. Middleman (1977) suggests that extremely complex flow fields in the vessel coupled with a wide variety of vessel and impeller geometries make fluid mechanical design approaches very difficult from an empirical viewpoint. Computational methods deal with these problems more efficiently.

In this chapter, the fundamentals of laminar mixing are presented. The development of correlations for the prediction of power consumption and for mixing and circulation times are covered in two sections of the chapter. Single and double flight helical ribbon impeller studies are discussed separately, addressing Newtonian and non-Newtonian fluid mixing in each case. A section dealing specifically with the physical and chemical behaviour of Carbopol is presented towards the end of the chapter. Finally, conclusions are made as to which studies are relevant to this work.

2.1 Laminar Mixing

The laminar mixing regime is employed for high viscosity fluids or fluids which can only experience low shear rates. These fluids frequently have non-Newtonian rheology and may also possess significant elasticity. It is the high (apparent) viscosity of these fluids which leads to laminar flow conditions. Although turbulence would lower processing times, the excessive power requirement associated with this leads to a low efficiency mixing process.

The objective of a mixing operation is to reach a specified level of homogeneity in an initially inhomogeneous system. In other words, the scale of segregation in the vessel must be reduced. Laminar mixing of high viscosity fluids is typically a macromixing process. This means that the segregates that are mixed together are several magnitudes larger than the molecular scale. Their size is reduced as mixing proceeds until a molecular level, or micromixing process results. Situations are often encountered where the level of homogeneity required is achieved by macromixing alone, and molecular level mixing is unnecessary. Three key mechanisms of macromixing are discussed by Edwards (1985), and are summarised below.

Laminar shear is the first mechanism. Here, relative motion across streamlines in the flow results in deformation of fluid elements (segregates) leading to increased interfacial areas between the liquids being mixed and reduced striation thicknesses. Tangential flow in a coaxial cylinder arrangement is generally considered as an idealised laminar flow field. The laminar shear mixing principle in such a flow field is illustrated in Figure 2.1.1. Here the inner cylinder (impeller) rotates while the outer cylinder (vessel wall) remains stationary. Batch fluid being mixed with a helical ribbon impeller experiences considerable laminar shear in this way. The shearing effect of the ribbon as it rotates is thought to be analogous to the Couette flow of the coaxial cylinder arrangement (Chavan, 1983).

Figure 2.1.1 The principle of laminar shear mixing

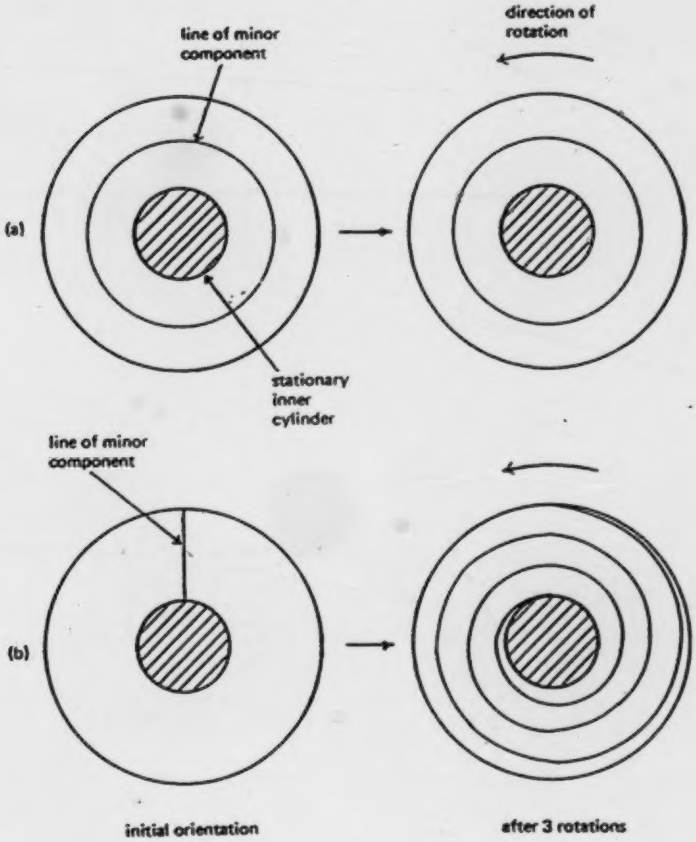
line of minor component
direction of rotation
(a)
stationary inner cylinder
line of minor component
(b)
initial orientation
after 3 rotations

source: Edwards, (1985) p. 205

Helical ribbon impellers generate radial flow in addition to tangential flow. Fluid elements often flow past each other in one dimensional shear flow. In this instance, the analogy of flow between parallel plates is made (Coulson, 1991), and it is envisioned as if one flat plate was moving at a speed V over a stationary plate. The fluid is sheared in the small gap, h, between the plates. The fluid is initially considered to be a rectangle of length, l, and width, w. After deforming in the flow field for a time, t, a streak of length l' and width w' results. The ratios of final to initial length and final to initial width have been shown to be

$$\frac{l'}{l} = \left(1 + [\dot{\gamma}_s t]^2\right)^{1/2} \tag{2.1.1}$$

$$\frac{w'}{w} = \left(1 + [\dot{\gamma}_s t]^2\right)^{1/2} \tag{2.1.2}$$

Spencer and Wiley (1951) have provided a general analysis of mixing for unidirectional flow based on changes of interfacial area for fluid elements. This is illustrated in Figure 2.2.2. The ratio of final to initial areas is determined as

$$\frac{S}{S_o} = \left[1 - 2\gamma_s \cos\alpha \cos\beta + \dot{\gamma}_s^{\,2} \cos\alpha\right]^{1/2} \tag{2.1.3}$$

Equation (2.1.3) determines the influence of orientation on mixing:

Figure 2.1.2 Effect of unidirectional laminar shear on interfacial area

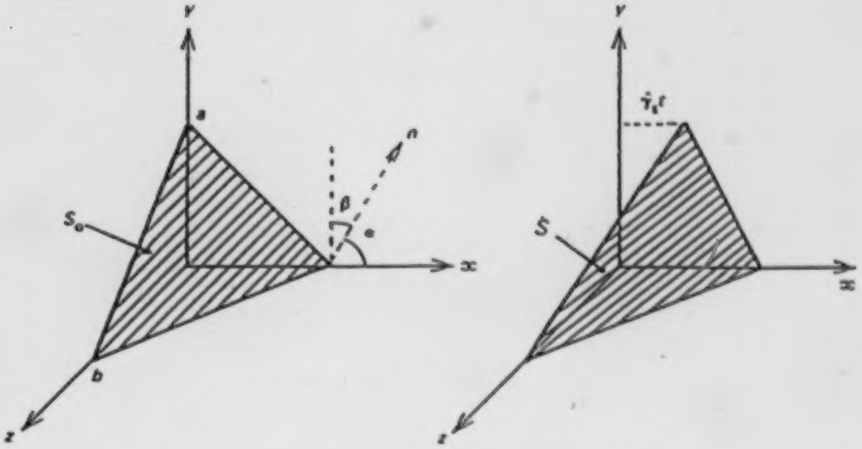
y
a
n
β
α
S_0
x
b
z
y
$\dot{\gamma}_s t$
S
x
z

$v_x = a\,y$ i.e. $\dot{\gamma}_s = v_x / y = a$

$v_y = 0$

$v_z = 0$

source: Edwards, (1985) p. 208

- $$\frac{S}{S_o} = 1 \qquad (2.1.4)$$

The surfaces are parallel to the x, y plane and no mixing occurs.

- $$\frac{S}{S_o} = 1$$

The surfaces are parallel to the x, z plane and no mixing occurs.

- $$\frac{S}{S_o} = \left(1 + \dot{\gamma}_s^{\,2}\right)^{1/2} \qquad (2.1.5)$$

the surfaces are initially parallel to the y, z plane and thus perpendicular to the plane of shear thereby providing an increased interfacial area between components and an improvement in mixing.

For real flows in a vessel agitated with a helical ribbon impeller, neither the tangential laminar shear, nor the parallel plate analogy for radial shear can sufficiently describe the mixing process. The flows are not unidirectional, but three dimensional, and a development on the Spencer and Wiley theory to accommodate this is the redistribution theory of Erwin (1978). He proposed that surface area generation is optimised by changing the direction of the instantaneous shearing action so that it always maintains angles $\alpha = \beta = 45°$ with the normal to the interface as shown in Figure 2.1.3. This is an optimal case for generating laminar shear and promoting mixing, and is more closely reached by helical ribbon flows than by simple Couette flow.

Figure 2.1.3 Effect of consecutive shearing with change in direction

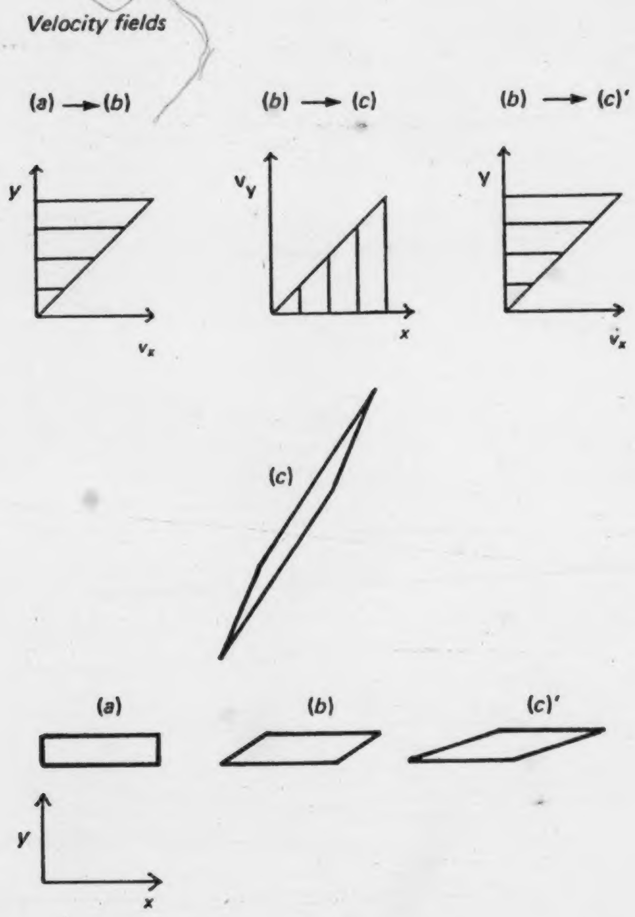
Velocity fields
(a) → (b)
(b) → (c)
(b) → (c)'
y
v_x
v_y
x
y
v_x
(c)
(a)
(b)
(c)'
y
x

source: Edwards, (1985) p. 210

Elongational laminar flow, sometimes referred to as extensional laminar flow, has been described in its simplest form and is the second mechanism of macromixing. Chavan, (1983) suggested that this effect is prominent in the small gap between the blades of a rotating helical ribbon impeller and the vessel wall. The complex three dimensional flow patterns generated in the vessel ensure reasonably efficient fluid transfer from the relatively unsheared central core into this high shear region. The fluid experiences elongational flow between the blades and the wall and is caused to "roll" over the blade. This concept is illustrated in Figure 2.1.4.

The third mechanism of macromixing is *distributive mixing*, where the "slicing and folding" of layers of fluid by the flow patterns in the vessel, and by the two previous mechanisms, generate spatial redistribution, increased interfacial area and reduced striation thickness. This is essential in reducing the size of segregates and moving towards the end objective of the mixing process. An idealised case of distributive mixing is illustrated in Figure 2.1.5.

A fourth mechanism of *dispersive mixing* has been described (Edwards, 1985), but is normally discussed in terms of the dispersion of a solid or gaseous phase through the liquid. Furthermore this might be considered as a macromixing process or a micromixing process depending on the size of the dispersant particles. This area of mixing has not been studied in this work and so will not be elaborated on.

Figure 2.1.4 Velocity profile and flow patterns in the mixing vessel

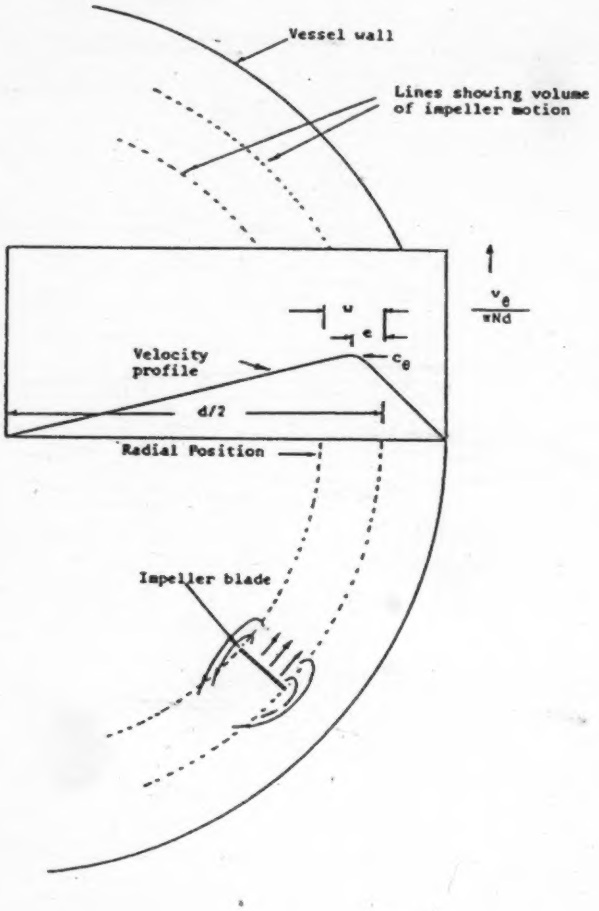
Vessel wall
Lines showing volume of impeller motion
$\frac{v_\theta}{\pi N d}$
w
e
Velocity profile
c_θ
d/2
Radial Position
Impeller blade

source: Chavan, (1983) p.178

Figure 2.1.5 Distributive mixing by slicing and rotating

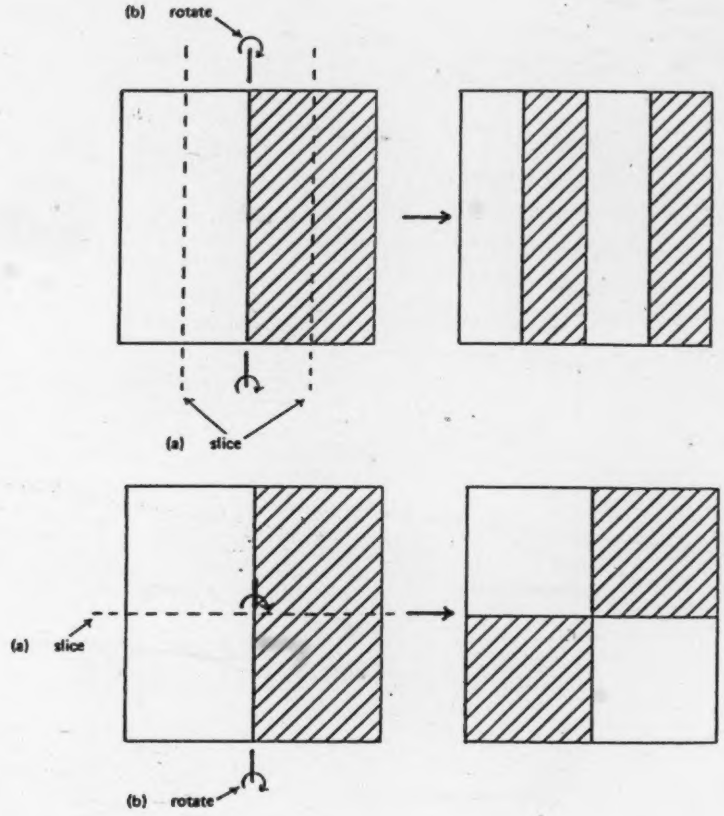
(b) rotate
(a) slice
(a) slice
(b) rotate

source: Edwards, (1985) p. 216

2.2 Power Consumption

The hydrodynamic equations governing mixing operations are complex and difficult to solve. Furthermore, they only approximate the fluid dynamics of the process. It is for these reasons that most mixing studies are based on analysis of the integral physical quantities involved, mainly power consumption, circulation capacity and mixing time. There is considerable use of dimensional analysis to correlate experimental data and to interpret results from models (Skelland, 1985).

The power per unit volume, and the relative cost of mixing equipment to vessel size are high when compared to turbulent mixing (Tatterson, 1991). A demand for well established power correlations exists because of this. The viscous mixing power correlations have a more fundamental basis than those used in turbulent mixing since turbulent mixing is often inhomogeneous with irregular fluctuations of velocity and pressure in the flow. This adds to the complexity of the hydrodynamic equations for flow prediction.

Power consumption is taken to be the energy transferred from the impeller to the fluid per unit time. Energy consumption is a useful tool in determining the efficiency of the mixer and is often a function of:

- flow regime
- tank and impeller geometry
- fluid rheology

These factors contribute to the power consumption correlations. The flow regime employed governs how the mixing process proceeds. Since the fluid rheology and the geometrical configuration largely govern the flow regime, then if these two quantities are fixed, the power consumption and flow pattern can be directly related. It is from this relation, that the energy efficiency of the mixing operation to reach a desired level of homogeneity can be inferred.

The power required to rotate an impeller in a vessel filled with a Newtonian fluid may be expressed as a general function of the variables which contribute to the three physical concepts noted above:

$$P = f(d, D, h, H, c, w, s, b, \rho, \mu, g, N) \qquad (2.2.1)$$

From this, dimensional analysis gives (Skelland, 1985):

$$\frac{P}{d^5 N^3 \rho} = Po = f\left[\left(\frac{D^2 N \rho}{\mu}\right), \left(\frac{DN^2}{g}\right), \left(\frac{D}{d}\right), \left(\frac{H}{d}\right), \text{other dimensions}\right] \qquad (2.2.2)$$

The first three dimensionless groups are the Power number (Po), Reynolds number (Re) and Froude number (Fr). When the geometry of the mixer is fixed, the remaining dimensionless groups are constant and hence,

$$Po = f(Re, Fr) \qquad (2.2.3)$$

When the rotating fluid has a flat surface and no vortices are present, the Froude number can be eliminated from equation (2.2.3). This situation is common with high viscosity fluids, but applies for a general fluid for Reynolds numbers less than 300 (Edwards, 1985). The relationship of equation (2.2.3) can be investigated experimentally for a fixed system geometry. The power requirement can be evaluated from torque measurements made on the impeller as it rotates through the fluid. The power delivered to the fluid is calculated from (King, 1985):

$$P = 2\pi NM \qquad (2.2.4)$$

If the impeller is rotated at different speeds in fluids of varying density or viscosity, a power curve can be developed to define equation (2.2.3) more precisely. A typical curve is shown in Figure 2.2.1 (Edwards, 1985). Generally, for Reynolds number less than 10, a laminar flow region exists where viscous forces predominate and the power-flow relation takes the form

$$Po = Kp\, Re^{-1} \qquad (2.2.5)$$

Since this study is devoted exclusively to laminar mixing, transitional and turbulent flows will not be discussed.

Figure 2.2.1 General characteristics of a power curve

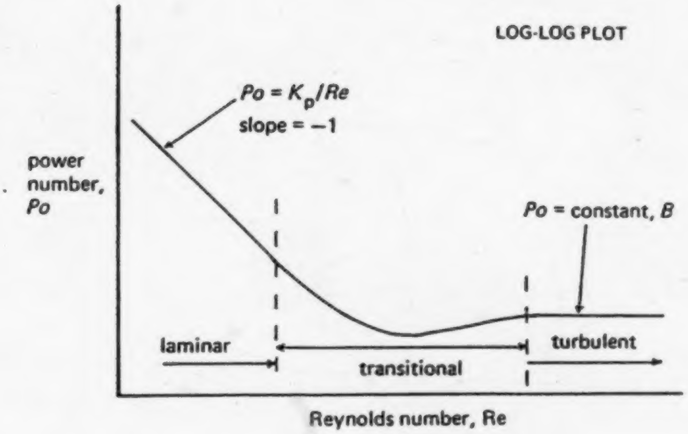

source: Edwards, (1985) p. 133

Thus far, the discussion has been restricted to Newtonian fluids. The fluid under investigation in this study, Carbopol, is non-Newtonian. Shear rate variations at different distances from the vessel walls give rise to varying apparent viscosity for non-Newtonian fluids, and the rheology evolves as mixing progresses. A simple relationship has been shown to exist between the power consumption data of Newtonian and non-Newtonian fluids in the laminar flow regime using the classical approach of Metzner and Otto, (1957). The basis of the relationship is that the shear rate generated by the impeller as it rotates through the fluid is directly proportional to the speed of the rotation:

$$\bar{\dot{\gamma}} = k_s N \qquad (2.2.6)$$

The average shear rate that is obtained from equation (2.2.6) can be combined with viscometric data of the test fluid to evaluate the apparent viscosity of the fluid at any impeller rotational speed. When the apparent viscosity of the fluid being mixed in the vessel can be ascertained, a non-Newtonian Reynolds number can be readily determined from:

$$\mathrm{Re}_a = \frac{N d^2 \rho}{\eta_a} \qquad (2.2.7)$$

For a given non-Newtonian fluid, viscometric data can be used to assign a value of apparent viscosity to a particular shear rate. In steady state viscometric tests, a plot of shear stress versus shear rate using the test data is very useful in selecting an appropriate rheological model which can then predict apparent viscosity of the fluid at any shear rate. This approach has been used to characterise the rheology of the Carbopol fluids under investigation (Section 3.2.1), and to calculate Reynolds numbers for the flow in the mixing vessel. However, to fit a rheological model successfully, a large number of experimental viscometric data are required. Fischer et al., (1961) have shown that Carbopol fluids are well characterised by a Herschel-Bulkley rheological model. The model is an empirical combination of the Bingham plastic and Ostwald-de-Waele (power) laws, (Brodkey, 1967), and is expressed mathematically as:

$$\frac{dU_x}{dy} = 0, \qquad \overline{\overline{\tau}}_{yx} \leq \tau_o$$

$$\overline{\overline{\tau}}_{yx} - \tau_o = K\left|\frac{dU_x}{dy}\right|^{n-1}\left(-\frac{dU_x}{dy}\right) \qquad (2.2.8)$$

For the calculation of apparent viscosity this can be more simply written as,

$$\eta_a = \frac{\tau_y}{\dot{\gamma}} + K|\dot{\gamma}|^{n-1} \qquad (2.2.9)$$

The shear rate on the fluid in the vessel, as proposed by equation (2.2.6), seems to be widely accepted. The problem arises in the evaluation of the constant, k_s, in equation (2.2.6). A number of correlations have been proposed to account for this, and they seem to be unanimous in predicting that k_s is very much dependent on the geometry of the mixing system. For close clearance impellers, there appears to be two distinct categories from which k_s is determined.

The first of these considers that the majority of the shearing on the fluid takes place in the small gap between the walls of the vessel and the close clearance impeller. In this analogy, the fluid is believed to be sheared as if it were in Couette flow between two concentric cylinders, the inner cylinder rotating and the outer cylinder stationary. This concept is illustrated in Figure 2.2.2. The analogy is more thoroughly described by Chavan, (1983) and Cheng and Carreau, (1994). Because steady state rheological characterisation in this study has used Couette flow viscometry, this analogy to relate rheology in the mixing vessel is given considerable attention. A theoretical treatment of Couette flow is given in section 2.2.2.

The second category considers that shearing occurs as a result of the blades of the impeller passing through the fluid as they rotate, and the resulting drag from this contributes to the overall power consumption. The theory, developed from a drag-based analogy, is well documented by Yap et al. (1979) and is reviewed by Tatterson, (1991). A theoretical treatment of the drag based analogy is given in Section 2.2.3.

The details of the correlations that have been developed which are necessary to determine power consumption will now be discussed specifically for mixers employing single and double flight helical ribbon impellers.

Figure 2.2.2 Two dimensional Couette flow

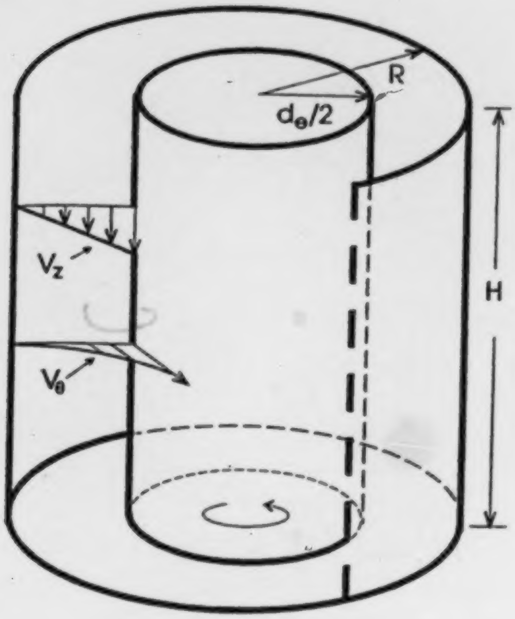
R
$d_e/2$
H
V_z
V_θ

source: Cheng and Carreau, (1994) p. 419

2.2.1 Dimensional Analysis

In the previous section, it was established that dimensional analysis is invaluable in describing the mixing process in a way which has practical engineering value. From dimensional analysis, a power-flow relationship is developed to describe mixer efficiency and for laminar mixing operations this has been shown to have a general form of equation (2.2.5). The Power number is based on a Stokes drag velocity mechanism which is theoretically described by Brito, (1992). The dimensionless number, Kp, from equation (2.2.5) is a function of geometry only for Newtonian fluids:

$$Po \cdot Re = \frac{P}{N^2 d^3 \eta_a} = Kp \qquad (2.2.10)$$

Kp typically varies between 100 and 1000 depending on the mixer geometry (Käppel, 1979; Shamlou and Edwards, 1985). For a Herschel-Bulkley type fluid, the Reynolds number can be expressed by substitution of equation (2.2.9) into (2.2.7):

$$Re_a = \frac{k_s N^2 d^2 \rho}{\left[\tau_y + K|k_s N|^n\right]} \qquad (2.2.11)$$

By using the power-flow relation of equation (2.2.5) and the definitions of Power number from equation (2.2.2), and non-Newtonian Reynolds number from equation (2.2.11), the dimensionless number, Kp, can be determined for the Herschel-Bulkley fluid as:

$$\mathrm{Kp} = \frac{k_s P}{N d^3 \left[\tau_y + K (k_s N)^n \right]} \tag{2.2.12}$$

Hall and Godfrey, (1970) developed a generalised equation to predict power consumption in Newtonian and non-Newtonian fluids using helical ribbon impellers in a variety of geometrical arrangements:

$$\mathrm{Po} = 66\,\mathrm{Re}_a^{-1} \left(\frac{s}{d}\right)^{-0.73} (B) \left(\frac{h}{d}\right) \left(\frac{w}{d}\right)^{0.5} \left(\frac{c}{d}\right)^{-0.6} \tag{2.2.13}$$

Shear rates were calculated using the Metzner and Otto approach, equation (2.2.6), to evaluate Re_a, and the fluid rheology was approximated by the Ostwald-de-Waele law. They found that the correlation was independent of the scale of the equipment and an average calculated value of k_s was 27. They also reported that power consumption approximately doubled when moving from a single flight impeller to a two flight impeller.

An experimental equation to predict power consumption in Bingham plastic fluids was proposed by Nagata et al., (1970). The rheological model used for the fluids was

$$\tau - \tau_y = \eta \dot{\gamma} \tag{2.2.14}$$

and the final power consumption equation was

$$\mathrm{Po} = \beta (\mathrm{Re}_a)^{-1} + \alpha\ \mathrm{Ny} + I \tag{2.2.15}$$

In this equation, Ny is a dimensionless number given by

$$Ny = \frac{\tau_y}{\rho N^2 d^2} \qquad (2.2.16)$$

Re_a is defined by equation (2.2.7). For mixing in the laminar flow regime, a linear plot of PoRe versus NyRe can be generated, with slope, α, and intercept, β. These can be used in equation (2.2.15). I is an inertial force. Nagata et al., (1970) found I to be 0.2 for a double ribbon impeller using geometry d/D=0.95 and b/D=0.095. The fluid was a $CaCO_3$-water dispersion having yield stress 700 g/cms^2 and viscosity 1.52 poise. The authors suggest that the value of I should be taken as the Power number for turbulent fluid mixing, which is a constant. α can be obtained from a theoretical viewpoint based on the resisting force per unit area as the impeller rotates using torque measurements:

$$Mg = \frac{Fwd^2B}{4} \qquad (2.2.17)$$

$$\alpha = \left(\frac{\pi}{2}\right)\left(\frac{F}{\tau_y}\right)\left(\frac{w}{d}\right)B \qquad (2.2.18)$$

The results obtained by Nagata et al., (1970) are in good agreement with theoretical studies of resisting forces acting on the surface of materials moving in Bingham fluids (Boardman, 1950). Nagata et al., (1970) have suggested equation (2.2.15) is useful for power prediction of ribbon, anchor, turbine and paddle type impellers in Bingham fluids. Equation (2.2.15) can be written alternatively as

$$Po = \beta(Re_a)^{-1} + \alpha He(Re_a)^{-2} \tag{2.2.19}$$

Here, He is the dimensionless Hedstrom number, defined as

$$He = \frac{\tau_y \rho d^2}{\eta_a{}^2} \tag{2.2.20}$$

The analysis of Nagata et al. (1970) essentially models the fluid flow in two parts; the first overcomes the internal structure of the viscoplastic fluid and the second overcomes the viscous resistance of the flow. This work has been investigated numerically by Tanguy et al. (1996). In their analysis, a dimensionless Bingham number, Bi, is used and is defined as

$$Bi = \frac{He}{Re_a} = \frac{\tau_y}{\eta_a N} \tag{2.2.21}$$

Their final power-flow correlation is expressed as

$$Po = Re_a{}^{-1}\left[Kpk_s{}^{-1}(k_s - 1)(Bi + 1)^{-1} + k_s{}^{-1}\right] \tag{2.2.22}$$

This correlation follows the theory of Rieger and Novak, (1973) where these authors showed a relationship of the form

$$Kp(n) = Po\,Re \tag{2.2.23}$$

i.e. Kp is a function of mixer geometry and power law index, n. In equation (2.2.22) the term in square brackets is simply a power constant for the Bingham fluid which depends on Bi only. The work of Tanguy et al. (1996) has suggested that the Metzner and Otto correlation of equation (2.2.6) can be succesfully used for viscoplastic fluids and that k_s is essentially constant for Bi ≤ 7500.

An analysis examining shear rates in a mixing vessel when the fluid present exhibits Herschel-Bulkley rheology has been provided by Rauline, (1998). If we assume that the Metzner-Otto correlation of equation (2.2.6) holds, then the power-flow relationship for such a fluid can be expressed as

$$Po = \frac{Kp}{\rho N d^2}\left(\frac{\tau_y}{k_s N} + K k_s^{\,n-1} N^{n-1}\right) \tag{2.2.24}$$

Defining a generalised Bingham number as a Herschel-Bulkley number, HB:

$$HB = \frac{\tau_y}{N^n K} \tag{2.2.25}$$

The Reynolds number for a Herschel-Bulkley fluid can then be expressed as

$$\mathrm{Re}_{hb} = \frac{\rho N^{2-n} d^2}{K + \dfrac{\tau_y}{N^n}} \tag{2.2.26}$$

A revised form of the power-flow relationship of equation (2.2.24) can now be used

$$\mathrm{Po} = \frac{1}{\mathrm{Re}_{hb}} \left[\frac{\mathrm{Kp}}{k_s} \left(1 + \frac{k_s^{\,n} - 1}{\mathrm{HB} + 1} \right) \right] \tag{2.2.27}$$

Rauline, (1998) citing Roels (1974) has shown

$$\frac{\mathrm{Kp}}{k_s} = \frac{M_0}{\tau_y} \frac{2\pi}{d^3} \tag{2.2.28}$$

In equation (2.2.28), M_0 is the torque on the impeller as the rotational speed approaches zero. The ratio of Kp/k_s is readily determined from equation (2.2.28) when a rheological characterization of the fluid has been established. For a range of rotational speeds, Re_{hb} can be tabulated using equation (2.2.26). A plot of Po versus Re_{hb} can then be made using measured values of Po at the given Re_{hb}. From the slope of the resultant plot and using equation (2.2.28), a prediction of k_s for the particular fluid and the given vessel geometry can be made.

Nagata et al., (1971) extended the work reported in Nagata et al. (1970), to predict power consumption in pseudoplastic fluids possessing a yield stress; in other words, fluids which obey a Herschel-Bulkley rheology. Again, the average shear rate concept of Metzner and Otto is used. Once the value of k_s has been predicted by an appropriate correlation, rearrangement of equations (2.2.29) and (2.2.30) yields values of α and β.

$$\alpha = \frac{\beta}{k_s} \tag{2.2.29}$$

$$\alpha = \frac{f\beta_N N}{k_s} \tag{2.2.30}$$

In equation (2.2.30), f is a correction factor due to the difference between Bingham and pseudoplasticity and is suggested to have a value of 0.575 by Nagata et al., (1971). The reasoning behind this assumption is not given. The parameter β_N is determined by its replacement for Po in equation (2.2.41) given later.

Nagata et al., (1972) presented a power correlation for the mixing of high viscosity non-Newtonian fluids. They used a range of ribbon impellers, including single and double flight ribbons and ribbon screw combinations. The correlation they developed is:

$$\mathrm{Po} = 52.5\left\{\frac{(\mathrm{D}-\mathrm{d})}{\mathrm{d}}\right\}^{-0.5}\left(\frac{\mathrm{Bd}}{\mathrm{s}}\right)^{0.5}\mathrm{Re}_{a} \qquad (2.2.31)$$

The dimensions of geometric parameters in equation (2.2.31) are in centimetres. They found that power increased with decreasing pitch and increasing number of blades. The impeller with optimum efficiency was a double flight impeller with unit pitch. Anchor impellers, having infinite pitch, were found to be much less efficient. Single ribbon impellers were suggested to be less efficient than double ribbon impellers because of the formation of stagnant mixing lumps, or effectively dead zones, between the blades.

Novak and Rieger, (1974) studied the homogenisation efficiency of three Newtonian fluids in the viscosity range 1cP to 9000cP, using anchor, pitched blade anchor and double helical ribbon agitators. From their results on helical ribbo[illegible]es, they found that

$$\mathrm{Po}\cdot\mathrm{Re} = 296 \pm 3.3 \qquad \text{for } \mathrm{Re} < 60 \qquad (2.2.32)$$

Nagata, (1956), cited by Novak and Rieger, (1974), suggested a value of 300 in equation (2.2.32). It was established by Novak and Rieger that the double ribbon impeller was the most efficient for laminar flow mixing of high viscosity fluids.

Sawinsky et al. (1976) studied the power consumption of a variety of helical ribbon and anchor agitators in both Newtonian and non-Newtonian fluids. Based on published data at the time, and on their own experimental results, they proposed the following correlations for Power number for Newtonian fluids,

$$\mathrm{Po} = 19\,\mathrm{Re}^{-1}\left(\frac{D}{c}\right)^{0.45}\frac{(B)(h)\left[1+\left(\frac{d\pi}{s}\right)^{2}\right]^{0.5}}{d} \qquad (2.2.33)$$

and for Non-Newtonian fluids,

$$\mathrm{Po} = \mathrm{Re}_a^{\ -1}\,\mathrm{Kp}\,\exp\left[(n-1)\left\{4.2\left(\frac{d}{D}\right)-0.5\right\}\right] \qquad (2.2.34)$$

Re_a has been previously defined for a Herschel-Bulkley fluid in equation (2.2.11). Sawinski et al. (1976) based their work on a shear thinning "power law" fluid where

$$\mathrm{Re}_a = \frac{\rho N^{2-n} d^2}{K(k_s)^{n-1}} \qquad (2.2.35)$$

Käppel, (1979) provided a detailed overview of Newtonian laminar mixing with helical ribbon impellers. Some of the works cited by Käppel, (1979) relating to Power number correlations include:

Käppel and Seibring, (1970),

$$\mathrm{Po} = 14\,\mathrm{Re}^{-1}(\mathrm{B})^{0.9}\left(\frac{\mathrm{s}}{\mathrm{d}}\right)^{-0.66}\left[\frac{\left(\frac{\mathrm{D}}{\mathrm{d}}\right)^{2}}{\left(\frac{\mathrm{D}}{\mathrm{d}}\right)^{2}-1}\right] \qquad (2.2.36)$$

and Reher and Böhm, (1970),

$$\mathrm{Po} = 10.5\,\mathrm{Re}^{-1}\left(\frac{\mathrm{D}}{\mathrm{c}}\right) \quad \text{for } 12.5 < \left(\frac{\mathrm{D}}{\mathrm{c}}\right) < 200 \qquad (2.2.37)$$

and also Schlüter, (1972)

$$\mathrm{Po} = 16.9\,\mathrm{Re}^{-1}(\mathrm{B})^{0.9}\left(\frac{\mathrm{h}}{\mathrm{d}}\right)\left[\frac{1}{1-\left(\frac{\mathrm{d}}{\mathrm{D}}\right)^{2}} + 11.5\frac{\left(\frac{\mathrm{w}}{\mathrm{D}}\right)\left(\frac{\mathrm{d}}{\mathrm{D}}\right)}{\left(\frac{\mathrm{s}}{\mathrm{D}}\right)^{2}}\right] \qquad (2.2.38)$$

Based on his own results, Käppel (1979) proposed the following correlation:

$$\mathrm{Po} = 60\,\mathrm{Re}^{-1}\left(\frac{\mathrm{s}}{\mathrm{d}}\right)^{-0.5}(\mathrm{B})^{0.8}\left(\frac{\mathrm{c}}{\mathrm{d}}\right)^{-0.3} \qquad (2.2.39)$$

Equation (2.2.39) was based on twelve geometric arrangements for helical ribbon impellers. The overall findings of Käppel, (1979) suggested that at large clearances Power number was consistent amongst the various authors cited, however, larger discrepancies were found at close wall clearance.

Bourne et al. (1979) analysed the results of many studies and obtained the correlation:

$$Po = 134\,Re^{-1}\left(\frac{h}{d}\right)\left(\frac{s}{d}\right)^{-0.3}\left(\frac{c}{d}\right)^{-0.3} \qquad (2.2.40)$$

Blasinski and Rzyski, (1980), citing one of their earlier papers from 1978, proposed a correlation for double helical ribbon impellers

$$Po = 74.3\,Re^{-1}\left(\frac{D-d}{d}\right)^{-0.5}\left(\frac{s}{d}\right)^{-0.5} \qquad (2.2.41)$$

In their paper, the authors analysed both published data and their own experimental results and proposed

$$Po = 34.1\,Re^{-1}\left(\frac{s}{d}\right)^{-0.63}(B)^{0.79}\left(\frac{H}{d}\right)^{0.45}\left(\frac{h}{d}\right)^{1.01}\left(\frac{c}{d}\right)^{-0.53}\left(\frac{w}{d}\right)^{0.14} \qquad (2.2.42)$$

A summary of the geometrical configuration of previously reported studies that used helical ribbon impellers is given in Table 2.2.1.

Table 2.2.1 Power Consumption Data for Helical Ribbon Impellers

Author	D/d	s/d	w/d	h/d	B	Kp
Gray (1963)	1.058	0.753	0.118	0.941	2	420
Hoogendoorn & den Hartog (1967)	1.042	0.610	0.091	1.0	2	609
Hall and Godfrey (1970)	1.10-1.114	0.50-1.0	0.097-0.135	0.94-1.01	1 or 2	130-250
Nagata et al. (1970, 1971)	1.053	1.0	0.1053	1.0	1 or 2	----------
Nagata et al. (1972)	1.053	0.5-1.0	0.105	1.0	1 or 2	210-400
Ho and Kwong (1973)	1.053	0.5-1.0	0.10	1.0	1 or 2	270-430
Rieger and Novak (1973)	1.053	1.0	0.10	1.0	2	300
Novak and Rieger (1975)	1.053	1.0	0.10	1.0	2	296.3±3.3
Sawinski et al. (1976) [Newtonian fluids]	1.042-1.19	0.36-1.3	0.084-0.12	0.8-1.1	1 or 2	250-350
Sawinski et al. (1976) [Non-Newtonian fluids]	1.042-1.19	0.36-1.3	0.084-0.12	0.8-1.1	1 or 2	----------
Käppel (1979)	1.02-1.1	0.5-1.0	0.10-1.10	1.0	1 or 2	140-450
Bourne et al. (1979)	------	------	------	------	------	300-500
Blasinski &Rzyski (1980)	1.02-1.19	0.36-1.3	0.07-0.17	0.862-1.11	1 or 2	100-300
Rieger et al. (1986)	1.05-1.12	1.0-1.5	0.1-0.2	1.0	1 or 2	190-400

2.2.2 Couette Flow Analogy

The mixing of a fluid in a cylindrical tank using a helical ribbon impeller has been considered analogous to the flow developed when one cylinder rotates inside a second, stationary cylinder. This is referred to as Couette flow and has been well described (Brodkey, 1967; White, 1974; Tatterson, 1991). The concept of the Couette flow analogy is illustrated in Figure 2.2.2. A mathematical analysis of the fluid behaviour in Couette flow begins with a force balance on the system or the equations of motion (Brodkey, 1967):

$$\frac{\partial\left(r^2\tau_{r\theta}\right)}{\partial r}=0 \qquad (2.2.43)$$

The shear stress, $\tau_{r\theta}$, is found by integration of equation (2.2.43) using $-T_o/2\pi$ as the constant of integration:

$$\tau_{r\theta}=\frac{-T_o}{2\pi r^2}=-K\left(r\frac{\partial\left(V_\theta/r\right)}{\partial r}\right)^n \qquad (2.2.44)$$

$$r\frac{\partial\left(V_\theta/r\right)}{\partial r}=-r^{-2/n}\left(\frac{T_o}{2\pi K}\right)^{1/n} \qquad (2.2.45)$$

K and n are parameters of the power law model in this case. On further integration:

$$\frac{V_\theta}{r} = \left(\frac{T_o}{2\pi K}\right)^{1/n}\left(\frac{n}{2}\right)\left(r^{-2/n}\right) + c \qquad (2.2.46)$$

evaluating the integration constant, *c*, at $r = r_2$ where $V_\theta = 0$ gives:

$$\frac{V_\theta}{r} = \left(\frac{T_o}{2\pi K}\right)^{1/n}\left(\frac{n}{2}\right)\left(r_1^{-2/n} - r_2^{-2/n}\right) \qquad (2.2.47)$$

Evaluating at r_1:

$$\Omega = \left(\frac{T_o}{2\pi K}\right)^{1/n}\left(\frac{n}{2}\right)\left(r_1^{-2/n} - r_2^{-2/n}\right) \qquad (2.2.48)$$

$\Omega = 2\pi N$ in equation (2.2.48). Rearranging for the unknown torque, T_o:

$$\left(\frac{T_o}{2\pi K}\right)^{1/n} = \frac{\left(2/n\right)\Omega}{r_1^{-2/n} - r_2^{-2/n}} \qquad (2.2.49)$$

Hence from equation (2.2.46), the shear rate at any radius is:

$$\bar{\dot{\gamma}} = -r\frac{\partial\left(V_\theta/r\right)}{\partial r} = \left(\frac{1}{r}\right)^{2/n}\frac{\left(2/n\right)\Omega}{r_1^{-2/n} - r_2^{-2/n}} \qquad (2.2.50)$$

At $r = r_1$, the radius of the inner cylinder:

$$\bar{\dot{\gamma}} = \frac{\left(\frac{2}{n}\right)\Omega}{1-\left(\frac{r_1}{r_2}\right)^{\frac{2}{n}}} \tag{2.2.51}$$

In terms of a mixing analogy with a helical ribbon, there are two limits of interest for equation (2.2.51). For fluid being sheared very close to the impeller blade, $r_1/r_2 \to 0$, and

$$\bar{\dot{\gamma}} = \frac{4\pi N}{n} \tag{2.2.52}$$

In this case, the impeller behaves as if it was rotating in an infinite fluid. In the second limit as $r_1/r_2 \to 1.0$, the impeller behaves as if it was rotating with very close clearance to the walls of the vessel:

$$\bar{\dot{\gamma}} = \frac{2\Omega r_2^2}{r_2^2 - r_1^2} \tag{2.2.53}$$

The important conclusion from equations (2.2.52) and (2.2.53) is that a linear relationship exists between $\bar{\gamma}$ and N such as that proposed by equation (2.2.6). The constant k, takes a maximum value of 4π in the limit as $(r_1/r_2) \to 0$.

Equation (2.2.53) suggests that the shear rate exerted on fluid close to the wall of the vessel is influenced by the amount of clearance between the impeller blade and the wall. The knowledge of shear rates in stirred mixing vessels is important for power consumption calculations and scale-up procedures. Some of the correlations to determine k_s and hence $\bar{\gamma}$ will now be addressed.

2.2.2.1 Shear Rates in the Mixing Vessel

For a fixed value of n, the shear rate in the mixing vessel is linearly related to impeller rotational speed as shown in equations (2.2.52) and (2.2.53), and has been discussed by Metzner and Otto, (1957). Their equation is provided here as (2.2.6). Although many workers have considered k_s to be a constant for a given impeller geometry, some have doubted the validity of this, (e.g. Ulbrecht and Carreau, 1985), especially for high shear thinning flows where shear rates have been significantly higher than those predicted by equation (2.2.6). To accommodate this, some authors have incorporated the fluid property parameters in equations to predict k_s. In this review, only correlations related to helical ribbon impellers will be addressed.

Blasinski and Kuncewicz, (1981) studied heat transfer in the mixing of pseudoplastic fluids using helical ribbon impellers. To calculate the Reynolds number in their heat transfer correlation they used the Metzner and Otto correlation to calculate shear rates in the vessel. The authors cited the work of Mitsuishi and Miyairi, (1973) who determined k_s to be

$$k_s = \frac{\sqrt{2}\pi d}{(D-d)} \tag{2.2.54}$$

These workers used a double ribbon impeller where *d* = 0.400m and *d/D* = 0.95.

Kuriyama et al. (1983) performing similar heat transfer studies again used equation (2.2.6) and determined k_s from

$$k_s = 8.9\left(\frac{c}{D}\right)^{-1/3} \tag{2.2.55}$$

3 and 5wt% solutions of CMC were used in the studies with $0.35 \le n \le 0.75$; however, equation (2.2.55) takes no account of n.

Takahashi et al. (1984) studied power consumption in viscous pseudoplastic liquids using helical ribbon impellers. They used a power law model for the fluid where $0.44 < n < 0.77$ and proposed an empirical correlation for k_s for use in equation (2.2.6):

$$k_s = 11.4\left(\frac{c}{D}\right)^{-0.411}\left(\frac{s}{D}\right)^{-0.361}\left(\frac{w}{D}\right)^{0.164} \tag{2.2.56}$$

Shamlou and Edwards, (1985) reported power consumption measurements for helical ribbon mixers in viscous Newtonian and non-Newtonian fluids. They followed the Metzner and Otto concept for shear rate in the vessel. Using their own experimental results, and those of others, they proposed the following power-flow correlation for laminar mixing:

$$\mathrm{Po} = 150\,\mathrm{Re}^{-1}\left(\frac{h}{d}\right)\sqrt{\frac{B}{\left(\frac{s}{d}\right)\left(\frac{c}{w}\right)^{0.67}}} \tag{2.2.57}$$

They found k_s to be

$$k_s = 34 - 144\left(\frac{c}{d}\right) \tag{2.2.58}$$

Again, contrary to Couette flow analogy, these authors also find that that k_s is independent of n and is found to be only reliant on the impeller clearance from the wall. Shamlou and Edwards, (1985) found that as clearance increases in the range $0.062 < c/d < 0.1637$, a limiting value of k_s is found to be 11.5. Values similar to this have been reported for turbine and paddle type impellers (Metzner and Otto, 1957; Metzner et al. 1961; Calderbank and Moo-Young, 1961). Shamlou and Edwards, (1985) found that power input was independent of the direction of rotation of the impeller for both single and double flight impellers. These authors additionally discussed the relevant merits of power consumption calculations based on Couette flow or drag-based analogies. Flows in both of these methods are addressed and estimations of errors in resulting power consumption calculations are presented. The conclusion is that these methods only provide accurate prediction of power consumption for one mixer configuration: $w/d = 0.1$; $s/d = 0.5$; $B = 1$.

Another method for determining power requirements in a laminar flow mixer is available which does not rely on any relationship between average shear rate and impeller rotational speed. This analogy has been termed the extended Couette flow analogy by Tatterson, (1991). In this analogy, power is calculated directly as a product of the shear stress, $\tau_{r\theta}$, area, A, and velocity, (πdN).

$$P = \left(\tau_{r\theta}\right)A\left(\pi\, dN\right) \tag{2.2.59}$$

The analysis of a helical ribbon impeller rotating in a cylindrical vessel has been made by Brito, (1992) using this approach. $\tau_{r\theta}$ for a power law fluid is given by equation (2.2.44). The velocity, or tip speed of the impeller, is $\Omega d/2$. The area, A, is taken to be the surface area of a cylinder of diameter, d, in the extended Couette flow analogy, so $A = 2\pi r_1 h$. Then equation (2.2.59) can be expressed as

$$P = K\left[\frac{r\,\partial\left(V_\theta/r\right)}{\partial r}\right]^n \left(2\pi\, r_1 h\right)\left(\Omega r_1\right) \tag{2.2.60}$$

Substitution for the shear rate at the inner cylinder given by equation (2.2.51) leads to

$$P = \frac{Kh\Omega\pi D^2 d^2 (2\Omega/n)^n}{2\left(D^{2/n} - d^{2/n}\right)^n} \qquad (2.2.61)$$

This is expressed in dimensionless form as

$$\mathrm{Po}\,\mathrm{Re}_a = \pi^2 \left(\frac{h}{d}\right)\left(\frac{D^2}{d^2}\right)\left[\frac{4\pi}{n\left(\frac{D^{2/n}}{d^{2/n}} - 1\right)}\right]^n \qquad (2.2.62)$$

Bourne and Butler, (1965) used the extended Couette flow analogy to describe the flow produced by a helical ribbon impeller in a cylindrical vessel. In upward pumping mode, the ribbon generated a deep central vortex produced by the flow field between the central shaft and the ribbon. Low shear rates are experienced by the fluid in this regional core. Power consumption in agitation was considered to be due to overcoming tangential viscous drag forces generated between the wall of the vessel and the vortex core. The authors also found a 30% increased power requirement in an upward pumping mode.

In continued studies, Bourne and Butler, (1969) showed that fluid is highly sheared in the annular space between the blades of the impeller and the vessel wall. The authors studied power requirements of Newtonian fluids and pseudoplastic fluids where $0.4 \le n \le 1.0$. They concluded that the direction of rotation had no influence on power consumption and that as d/D → 1.0, i.e. as the wall clearance approached zero, the extended Couette flow analogy failed to accurately predict power consumption.

Chavan and Ulbrecht, (1972) used the extended Couette flow analogy and provided an equivalent diameter, d_e , for the ribbon impeller. Using this, an average shear rate in the gap between the tank wall and the impeller can be determined. d_e is found from

$$\frac{d_e}{d} = \frac{D}{d} - \frac{2\left(w/d\right)}{\ln\left[\dfrac{\left(D/d\right) - \left[1 - \left(2w/d\right)\right]}{\left(D/d\right) - 1}\right]} \qquad (2.2.63)$$

and the resulting power-flow correlation is

$$Po = 2.49\pi\alpha\left(\frac{d_e}{d}\right)\left(\frac{D}{d_e}\right)^2\left(\frac{4\pi}{\left\{n\left[\left(D/d_e\right)^{2n} - 1\right]\right\}}\right)^n Re_a^{-1} \qquad (2.2.64)$$

Chavan and Ulbrecht, (1972) based their studies on power law fluids where $0.35 \leq n \leq 1.0$. α was determined based on the ribbon geometry, from

$$\alpha = \frac{\left(h/d\right)\left(s/d\right)}{3\pi}\left[\frac{\pi\sqrt{\left(s/d\right)^2 + \pi^2}}{\left(s/d\right)^2} + \ln\left(\frac{\pi}{\left(s/d\right)} + \frac{\sqrt{\left(s/d\right)^2 + \pi^2}}{\left(s/d\right)}\right)\right]\left[1 - \left\{1 - 2\left(w/d\right)\right\}^2\right]$$

(2.2.65)

Chavan, (1983) developed a physical model for flow between the wall and the ribbon of a rotating impeller based on tangential shear rates at the wall. For Newtonian fluids, it was proposed that

$$\mathrm{Po\,Re} = \left[\frac{c_\theta}{1 + B\xi}\right]\left[\frac{2\pi^3\left(D/d\right)^2\left(h/d\right)}{\left(D/d\right) - 1 + 2\left(\varepsilon/d\right)}\right] \qquad (2.2.66)$$

Chavan, (1983) cited the work of Käppel, (1979), and using his published data suggested $\varepsilon=0.5(w/d)$ and $\xi=0.3$ in equation (2.2.66). He also proposed that

$$c_\theta = 0.532 - 0.238\left(s/d\right) \qquad (2.2.67)$$

The prediction of c_θ from equation (2.2.67) gave good agreement with experimental results of Carreau et al. (1976). Using equation (2.2.64) proposed by Chavan and Ulbrecht, (1972) and coupled with the Metzner and Otto approach to determine k_s, Brito, (1992) has shown

$$k_s = \frac{4\pi\left[\left(D/d_e\right)^2 - 1\right]^{\frac{1}{n-1}}}{\left[n\left\{\left(D/d_e\right)^{2/n} - 1\right\}\right]^{\frac{n}{n-1}}} \tag{2.2.68}$$

Equation (2.2.68) can be used to predict an apparent Reynolds number in the vessel and thereby solve the power correlation of equation (2.2.64) for a non-Newtonian fluid. Kai and Shengyao, (1989) proposed a further correlation to determine shear rate in the mixing vessel. They performed power and heat transfer studies using a range of impeller types, in a number of flow regimes, and for shear thinning fluids in the range $0.49 < n < 0.92$, they proposed

$$k_s = 0.4^{1/n} \tag{2.2.69}$$

for the laminar flow regime.

Brito et al. (1997) studied the mixing of nine rheologically complex fluids with helical ribbon impellers. The fluids were largely described by a power law rheology with $0.14 < n < 0.65$. The Metzner and Otto correlation of equation (2.2.6) was found to have good prediction of shear rate and the constant k_s was correlated as

$$k_s = \left[38.27\left(\frac{w}{d}\right)^{-0.024}\left(\frac{s}{d}\right)^{-0.135}\right](0.814)^{1/n} \tag{2.2.70}$$

From the studies that have been performed to evaluate shear rates in the mixing vessel, it seems that the empirical relationship such as that proposed by Metzner and Otto, (1957) generally holds, and that k_s is largely a function of mixer geometry, although much more experimental and theoretical work is required to confirm the role of the rheological parameters of non-Newtonian fluids in accurately predicting k_s.

2.2.3 Drag Forced-Based Analogy

In the drag-forced based analogy, power consumption is considered to result from the drag exerted by the fluid on the impeller blade as it rotates. The overall force is expressed as the torque on the impeller. The analogy has been theoretically described by Patterson et al. (1979). The overall drag on the rotating impeller blade has two components: normal, or form drag, caused by the dynamic pressure of the stream velocity acting normal to the blade; and friction or skin drag due to the tangential stresses of fluid elements sliding over the blade. The torque on the impeller blades is given by

$$\tau = \iint A - \left[n \cdot \left(\underline{\tau} + p\underline{\delta}\right)\right]_{\theta} r\,dA \qquad (2.2.71)$$

where the term in brackets is the force per unit area in the direction of rotation. For helical ribbon impellers,

$$\tau = F_{k\theta} B \qquad (2.2.72)$$

where $F_{k\theta}$ is the drag force in the θ-direction. The power is determined from

$$P = \tau(2\pi N) = 2\pi BNF_{k\theta} \tag{2.2.73}$$

The drag force, $F_{k\theta}$, is expressed in terms of the drag coefficient, C_D, as

$$F_{k\theta} = C_D\left(\tfrac{1}{2}\rho V_\theta^2\right)A \tag{2.2.74}$$

V_θ is the angular component of the fluid velocity and A is the blade surface area. Correlations for power consumption based on the drag-forced based analogy differ largely through the definition of C_D. Patterson et al. (1979) citing Whittaker, (1968) use

$$C_{D_n} \approx \frac{5.8}{(Re)^{0.44}} \qquad 2 \le Re \le 20 \tag{2.2.75}$$

for normal flow, and

$$C_{D_t} \approx \frac{3.6}{(Re)^{0.7}} \qquad 2 \le Re \le 20 \tag{2.2.76}$$

for tangential flow.

The overall semi-empirical correlation for Newtonian fluids proposed by Patterson et al. (1979) is

$$\mathrm{Po} = 7.9\mathrm{B}\left(\frac{w}{d}\right)^{0.16} \frac{\left[5.8(\mathrm{Re})^{0.26}\sin\varphi + 1.8\cos\varphi\right]}{\left(\frac{d^2N\rho}{\mu}\right)^{0.93}\left(\frac{D}{d}\right)^{0.91}\left(\frac{\ell}{d}\right)^{1.23}} \qquad (2.2.77)$$

The impeller blade length, ℓ, in equation (2.2.77) is given by

$$\ell = h\sqrt{1+\left(\frac{d\pi}{s}\right)^2} \qquad (2.2.78)$$

An error of 8% is reported for the correlation by the authors, based on calculations using previously published data.

The theory proposed by Patterson et al. (1979) has been extended by Yap et al. (1979) to account for non-Newtonian fluids. They use a Carreau model for fluid rheology:

$$\eta_a = \frac{\eta_o}{\left[1+(t_1\gamma_a)^2\right]^S} \qquad (2.2.79)$$

Shear rates are determined using the Metzner and Otto approach. From experimental results using seven shear thinning fluids in the range $0.166 \le n \le 0.65$, Yap et al. (1979) proposed

$$k_s = 4^{1/2s}\left[\left(\frac{d}{D}\right)^2\left(\frac{\ell}{d}\right)\right] \qquad (2.2.80)$$

The apparent Reynolds number in this model is taken from

$$\mathrm{Re}_a = \frac{\rho N d^2\left(t_1\bar{\dot{\gamma}}_a\right)^{2s}}{\eta_o} \qquad (2.2.81)$$

Takahashi et al. (1980) studied power consumption in viscous Newtonian fluids. They used a drag coefficient

$$C_D = \frac{8\pi\mu V_\theta}{2\ln\left[4+8\left(\frac{c}{w}\right)\right]-1} \qquad (2.2.82)$$

Their power-flow correlation was then

$$\mathrm{Po}\,\mathrm{Re} = \left\{\frac{16\pi^3}{2\ln\left[4+8\left(c/w\right)\right]-1}\right\}\left(\frac{\ell}{d}\right)f\left(\frac{D}{c}\right)\left(\sin\theta_B{}^{0.50}\right) \qquad (2.2.83)$$

where,

$$f\left(\frac{D}{c}\right) = 1+0.00735\left(\frac{D}{c}\right)^{0.832} \qquad (2.2.84)$$

$$\sin\theta_B = \frac{s}{\sqrt{(\pi d)^2 + s^2}} \tag{2.2.85}$$

The model developed is based on the following geometry variations: B=2; $1.067 \le D/d \le 1.245$; $0.109 \le w/d \le 0.127$; $1.042 \le h/d \le 1.216$; $0.52 \le s/d \le 1.22$.

2.2.4 Discussion of Power Consumption Correlations

In Section 2.2, a number of correlations were presented to account for power consumption in a vessel being agitated with a helical ribbon impeller. All of the experimental work that has been performed for this study uses non-Newtonian Carbopol solutions; however, a number of the power-flow correlations that have been presented apply to Newtonian fluids. The suitability of these correlations is later examined based on the experimental results of Hayes et al. (1998), who used the same equipment that has been employed in this work; however, viscous Newtonian polyethylene glycol solutions were studied. Furthermore, Hayes et al. (1998) did not make any direct measurements of power consumption. It is possible to determine the Reynolds number at a given impeller rotational speed for a Newtonian fluid and a power number is generated from the correlations that have previously been outlined. Power-flow curves for the different correlations can then be compared. This work is found in Section 4.4.

It is very apparent from the literature review of non-Newtonian mixing using helical ribbon impellers, that accurate prediction of the shear rate in the vessel is critical to developing a good power-flow relationship. The suggestion is that the Metzner and Otto approach can be equally applied to both Newtonian and non-Newtonian rheologies, even yield stress fluids (Tanguy et al. 1996), when mixing by helical ribbon impellers is considered to be analogous to Couette flow. The problem associated with solving the Metzner and Otto equation, given here as (2.2.6), is accurately dtermining the "constant", k_s. Although a number of correlations have been developed to do this, they often have restrictions either geometrically, rheologically, or both. The applicability of a correlation to predict k_s must be scrutinized for these reasons. Many correlations for k_s in early studies are based on mixing using turbine and paddle-type impellers (Calderbank and Moo-Young, 1961). These are not described in this work, and only those correlations related to helical ribbon impellers have been discussed. The more important correlations are summarised in Table 2.2.2, together with the range of the power law index, n, for which studies have been made using the correlation.

Based on the value of k_s generated from the different correlations of Table 2.2.2, the Metzner-Otto equation of (2.2.6) is used to calculate γ. This result is used in the Herschel-Bulkley rheological model of equation (2.2.9), together with measured values of K, τ_y and n, from a rheological characterisation of the fluid under investigation, and then a Reynolds number for the fluid in the mixing vessel can be calculated.

Table 2.2.2 Correlations to determine k_s from literature

Author	Equation	Rheological Restriction	Geometric Restriction
Mitsuishi & Miyairi, (1973)	(2.2.54)	----------	$d/D = 0.95$
Kuriyama et al. (1983)	(2.2.55)	$0.35 \leq n \leq 0.75$	$c/D = 0.024 \rightarrow 0.07$
Takahashi et al. (1984)	(2.2.56)	$0.44 \leq n \leq 0.77$	$c/D = 0.0227 \rightarrow 0.0431$
Shamlou & Edwards, (1985)	(2.2.58)	----------	$c/D = 0.062 \rightarrow 0.1637$
Brito-de-la-Fuente, (1992)	(2.2.68)	$0.35 \leq n \leq 1.0$	------------
Kai & Shengyao, (1989)	(2.2.69)	$0.49 \leq n \leq 0.92$	------------

2.3 Methods to Study Mixing

Some approach to measure the degree of mixing, both qualitatively and quantitatively, is required to design batch mixing systems. Power consumption, which has been previously described, is one of the most common ways to do this. Two other approaches are often also used. These are measurements of circulation time, t_c, and mixing time, t_m. t_c and t_m are not physical quantities, but are inferred from the results of particular experimental techniques to assess mixer performance. Before definitions of mixing and circulation times are given, some of the experimental techniques used for their measurement will be described.

The physical process of laminar mixing has been described in Section 2.1. As the process proceeds, a new level of homogeneity is reached from the point when a specified change in the system has been made. It has been established that viscous mixing is essentially a macromixing process. An experimental technique to monitor mixing as it proceeds requires that the starting point of the mixing process can be well identified, that the endpoint of mixing can be well established and that in the intermediate period, the transition to homogeneity can be determined. Clearly, the physical change occurring in the system is measured with respect to time. The following techniques are most commonly employed to achieve these goals:

- Conductivity or pH method
- Thermal technique
- Colorimetry

- Decolourisation by fast chemical reaction
- Schlieren method

All of these techniques essentially use a tracer and monitoring instrument to quantify mixing. The Schlieren method relies on density differences in the mixing vessel, monitored by an optical technique. Since many of these techniques have a complex set up and can be expensive, the simpler techniques of colorimetry and the thermal method have been used in this study and have been found to give reasonably good results. A discussion of the advantages and disadvantages of the various methods to study mixing has been given by Hoogendoorn and Den Hartog (1967), Ford et al. (1972), and Hiby (1981). An important requirement of the technique used is that the rheological properties of the bulk fluid are not significantly changed on addition of the tracer sample.

In the thermal technique, temperature differences in the mixer are used to quantify the degree of mixing. Typically, a portion of fluid is heated externally to several degrees above the temperature of the bulk fluid in the vessel. The heated aliquot is introduced to the bulk fluid and mixing is initiated. Temperature is monitored at various locations in the vessel by inserting thermistors or thermocouples in the bulk fluid for example (Landau and Prochazka, 1960). The technique often requires a large volume for the injected aliquot; Tanguy et. al., (1992) used 2% of the vessel volume. Higher temperature differences between the bulk fluid and the injected aliquot often also give better results, however, the physical properties of the aliquot and the bulk fluid should be approximately the same, and larger temperature differences will tend to compromise this. The endpoint of mixing is often difficult to define and to predict using a thermal technique, as the approach to the fully mixed condition is asymptotic (Käppel, 1979). Errors in estimation of mixing and circulation times are potentially large (Godfrey, 1985)

2.4 Mixing Time

The purpose of the mixing process is to reach a desired level of homogeneity in the mixing vessel and the methods by which this is achieved have been described in Section 2.1. The mixing time, t_m, is generally accepted as the time needed to reach a specified degree of homogeneity from the point when mixing is initiated. Hiby (1981) has suggested that the degree of mixing, M, should be defined as

$$M = 1 - \varepsilon \qquad (2.4.1)$$

where ε is the relative deviation from the required level of homogeneity. However, the author has recognised five possible definitions of ε which are related to the frequency distribution curve of the trace which is used to create inhomogeneity. ε is then defined from statistically derived parameters of ε. Ogawa and Ito, (1975) use probability theory to explain the mixing phenomena. The volume of the mixing tank is divided into *i* subdomains of equal volume and the theory relies on measured trace changes in these *i* subdomains which are then summed over the entire tank volume.

From the most general definition of mixing time, it is clear that it is an entirely experimental criterion which can be used to compare mixing with impellers of different geometry. The concept of mixing time has been criticised for being unreliable and with good reason. Most of the techniques used in its determination are prone to have large errors associated with them.

Hoogendoorn and Den Hartog, (1967) have suggested that t_m is the time, t, at which

$$\forall t \geq t_m ;\ 0.9 \leq \frac{\theta(t) - \theta(i)}{\Delta\theta_\infty} \leq 1.1 \qquad (2.4.2)$$

where $\theta(t)$ is the temperature at time t, and $\Delta\theta_\infty$ is the difference between the final temperature, θ_f and the initial temperature, θ_i. Because of the asymptotic approach to θ_f previously described, the actual value of θ_f is difficult to assign and in this work has been estimated based on the resultant thermograms, and in some instances, has been based on an extrapolation of the thermogram, forward in time. The proposal of Hoogendoorn and Den Hartog, (1967) in equation (2.4.2) is based on studies using a number of different impeller types including helical ribbons. Brito et al. (1990) use a similar definition for t_m based on the thermal technique.

$$\forall t \geq t_m ;\ \left|\theta(t) - \theta_f\right| \leq \frac{\Delta\theta_\infty}{2} \qquad (2.4.3)$$

The authors propose less scatter of data using the approach of equation (2.4.3) over equation (2.4.2).

In the mixing process, mixing time is typically correlated in the literature (Tatterson, 1991) as

$$Nt_m = f(Re) = k_m \tag{2.4.4}$$

and k_m is the mixing or homogenisation number. It is generally considered that for a given impeller geometry, k_m is constant in the laminar flow regime and is independent of Reynolds number. k_m then represents the number of revolutions required to achieve a specified level of homogenisation.

In comparing the performance of different agitators, power consumption and mixing times are combined and the energy of mixing is analysed. The current study is restricted to helical ribbon impellers but the reader is directed to the review of Tatterson, (1991) for elaboration on the energy of mixing concept.

The mixing time is the time required to obtain fairly complete dispersion of dye in colorimetry or the time to reach an equilibrium temperature in the thermal method. Nagata et al. (1956) cited by Tatterson (1991) used a decolourisation method by fast chemical reaction to study mixing times of highly viscous liquids. k_m from equation (2.4.4) was found to be 33 for helical ribbon impellers and the authors showed no effect on this due to vessel diameter. They proposed that upward pumping at the vessel wall produced the lowest mixing times and best overall mixing efficiency however no data were supplied to confirm the proposal.

Gray, (1963) found k_m to be 25 for the mixing of Newtonian fluids in the viscosity range 25 to 50 Pas. Helical ribbon impellers were used and mixing times were determined using colorimetry. The author concluded that the helical ribbon impeller had far superior mixing efficiency by an order of magnitude over combined screw-ribbon impellers and turbine-type impellers.

Hoogendoorn and Den Hartog, (1967) compared mixing performance with several agitators by measuring mixing time and power input. For helical ribbon impellers they found k_m to be 65. The geometrical configuration of the mixer in this work has been previously described by Hayes et. al., (1998).

Zlokarnik (1967) cited by Brito (1992) found k_m to be dependant on Reynolds number in the laminar flow regime, according to

$$k_m = 47\,\mathrm{Re}^{0\,1} \qquad (2.4.5)$$

The geometry of the mixer used in the study was D/d = 1.02; h/d = 1.0; w/d = 0.1. Newtonian fluids were investigated in the viscosity range 0.1 to 40 Pas and $1 \leq \mathrm{Re} \leq 100$.

Nagata et al. (1972) used Newtonian and pseudoplastic fluids and a decolourisation method to determine k_m. Equation (2.4.4) was found to hold good and for double helical ribbon impellers k_m was 40. For single ribbon impellers, $100 \leq k_m \leq 150$. The authors suggested a double ribbon impeller with s/d = 1.0 had the best mixing efficiency.

Ho and Kwong (1973) reviewed the literature at that time to propose correlations for t_m based on experimental results from the literature. The findings of the authors are summarised in Table 2.4.1. An accuracy of ±30% is quoted by the authors and a contingency of ±50% should be added.

Novak and Rieger (1975) studied homogenisation efficiency for a variety of impellers and in a number of flow regimes. In laminar flow, where $Re < 40$, k_m was found to be approximately equal to 60 for helical ribbon impellers.

Carreau et al. (1976) used a decolourisation technique to measure mixing times in Newtonian and viscoelastic fluids with helical ribbon impellers. The authors found that Newtonian mixing times were as much as seven times less than those for viscoelastic fluids. A dimensionless mixing effectiveness factor was used, defined as

$$e_m = \frac{V}{Nd^3 t_m} \qquad (2.4.6)$$

where V is the bulk fluid volume in equation (2.4.6).

The effect of helical ribbon geometry on k_m has been studied by Bourne et al. (1979). For Newtonian fluids, $43 < k_m < 53$ in laminar flow. w/d had no effect on k_m and it was found that $s/d = 0.57$ created better mixing than $s/d = 0.87$. For optimum homogenisation, $d/D = 0.91$, $s/d = 0.57$, $w/d = 0.12$ was suggested.

Patterson et al. (1979) found k_m to vary between 22 and 49 for Newtonian fluids over a viscosity range of 0.1 to 0.8 Pas. They found that ribbons with wider blades were more efficient and a single ribbon agitator was more favourable than a double ribbon.

Figure 2.4.1 Mixing time correlations for helical ribbon impellers

Impeller Type	Correlation	Conditions
Single Ribbon Impeller	$Nt_m = 90$	$Re < 20$; $s/D = 0.5$
	$Nt_m = 126$	$Re < 20$; $s/D = 1.0$
	$Nt_m = 1640\ Re^{-0.6}$	$10 < Re < 200$
	$Nt_m = 122\ Re^{-0.19}$	$600 < Re < 25000$
Double Ribbon Impeller	$Nt_m = 48$	$d/D = 0.95$; $w/D = 0.095$; $h/D = 0.98$; $c/D = 0.025$; $s/D = 0.5$
	$Nt_m = 66$	$d/D = 0.95$; $w/D = 0.095$; $h/D = 0.98$; $c/D = 0.025$; $s/D = 1.0$

source: Ho and Kwong, (1973) p. 94-104

Yap et al. (1979), extending the work of Patterson et al. (1979) to non-Newtonian fluids found that pseudoplastic fluids behaved like Newtonian fluids with corresponding mixer geometry. A relative efficiency for mixer performance was used based on an arbitrary mixer configuration.

Käppel (1979) provided an exhaustive study of mixing time using twelve helical ribbon impeller geometries and Newtonian fluids in the viscosity range 2.5 to 35.8 Pas. A decolourisation technique was used to determine mixing time. The geometry studied varied as $0.5 < s/d < 1.0$ and $1.02 \leq D/d \leq 1.1$. For single ribbon impellers, $90 \leq k_m \leq 130$. For double ribbon impellers, $56 \leq k_m \leq 76$. Käppel (1979) found that k_m was weakly dependent on wall clearance as

$$k_m \propto \left(\frac{c}{d}\right)^{0.1} \qquad (2.4.7)$$

The author recommended s/d to be 1.0 and D/d to be 1.1 for both single and double flight helical ribbon impellers to achieve optimum mixing.

Takahashi (1982) used liquid crystal colorimetry and fourteen helical ribbon geometries to study the mixing of viscous Newtonian fluids. A recommended geometry for optimum mixing was suggested to be $c/D = 0.06$; $s/D = 0.9$; $w/D = 0.15$. The authors found a stronger dependence of wall clearance on k_m than Käppel (1979).

2.5 Circulation Time

The mixing performance of a helical ribbon impeller is related to the flow patterns and velocity distributions it develops in the vessel. The flow developed should enhance the mixing process described in Section 2.1 and reduce dead zones in the vessel. Mixing and circulation times are primarily used to quantify laminar macromixing and thereby assess the performance of the mixer.

Mixing time assessment has been previously discussed. Like mixing time, circulation time is very closely related to the experimental technique that is used in its measurement and methods for evaluation include the flow follower and probe based methods used to determine mixing time.

Chavan and Mashelkar, (1980) have defined the circulation time as the average time taken by a fluid element to complete one circulation loop in the vessel. In a flow follower technique, the motion of a freely suspended particle would be monitored with respect to a reference plane and a large number of observations would then be analysed statistically (Brito, 1992). From the definition of Chavan and Mashelkar, (1980), the problem still remains as to identifying what a circulation loop is, especially since the flow generated by a helical ribbon impeller is three dimensional. An alternative definition for t_c is proposed by Brito, (1992) citing Guerin et al. (1984): t_c is the time interval between two crossings of the tracer fluid in the same direction of a horizontal plane. The equatorial plane is naturally chosen as the arbitrary horizontal plane.

When probe based methods are used, circulation time is estimated from the periodicity of the response curve (Tanguy et al., 1996). The number of peaks that are observed depends on several factors. For the thermal technique, the number of peaks will depend on the rheology of the bulk and injected fluid, the initial temperature of the bulk and injected fluid, and also on the volume of the fluid injected to the bulk. Furthermore, the location of the thermocouples used to measure the transient temperature in the vessel has an important role in the results that are obtained for t_c by this method. In order that reproducible results are obtained, all of these influential factors must be kept as close to constant as is possible between separate runs.

The circulation time is related to the pumping capacity of the impeller and the liquid circulation flow rate is defined as

$$Q = \frac{V}{t_c} \tag{2.5.1}$$

The impeller pumping capacity and circulation times are related by the dimensionless circulation number, (Chavan et al., 1975):

$$Ci = \frac{Q}{Nd^3} = \frac{V}{t_c Nd^3} = k_Q \tag{2.5.2}$$

Circulation times are often also correlated by a dimensionless circulation time, Nt_c, which is the number of revolutions required to complete one circulation.

$$Nt_c = k_c \tag{2.5.3}$$

Ci and k_c are functions of the mixer geometry and it appears to be well accepted that for Re < 10, these are constants for a given mixer geometry and independent of Reynolds number (Ryan et al., 1988).

Circulation time data is sometimes also expressed as

$$n_c = \frac{t_m}{t_c} \tag{2.5.4}$$

There are few studies on circulation times using helical ribbon impellers, especially in the case of non-Newtonian fluid mixing. Bourne and Butler, (1969) provided a theoretical analysis of fluid flow over the blades of a helical ribbon impeller and showed Ci = 0.046 which was independent of mixer geometry or fluid rheology.

Carreau et al., (1976) studied t_c for Newtonian and shear thinning fluids using helical ribbon impellers. They used a flow follower technique and found $n_c \approx 3.5$ for Newtonian fluids which was independent of geometry. For shear thinning fluids, n_c was found to be in the range 5.7 to 9.4 and did have a dependence on geometry. Ci was found to be dependent on both mixer geometry and fluid rheology, with $0.05 \leq Ci \leq 0.15$ for Newtonian fluids and $0.047 \leq Ci \leq 0.098$ for shear thinning fluids.

Takahashi et al., (1982) estimated $0.0678 \le Ci \le 0.155$ for viscous Newtonian fluids using helical ribbon impellers. Their experimental and theoretical comparisons for Ci were satisfactory. They proposed Ci to be a function of impeller geometry.

Ryan et al., (1988) studied circulation time in a reactor using a helical ribbon impeller and a draught tube. Newtonian fluids in the viscosity range 0.001 to 23 Pas and shear thinning fluids with $0.6 < n < 0.75$ were used. For the Newtonian fluids with $Re < 500$, Nt_c was reported to be 9.5 ± 0.5. Nt_c was suggested to be higher for non-Newtonian fluids.

Takahashi et al., (1989) studied circulation times for shear thinning fluids with $0.69 \le n \le 0.93$ in a vessel equipped with a helical ribbon impeller. The authors proposed

$$Nt_c = \alpha_c Re^{\beta_c} \tag{2.5.5}$$

where α_c and β_c are fitting constants. The constants have been shown to vary experimentally as $8.4 < \alpha_c < 19.6$ and $0.044 < \beta_c < 0.117$ by the authors.

2.6 Conclusions on Circulation and Mixing Times

The theory and correlations that have been developed for determining mixing and circulation times have a less fundamental basis than those that have been established for power consumption. They are essentially based on experimental technique and procedure, and furthermore, the results thereby gained are left to personal interpretation. It is for these reasons to a certain extent that reported data often varies. Another reason for variability is that the analysis of the experimental data is statistical in nature.

What have been considered to be the more pertinent correlations to study mixing and circulation have been given above and these will be used in conjunction with the experimental results of this study in Section 4.3. A comparison and discussion on the appropriateness of these correlations will also be given in that section.

2.7 Carbopol: Chemistry and Physical Behaviour

Carbopol is a trade name of the B. F. Goodrich Company, USA. The Carbopol family of resins have been given the generic name “Carbomers” by the British Pharmacopoeia, the United States Adopted Names Council (USAN) and the Cosmetic, Toiletries and Fragrance Association (CTFA). Carbomer resins are high molecular weight, allylpentaerithritol-crosslinked, acrylic acid based polymers modified with C10-C30 akrylates (Allen, 1997). A generalised form of the organic monomer backbone of Carbopol is illustrated below, together with the monomer structure of poly(acrylic acid). The monomer of Carbopol 940 is a modified combination of these structures, as mentioned.

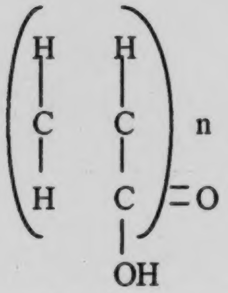

Generalised Carbopol backbone

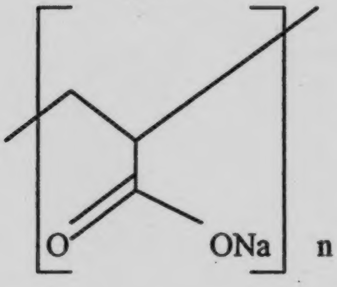

Poly(acrylic acid) monomer

Carbopol has a 2% maximum moisture content and a pKa of 6.0 ± 0.5. Aqueous dispersions have a pH in the range 2.5 to 3.5 depending on the concentration. For a

1.48wt% dispersion, pH has been observed to be 2.79. Semi-transparent organic gels are formed from aqueous dispersions of Carbopol and their viscosity rapidly increases upon neutralisation with concentrated sodium hydroxide. Carbopol 940 is the most efficient of all the Carbomer resins with excellent thickening efficiency at high viscosity. The viscoplastic rheology of these gels make them very effective in preparing suspensions, stable emulsions and preparations containing dissolved salts. The gels maintain their viscosity over a wide range of temperature (Ravissot, 1989). Carbopol 940 is very often used in topical pharmaceutical preparations and is a particularly common ingredient in transparent cosmetic gels, for the reasons outlined above.

Aqueous Carbopol gels have been shown to be composed of swollen deformable microgel particles which are packed into intimate contact when concentrated (Taylor and Bagley, 1974; 1977; Brown and Garret, 1959). The concept is illustrated in Figure 2.6.1. Carnali and Naser, (1992) used dilute solution viscometry to measure the intrinsic viscosity and overlap concentration of the gels. By these measurements, some understanding of the microstructure and therefore the behaviour of the gels could be inferred. The overlap concentration, c^*, is recognised as a reliable measure of the size of a gel's micronetwork and can be used to understand how the microparticles swell in water. The swelling profile can be established from standard theories for the free energy of a network using non Gaussian chain statistics. The reader is referred to the work of Carnali and Naser, (1992) for an elaboration of this theory. A crosslink density can also be determined and is expressed in terms of the number of monomer units between crosslinked sites. This density has been shown to be 1450 for Carbopol 940 by Carnali and Naser, (1992). These authors have further shown from mechanical spectroscopy that Carbopol gels contain a large number of cyclic structures and redundant crosslinks which is interpreted in a physical sense as the micronetworks having inherent defects. They cite the work of Wolfe and Scopazzi, (1989) and Antionetti et al., (1990), as confirmation of this. In accordance with the findings of Ketz et al., (1988), Carnali and Naser, (1992) also conclude that the rheology of Carbopol gels is a function of the microstructure, and since this contains inherent defects, absolute prediction of a steady rheology of the gels is not possible.

A schematic drawing of a molecule of Carbopol resin in its relaxed state is presented in Figure 2.6.2. In Figure 2.6.3 it is observed how a low viscosity solution results when such a resin is dispersed in water, since stronger hydrogen bonds then develop between polymer phase and the aqueous phase. In Figure 2.6.4 it can be seen that on the addition of concentrated sodium hydroxide the viscosity of the gels is caused to rapidly increase due to the formation of even stronger ionic-like bonds within the complex.

A rigorous treatment of the chemistry and physics of microgels is beyond the scope of this thesis, however the foregoing information has been included to provide some background as to the unusual rheological behaviour that has been observed with these gels and also to offer some explanation for the results obtained from rheological characterisation. The latter topic is presented in Section 4.1.

Figure 2.6.1 Aqueous linear polymer and microgel structures

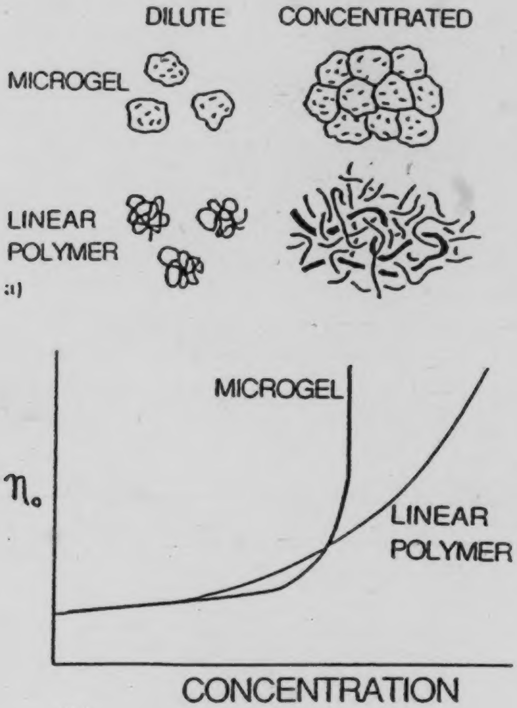
DILUTE
CONCENTRATED
MICROGEL
LINEAR POLYMER
MICROGEL
η_o
LINEAR POLYMER
CONCENTRATION

source: Ketz et al., (1988) p. 532

Figure 2.6.2 Schematic of Carbopol resin molecule in relaxed state

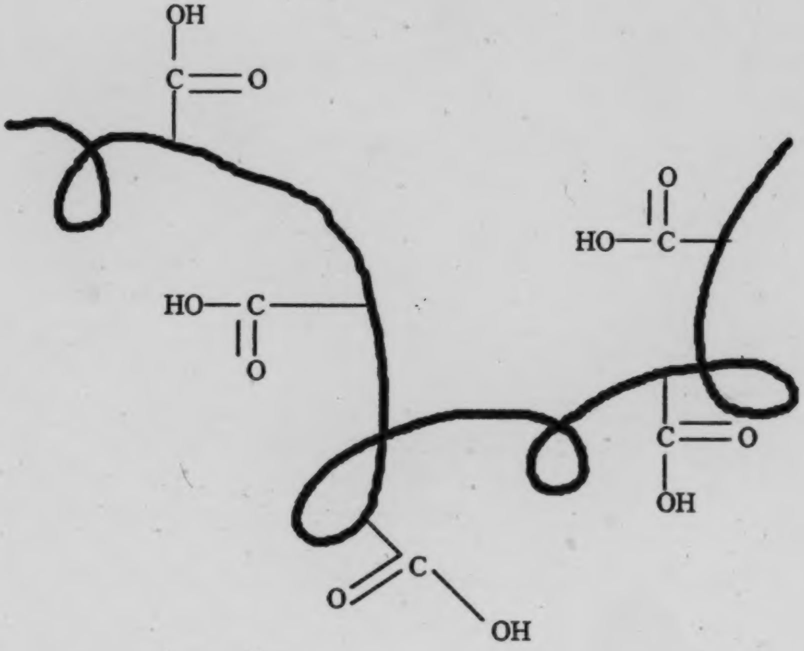
OH
C
O
O
HO—C
HO—C
O
C
O
OH
C
O
OH

Figure 2.6.3 Hydrogen bonding in aqueous Carbopol dispersions

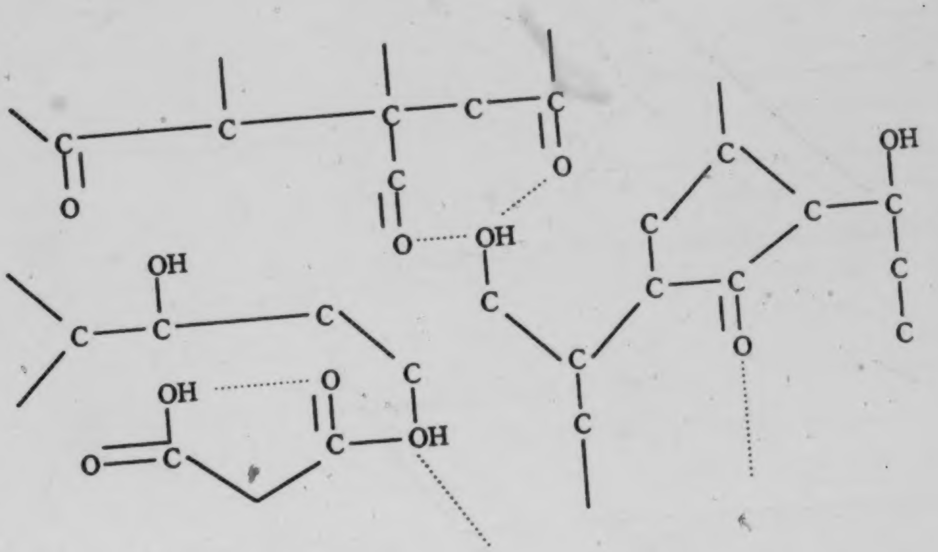

OH
OH
OH
OH
OH

······················ Hydrogen bonding

Figure 2.6.4 Ionic-type bonds from neutralisation with NaOH

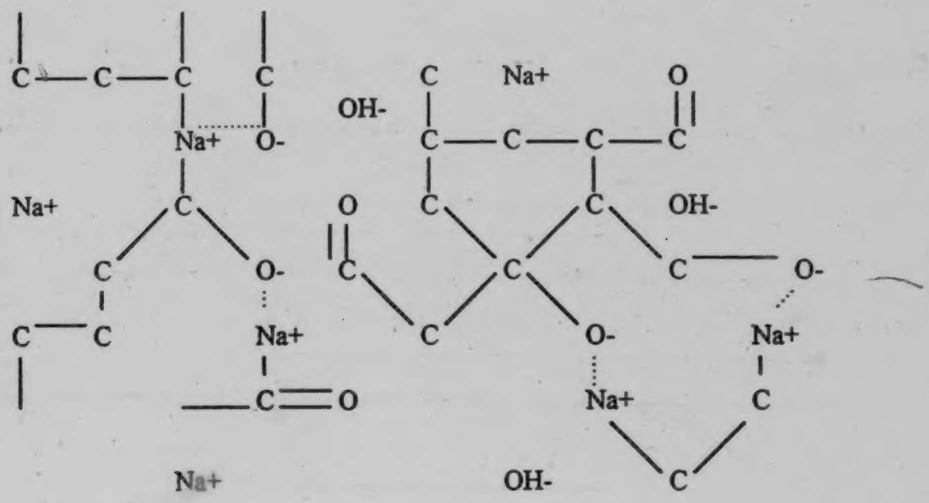
C
Na+
O-
Na+
C
O-
Na+
C
O
OH-
C
Na+
O
O-
Na+
OH-
Na+
OH-
C

Ionic-type bond

3. Experimental Procedure

3.1 Preparation of Carbopol Solutions

Extensive rheological tests were performed on aqueous solutions of Carbopol 940, a dry white powdered form of polymer supplied by the B. F. Goodrich Company, Michigan, USA. The chemical and physical behaviour of the polymer is described in Section 2.8.

The dry powdered form of Carbopol 940 has very low wettability which makes it difficult to produce a homogeneous solution. As a large number of samples of aqueous Carbopol were required for rheological characterisation, it was considered best to make a large batch of the aqueous polymer and small samples were drawn from this batch for use in the rheological tests.

Eight litre batches of aqueous Carbopol 940 were generated in the same vessel used in the mixing studies. This vessel and its associated components is described in Section 3.2.1.

Although some work was performed using a 0.48wt% Carbopol 940 solution, the majority of the work in this thesis focuses on aqueous solutions of 1.48wt% Carbopol 940. This is equivalent to 15 grams of the polymer in 1 litre of water[*]. For 8 litres of water, 120 grams of the solid polymer is required to give a 1.48wt% aqueous solution. The mass of the powder required was measured using a Mettler PC 2000 measuring balance with an accuracy of ± 0.01 gram. Typically, the mass of powdered polymer required for an 8 litre batch of water was weighed in a beaker. On transferral of the powder from the beaker to the mixing vessel, there was some unavoidable loss of mass because tiny amounts of powder cling to the walls and base of the beaker due to small flaws on the otherwise smooth glass surface, and some is also lost due to powder attachment to a stainless steel spatula used in the transferral process. This loss of mass has been estimated to be no more than 0.05 grams in a 120 gram transfer of powdered polymer. The final homogeneous solution is then 1.48wt% ± 1% error.

---

[*] All water referred to in this thesis is deionised water prepared by a process of reverse osmosis. It is taken to have a density of $1000 kgm^{-3}$ and any deviation from this assumption will be so small as to have negligible effect on any subsequent experimental results

The glass mixing vessel was cylindrical and flat bottomed with a maximum volume of 9.8 litres. In preparing the batches of aqueous Carbopol, the double flight helical ribbon impeller, DHR-1 was used exclusively. Refer to Section 3.2.1 for further details on the batch mixing vessel and associated components.

Water and Carbopol 940 powder were added to the mixing vessel in layers. To elaborate, 1 litre of water was added to the vessel, followed by 15 grams of Carbopol powder. The powder was visually observed to float on the water and remain dry. The impeller DHR-1 was plunged through the mixture by hand, to start the mixing. A second litre of water was then added to the vessel, followed by a further 15 grams of Carbopol powder. The vessel contents were plunged again as mentioned. Layers of water followed by powder, as described, were added to the vessel until 8 litres of water and 120 grams of Carbopol 940 powder were in the mixing vessel. The whole contents were then well plunged by the method described. The vessel was then locked into position and the ribbon impeller DHR-1 was secured in the drive shaft. The vessel contents were then mixed until an opaque, homogeneous solution was observed. The impeller DHR-1 was typically rotated at speeds from 40 to 50 rpm. The time required to reach a homogeneous solution was between 2 and 3 days. The rotational direction of the impeller was reversed every 12 hours.

A 23wt% aqueous solution of NaOH was prepared using solid sodium hydroxide supplied by Fisher Scientific.

The aqueous Carbopol 940 solution in the batch mixing vessel had a viscosity of around 10 Pas at zero shear rate. The pH of 1.48 wt.% solutions was measured as 2.79 and was found to be consistent over several batches that were made, the maximum error in pH measurement being estimated to be 3%. All pH measurements were determined using a Fisher Accumet 305 MP digital pH meter supplied by Fisher Scientific.

When the aqueous Carbopol solution is neutralised with sodium hydroxide, there is a rapid rise in viscosity until a viscosity plateau is reached for solutions having pH between 4 and 11. For pH higher than 11 the solution viscosity rapidly falls.

3.1.1 Sample Preparation for Rheological Studies

Dropwise additions of 23 wt.% sodium hydroxide were made to separate 100 ml. samples of 1.48 wt.% Carbopol solutions using a 1 cm^3 microsyringe. After additions were made the contents of the beaker were thoroughly mixed by hand using a clean stainless steel spatula. The pH was then measured using a Fisher Accumet 305 MP pH meter. The probe of the meter was cleaned three times before and after measurement, using toluene and water. Calibration of the probe was verified using buffer solutions of pH 3.0 and pH 10.0. All pH measurements were made three times for verification.

A titration curve for the 100ml. samples of Carbopol 940 solutions is shown in figure 3.1.1. Each of these points on the curve represents at least three repeated measurements of pH in two separate solutions prepared to have identical pH. The error associated with each point is not more than 2%.

3.1.2 Steady State Rheological Tests

Steady state rheological measurements were performed on the Carbopol 940 samples using a Contraves Rheomat 115 rotational viscometer. The viscosity as a function of shear rate was determined over a range of pH. All measurements were made at 25°C.

The Rheomat 115 operates according to a Couette-type flow analogy. The measuring bob of the system rotates inside a stationary cylindrical cup. The measuring substance is sheared in the annular space between the cup and the rotating bob. The breaking torque exerted on the bob by the test substance is measured. The shear rate on the substance is a function of the bob's rotational speed. The manufacturer's literature has data tables which provide the shear rate which corresponds to a given rotational speed. The viscosity of the substance can be deduced from these values and an appropriate rheological model.

Prior to use, the cup of the viscometer was cleaned with toluene and then water. Approximately 15 ml. of the Carbopol sample was transferred from the beaker to the cup. The bob was then slowly inserted into the cup while being gently rotated by hand. The

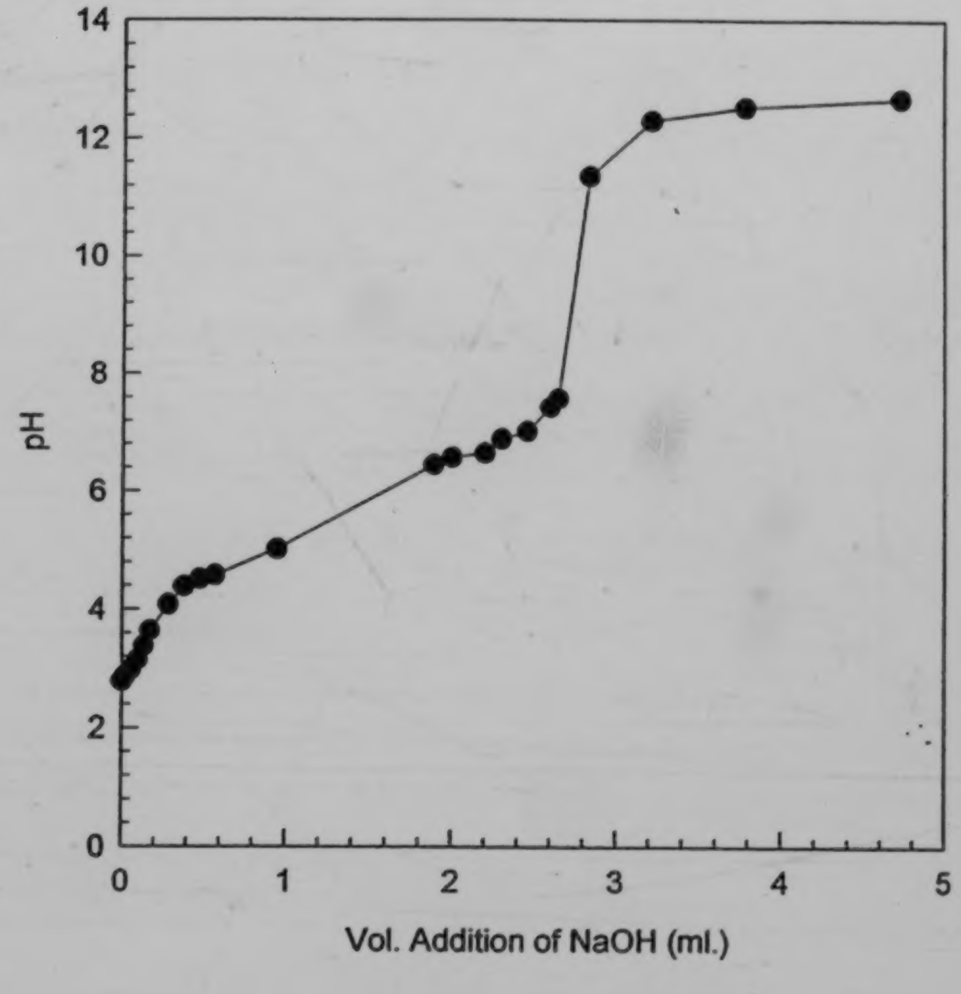

Figure 3.1.1 Titration curve for 1.48wt% aqueous Carbopol and additions of 23wt% aqueous NaOH .

gentle insertion and rotation of the bob prevents air pockets or discontinuities being generated in the sample.

The bob was rotated at fifteen different speeds in the range 5 to 780 min^{-1} starting from the lowest speed. At each speed step, the breaking torque was recorded.

For each pH, the procedure described above was repeated at least three times to verify the results obtained. The error between results of the tests was found to be no more than 5%.

It became apparent at any early stage that the information resulting from the runs was in error, and consistently so, suggesting that the shear rate data provided in the manufacturers literature might be in error. To verify this, the equipment was checked using an aqueous 46.7 wt.% polyethylene glycol solution. This solution is very viscous and Newtonian. The viscosity was measured using a Cannon-Fenske viscometer, No. 600599, with a viscosity constant of 21.053 at 40 °C. The Newtonian viscosity of the sample was found to be 7.063 Pas at 25°C. This sample was then tested in the Rheomat 115 using the prescribed shear rate data from the manufacturers literature shown in table 3.1. The apparent viscosity calculated from these values are shown in figure 3.1.2 and it is indeed evident that the viscosity appears to have a small dependence on shear rate. This is clearly false for a Newtonian fluid and therefore the manufacturer's data are false. New values for shear rate at a given bob speed were then calculated and are shown in table 3.1 and in Figure 3.1.3.

The results of the steady state rheological tests are presented in section 4.1.

Table 3.1: Shear Rate Data for Contraves Rheomat 115 Rotational Viscometer

Speed Step	Bob Speed (min^{-1})	Shear Rate (s^{-1}) (Manufacturers Literature)	Shear Rate (s^{-1}) (Calibrated)
1	5.15	6.65	8.01
2	7.37	9.51	11.40
3	10.54	13.61	16.34
4	15.09	19.48	23.21
5	21.6	27.9	33.16
6	30.9	39.9	47.44
7	44.3	57.2	67.78
8	63.4	81.8	96.73
9	90.7	117.1	138.21
10	129.8	167.6	194.52

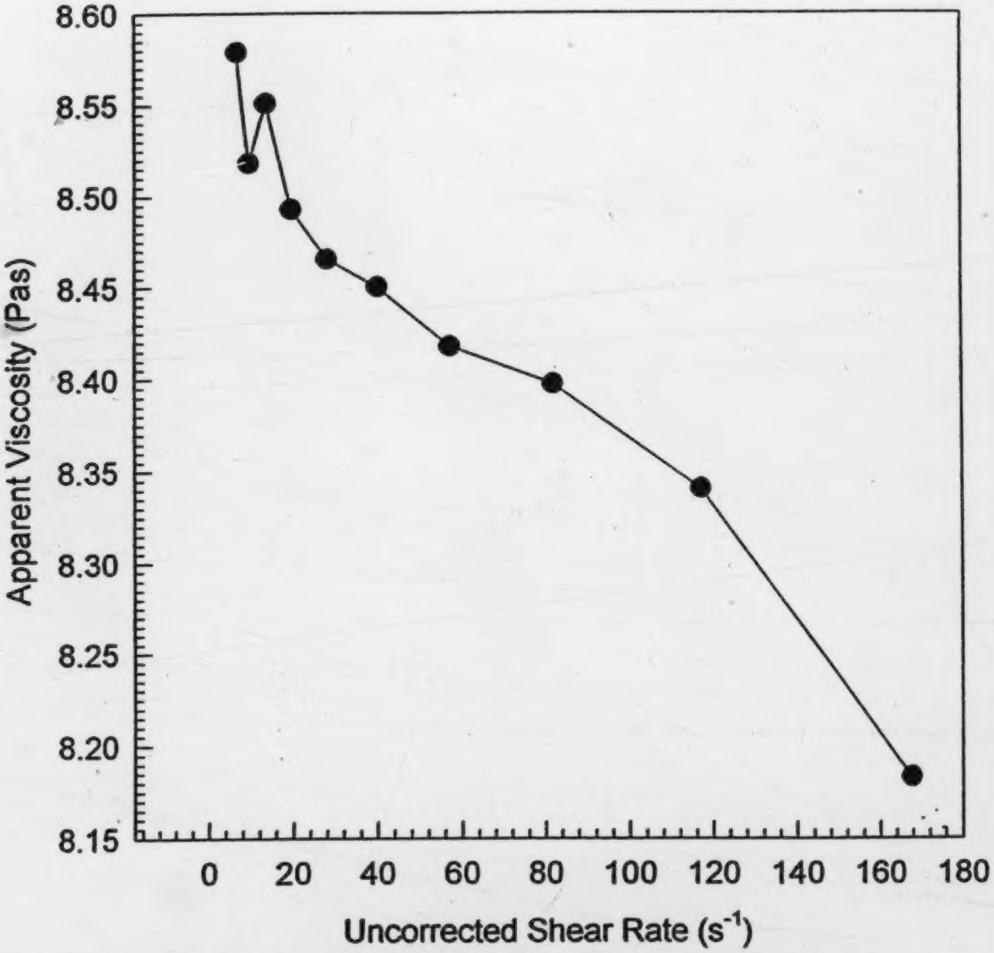

Figure 3.1.2 Measured data for 46.7wt% PEG solution in the Contraves Rheomat 115 viscometer before calibration

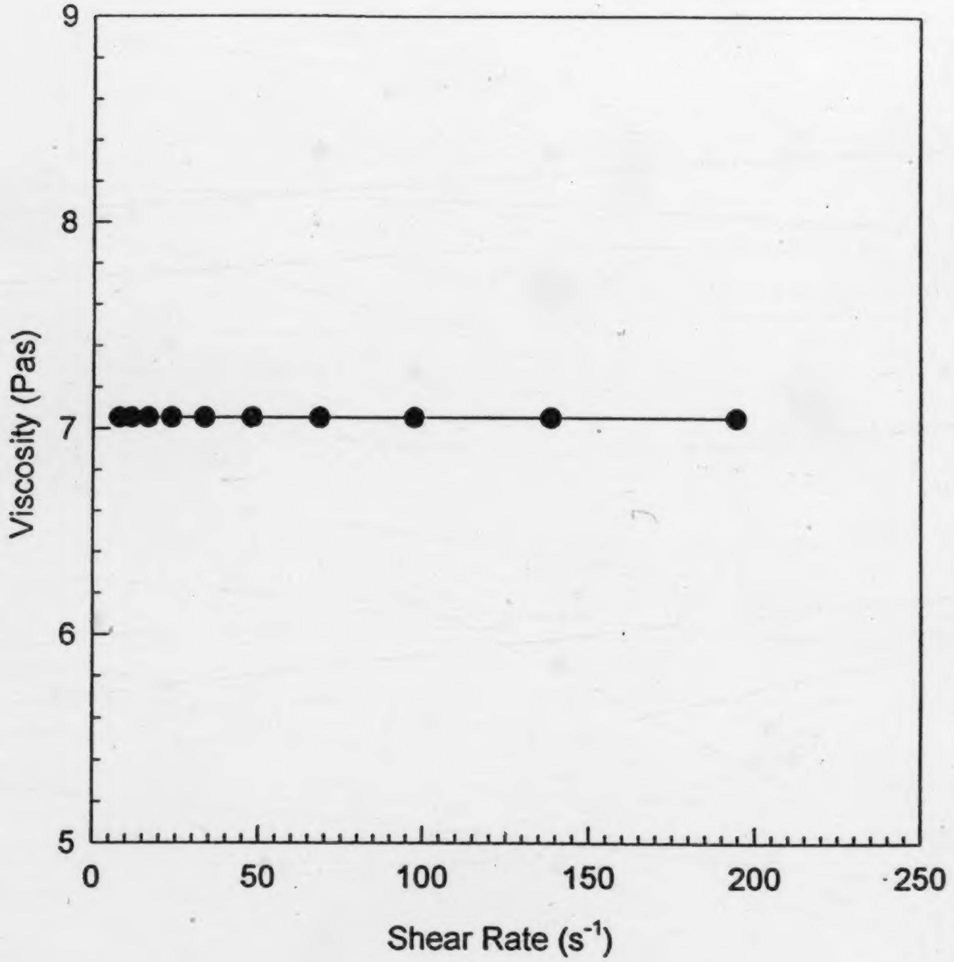

Figure 3.1.3 Measured data for 46.7wt% PEG solution in the Contraves Rheomat 115 viscometer after calibration

3.1.3 Dynamic Rheological Tests

It was established in Section 2.8 that the Carbopol solutions form microgels and that they have a certain degree of inherent microstructure. Hence, when under the influence of shear, the fluid will likely possess viscoelasticity and the microstructure may be damaged at high shear rates as is the case for many polymer solutions. To investigate this further, and to confirm the rheological findings of the steady state tests, Carbopol samples of prescribed pH's were subjected to dynamic rheological testing using a Rheometrics RMS 800 disk and plate rheometer. The testing was performed by Mr. Ibnelwaleed Hussein of the Department of Chemical and Materials Engineering, University of Alberta. A 25mm outer diameter disk and plate configuration was used. A small sample of the test fluid is confined in the gap between the disk and plate. The top disk is caused to rotate sinusoidally at a prescribed shear rate (rad s^{-1}). A data acquisition system records changes of the viscous and elastic moduli with time. For the pH range of samples that were subjected to dynamic testing there is some agreement with the steady state tests. The Carbopol solutions certainly also possess viscoelasticity. Results of these tests and further discussion is provided in section 4.1

3.2 Mixing Trials

3.2.1 Equipment

The mixing vessel and internals used to perform laminar mixing studies is shown in figure 3.2.1. The cylindrical flat bottomed glass vessel used has an inside diameter, D, of 0.208m and a height of 0.288m, providing a 9.8 litre capacity. The working volume was in the range 7.0 to 8.5 litres, ensuring a distance from the liquid surface to the lid of the vessel in the range 21mm to 72mm. The top of the impeller blade essentially scrapes the surface of the fluid when using a working volume of 7.0 litres. It is important to have the top of the impeller covered to a sufficient depth to ensure that the fluid surface remains essentially flat during mixing.

Two helical ribbon impellers were used: a stainless steel single flight helical ribbon impeller, HR-1B, and a double ribbon impeller, DHR-1, also of stainless steel construction. One important difference between the impellers is that for the same direction of rotation, the pumping direction is different between the two. The single ribbon impeller, HR-1B, pumps in an upward direction at the wall when rotating clockwise. The double ribbon impeller, DHR-1, pumps downwards at the wall when rotating in a clockwise direction. The dimensions of the impellers are the same; outside diameter, d, is 0.185m, as is the height, h, and the pitch, s. Both impellers have a ribbon width, w, of 0.03m and both have ribbon to wall clearance, c, of 0.0115m. The clearance between the bottom of the tank and the bottom of the impeller is 0.0104m in both cases also. Dimensionless geometric parameters can be summarised as:

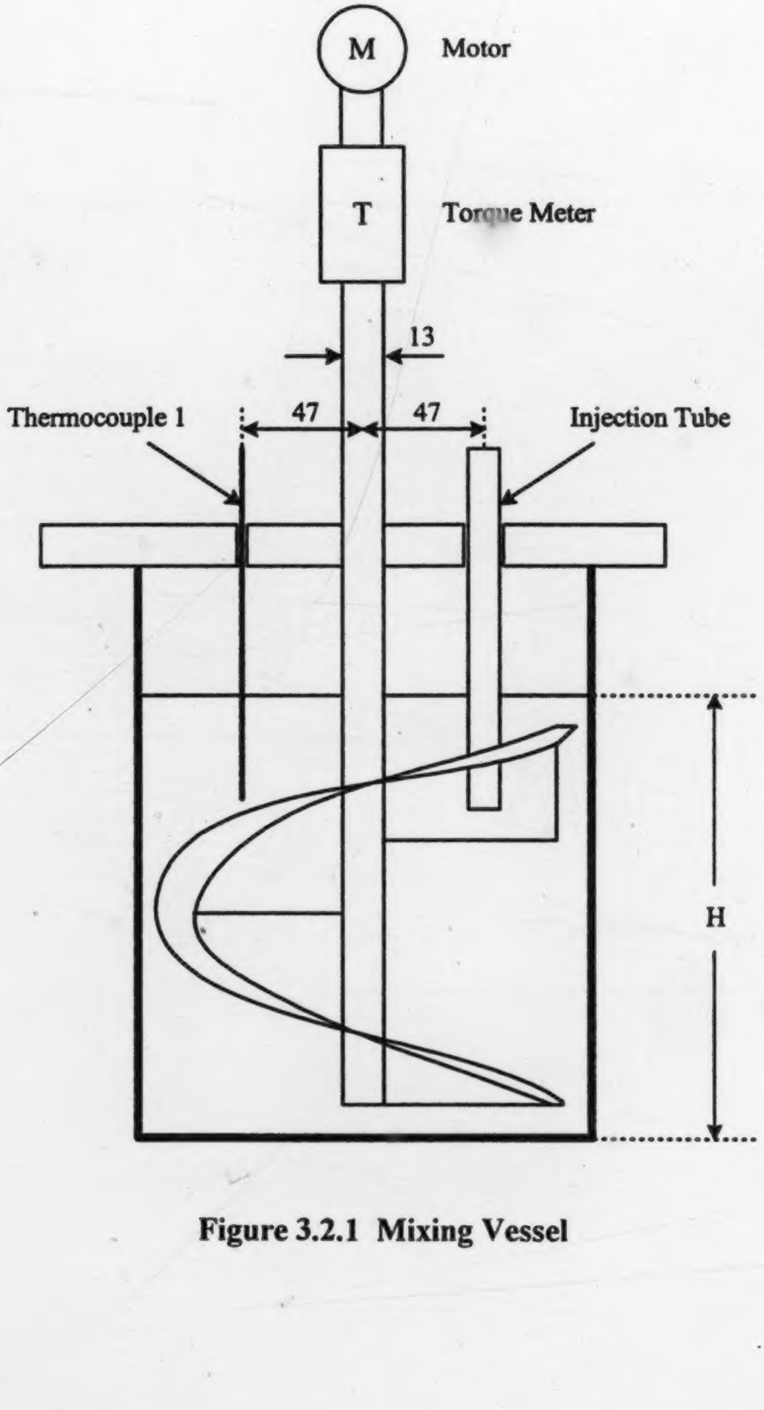
M
Motor
T
Torque Meter
13
Thermocouple 1
47
47
Injection Tube
H

Figure 3.2.1 Mixing Vessel

Tank Diameter / Impeller Diameter	D/d	1.124
Wall Clearance / Impeller Diameter	c/d	0.062
Ribbon Pitch / Impeller Diameter	s/d	1.0
Ribbon Width / Impeller Diameter	w/d	0.162
Impeller Height / Impeller Diameter	h/d	1.0

Table 3.2 Geometric Parameters for the Mixer used in this Study

The ribbons of the impellers are attached by three connecting rods to a central post. Connection between the top of the ribbon and the central post is made by an elbow rod. This allows accommodation of thermocouples in the vessel for mixing studies using the thermal technique. The horizontal portion of the elbow joints is 135mm below the lid of the vessel. The single ribbon impeller, HR-1B is shown in figure 3.2.2 and the double flight impeller, DHR-1 is shown in figure 3.2.3. Additionally, the PMMA coverplate seals tightly to the top of the vessel and is secured in place by four stainless steel posts which can be screwed into the assembly frame. The impeller of choice is bolted into the drive shaft assembly above the coverplate. It is driven by a Flexaline model TMQ1133-2, 0.45hp, 1750 rpm motor coupled to a 20:1 speed reduction box. A torque transmitter (model MCRT 3901X, S. Himmelstein and Co.) is fitted in-line on the drive shaft. The operating range is 0 to 100 lb-in (112.985 Nm). The drive motor could be run both clockwise and counter-clockwise.

Figure 3.2.2 Single Ribbon Impeller, HR1-B

Figure 3.2.3 Double Ribbon Impeller, DHR-1

Torque measurements, as a function of rotational speed are converted to power input by:

$$P = 2\pi NM \tag{3.2.1}$$

where P is the power input (W), N is the impeller rotational speed (rps) and M is the torque imparted on the impeller (Nm), (Nienow et al., 1985). M is determined from:

$$M(Nm) = \pm(readout - 50.00)(2lb_f in)\left(\frac{4.4482 kgm/s^2}{1lb_f}\right)\left(\frac{1m}{39.37in}\right) \tag{3.2.2}$$

The indicated torque when running the impeller with air in the vessel was essentially zero. This indicates that the torque owing to the bearings, couplings, etc. was not significant.

Two J-type thermocouples with stainless steel sheaths are inserted through the coverplate on the vessel at positions T1 and T2 (see figure 3.2.4). Thermocouple T1 was inserted at a depth of 120mm from the top of the coverplate and thermocouple T2 at 90mm from the top of the coverplate. The output from both thermocouples, and the torque transmitter were recorded as a function of time using an Opto 22 I/O system coupled to a an IBM personal computer.

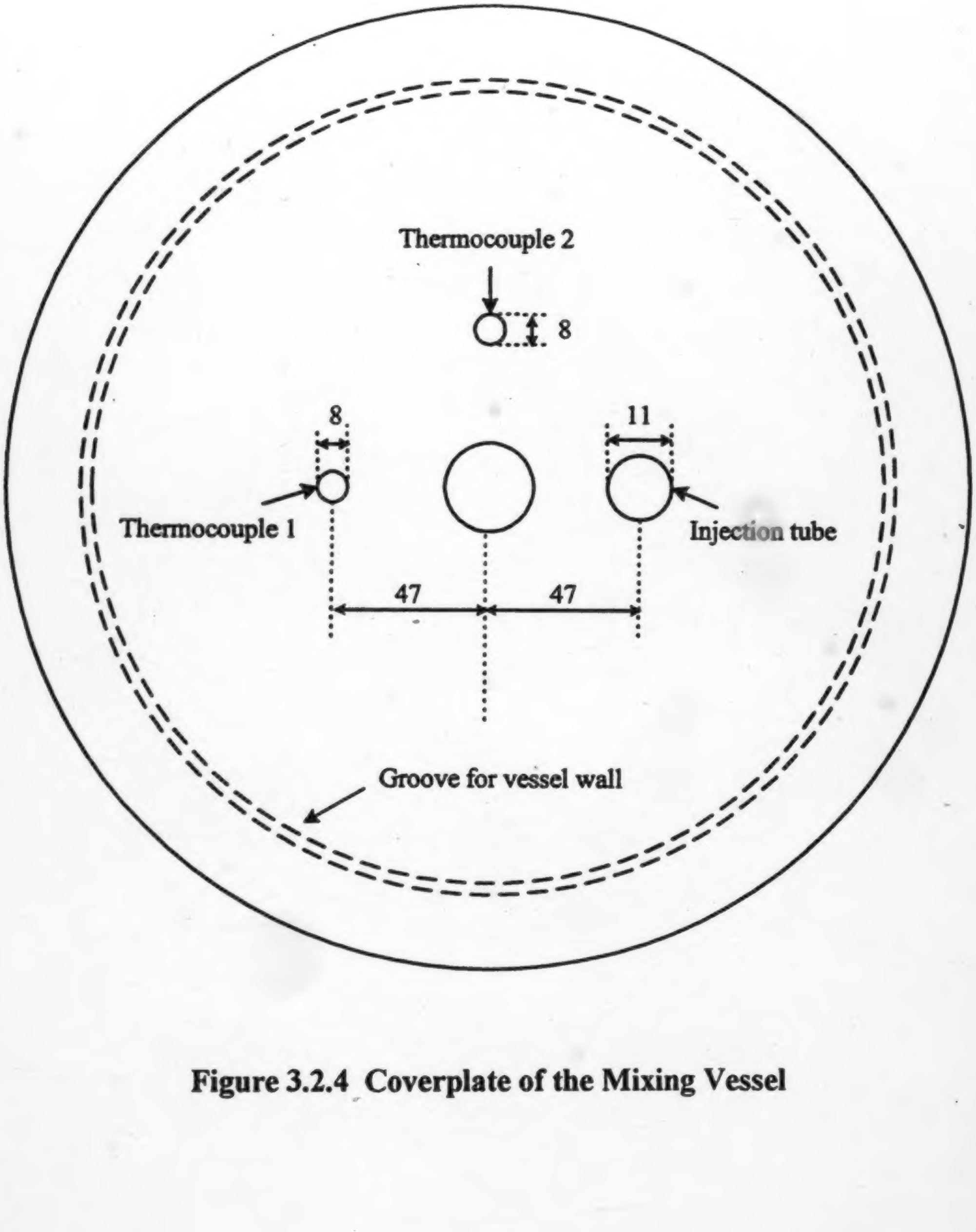
Thermocouple 2
8
8
11
Thermocouple 1
Injection tube
47
47
Groove for vessel wall

Figure 3.2.4 Coverplate of the Mixing Vessel

3.2.2 Mixing by Thermal Method

The underlying principles by which a thermal technique can be applied to assess mixing performance quantitatively were outlined in Section 2.7. These principles are relatively straightforward; an aliquot of hot fluid is injected into the batch mixing vessel containing similar fluid at a lower temperature. Mixing is initiated and the temperature change in the vessel is monitored with time. There are some practical considerations which are required in order that the experimental data are accurate and, most importantly, reproducible in successive runs. These considerations will be discussed here.

The probes which are used to monitor temperature in the vessel must be accurate and have a rapid response time. Thermistors or thermocouples are well suited for this purpose. To see if thermocouples could be used, their response was tested. Sample results of this simple test (figure 3.2.5) show that both the response time and accuracy of the thermocouple probes are sufficient.

The method of injection of the fluid into the vessel is important and to ensure that experimental results were accurate and reproducible the following points had to be adhered to as closely as possible:

- The injection method is simple, safe and relatively quick
- The injection position is the same
- The injection depth is the same
- The temperature and volume of the injected aliquot is the same

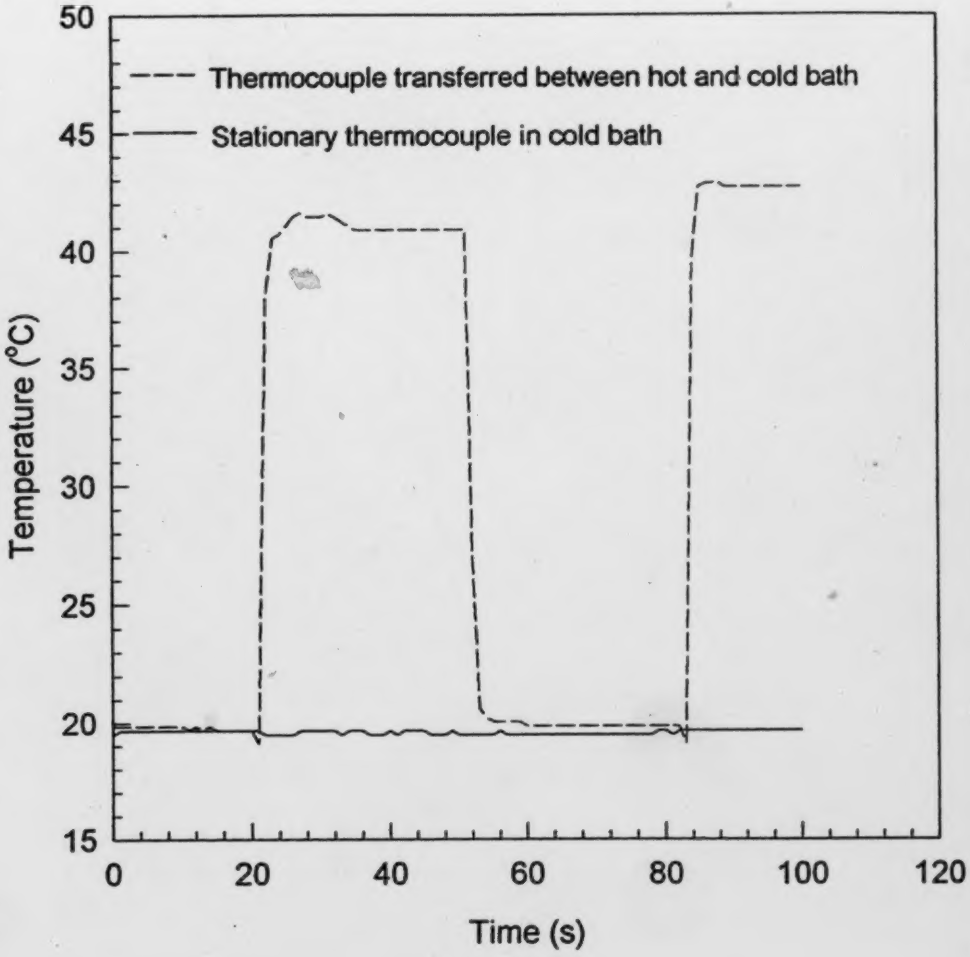

Figure 3.2.5 Response of J-type thermocouples used for thermal mixing trials

A 6mm stainless steel tube was attached to a threaded coupling for the coverplate. A syringe containing a heated aliquot of fluid could be attached at the end of the tube just above the coverplate and swift injection made. The injection depth was investigated to see its effect on the data collected. Optimum results were obtained using a depth of 120mm from the top of the coverplate (figure 3.2.4) The injection pipe was removed after injection. On removal, the DACS and stirrer motor were started simultaneously. In later work, the DACS was initiated and the stirrer started after a lagtime of 50 seconds which would establish the initial temperature in the vessel and aid in evaluating a mixing time. The position of the impeller prior to each injection was identical in all runs.

The temperature and volume of the injected aliquot has to be given careful consideration. The temperature difference between the injected aliquot and the batch fluid has to be sufficiently large so that several temperature peaks can be identified on the resulting temperature-time response curve, or thermogram. However, excessively large temperature differences might well result in significantly changing the rheological properties of the fluid which is undesirable. Experiments were performed initially using a 60 ml. syringe for injections. The bulk fluid temperature was typically around 20°C. A 250ml. Pyrex® beaker was filled with approximately 100ml. of the batch fluid. This solution was heated to around 65°C using a hotplate. The excellent reproducibility of the thermograms suggests that the injection technique was consistent. In later studies, larger volume injections were carried out using a larger illustrated in figure 3.2.6.

Mixing studies using the thermal technique have been applied to bulk fluids of two different levels of viscosity; lower viscosity fluid of pH 2.79 and high viscosity fluid of pH

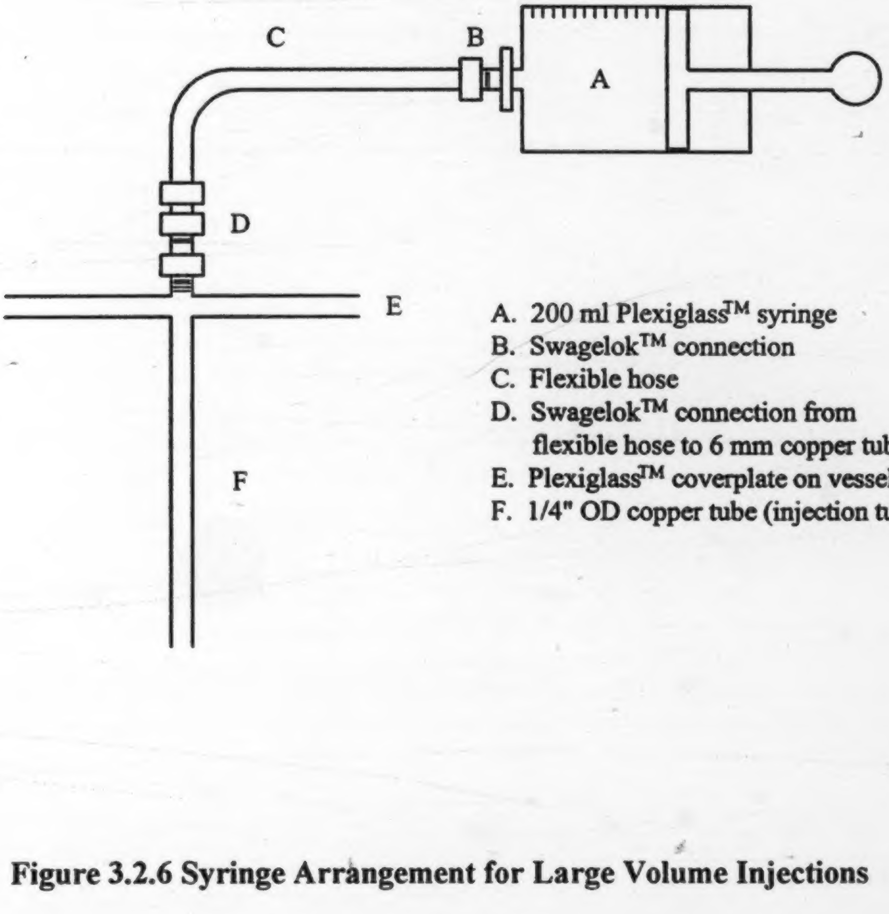

A. 200 ml Plexiglass^{TM} syringe
B. Swagelok^{TM} connection
C. Flexible hose
D. Swagelok^{TM} connection from flexible hose to 6 mm copper tube
E. Plexiglass^{TM} coverplate on vessel
F. 1/4" OD copper tube (injection tube)

Figure 3.2.6 Syringe Arrangement for Large Volume Injections

11.5. No problem was encountered in injecting aliquots of low viscosity fluid. However, fluid of pH 11.5 has a viscosity which is too high to be injected by hand using a syringe. In this case, the injected aliquot has a lower viscosity than the bulk, with a pH of around 3.4. Results of studies using the thermal technique are presented and discussed in section 4.2.

4. Results and Discussion

In Section 2, a review of the literature in the field of laminar mixing with helical ribbon impellers was presented and the more important correlations with which to assess mixing were described. In this section, these correlations are combined with the experimental findings reported in Section 3 to predict power consumption, flow regime and both mixing and circulation times for aqueous Carbopol solutions and for polyethylene glycol solutions.

In Section 4.1 the rheological characterisation of the non-Newtonian Carbopol solutions is addressed. In Section 4.2, the suitability of the various power-flow correlations is investigated for both Carbopol and polyethylene glycol solutions. In Section 4.3, experimental results are presented for mixing trials using the thermal method. An analysis of the results is made together with a comparison of results obtained by other workers. Section 4.3 reports the results of flow visualisation experiments. Comparisons are made between this technique and the thermal method.

4.1 Rheological Characterisation

Steady state rheological tests performed in a Contraves Rheomat 115 viscometer are described in Section 3.1. For each fluid sample that was tested in the viscometer, a shear stress-shear rate curve was generated. Three such curves are shown in Figure 4.1.1 for 1.48wt% Carbopol solutions at pH's 2.79, 4.51 and 11.36. The full set of experimental data for shear stress-shear rate measurements is provided in Appendix B1. It is evident from Figure 4.1.1 that in each case, the fluid has a yield stress and is shear thinning. Fischer et al., (1961) have previously found this behaviour with Carbopol solutions. Furthermore, these solutions have been traditionally described by a Herschel-Bulkley rheological equation, as given by equations (2.2.8) and (2.2.9). The stress-shear rate data reported in Appendix B1 were converted to apparent viscosity variation with shear rate. For each pH, the apparent viscosity was calculated over a range of shear rates. In Figure 4.1.2, the change in apparent viscosity of the fluid with pH at 6 different shear rates is presented. It is clear that apparent viscosity rises sharply between around pH 3.0 and pH 4.0, and again falls sharply at around pH 12.0. Between pH 4.0 and 12.0, the viscosity is relatively steady with some fluctuation around pH 7.0. The viscosity trend over this pH range is similar to that observed by Ravissot, (1989) and Moes, (1991), however they did not report these fluctuations. There is some evidence to suggest that the unsteady rheology may be due to an inherently defective microstructure (see Section 2.6). Certainly confirmation and perhaps explanation of the physico-chemical behaviour of the gels in this range of pH is an area requiring further investigation.

The rheological data of prime importance in this investigation are the parameters τ_y, K and n in equation (2.2.9) for yield stress, consistency and power law index, respectively. A least squares, multiple non-linear regression was performed on the rheology data of Appendix B1 to fit equation (2.2.9). The regression data are presented in Appendix B3. The optimum values for τ_y, K and n as a function of pH are shown in Figures 4.1.3, 4.1.4 and 4.1.5 respectively. The trend of yield stress in Figure 4.1.3 is similar to that found in Figure 4.1.2 for apparent viscosity. A similar, but less pronounced trend is suggested in

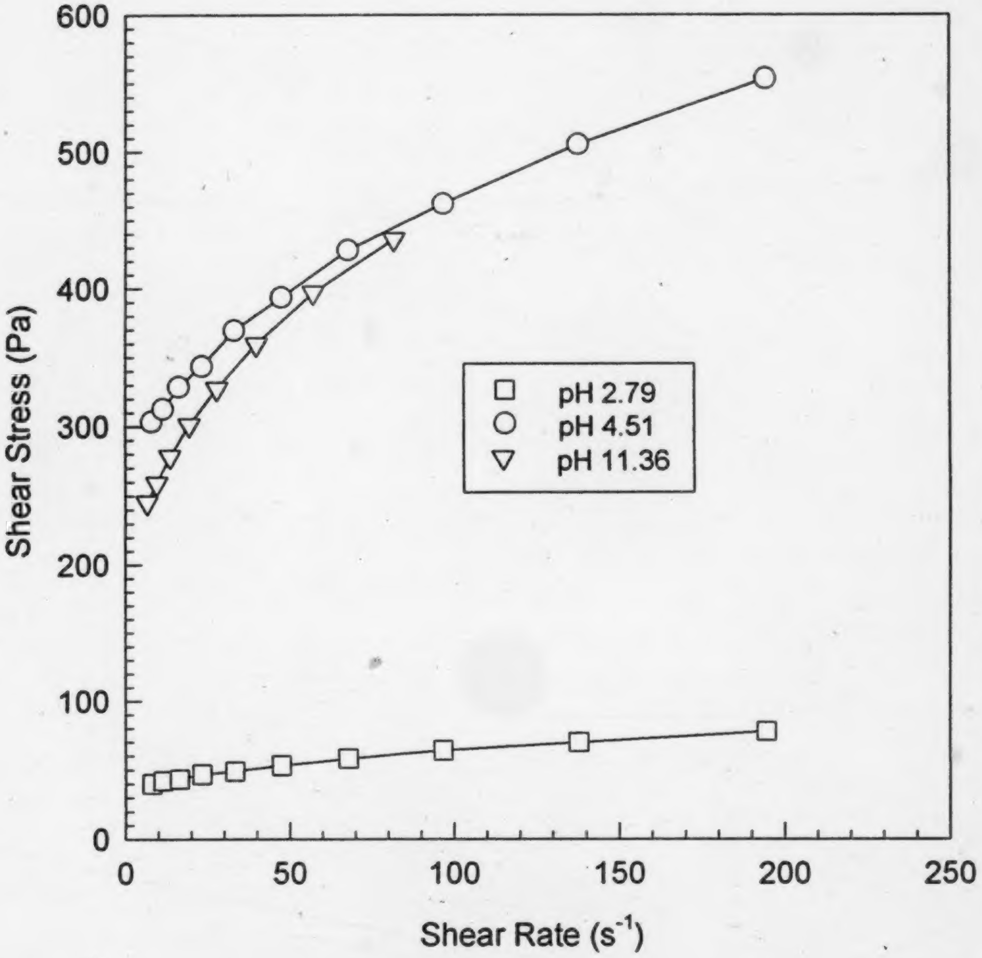

Figure 4.1.1 Shear stress-shear rate data from steady state tests on 1.48wt% Carbopol solutions of given pH

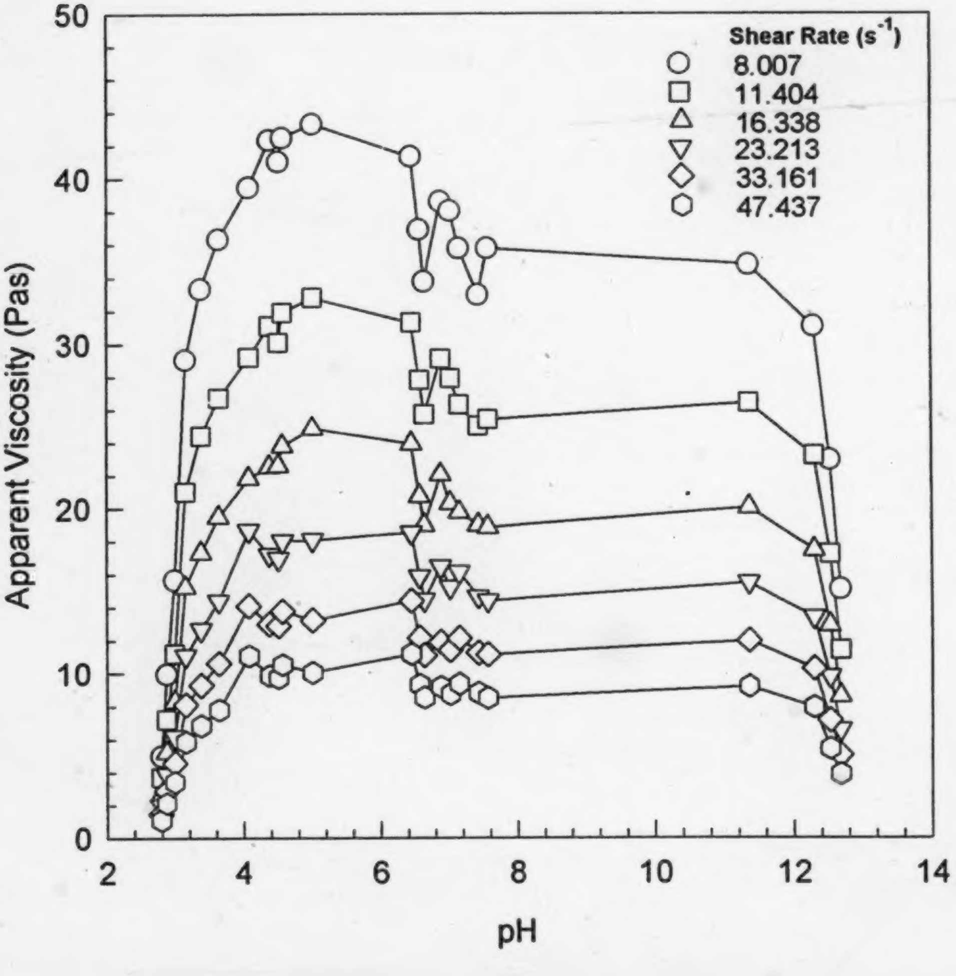

Figure 4.1.2 Variation of apparent viscosity with pH at the given sample shear rates, as measured in a Contraves Rheomat 115 rotational viscometer, using 1.48wt% Carbopol solutions and 23wt% aqueous NaOH

Figure 4.1.4 for K. Figure 4.1.5 appears to be very random with no observable trend, however, the value of n only fluctuates between around 0.44 and 0.62 over the whole pH range. Therefore, it is reasonable to assume a constant value for n over the pH range. This constant could be taken to be 0.52.

Dynamic viscometric tests have been carried out on a few samples spanning a range of pH roughly between 3.5 and 11. These are briefly described in Section 3.1.3. The purpose of these tests was to confirm the fluctuations in apparent viscosity which were observed in the pH range of 6 to 8 for steady state rheological tests in the Carbopol solutions. Steady state rheological measurements and dynamic rheological measurements can be related by the semi-empirical Cox-Merz rule (Cox and Merz, 1958). The rule states that steady state viscosity and dynamic viscosity should be the same if the steady shear rate is the same as the dynamic shear rate. These results can be compared using Figure 4.1.2 for steady state measurements and Figure 4.1.6 for dynamic measurements. In Figure 4.1.2, at a shear rate of 11.4 s^{-1} the apparent viscosity is approximately 25 Pas for steady state measurements. In Figure 4.1.6 at a dynamic shear rate of $10s^{-1}$, the dynamic viscosity is only around 4 Pas. It is concluded that the Cox-Merz rule does not apply for Carbopol solutions. This is in agreement with Ketz et al., (1988). Dynamic visometric testing does show a similar fluctuation in viscosity between pH 6 and 8 and so this behaviour that has been observed in steady state testing is believed to be a real phenomena for Carbopol solutions in this pH range.

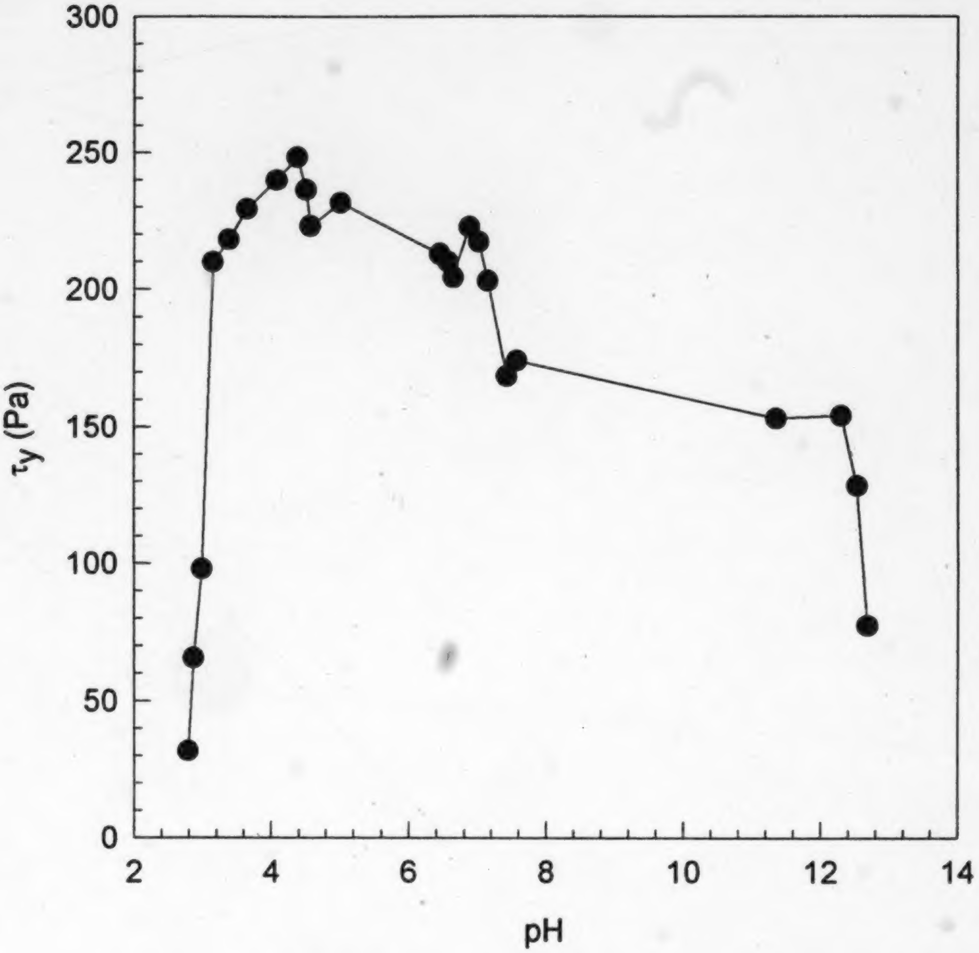

Figure 4.1.3 Variation of the rheological parameter, τ_y, with pH in the Herschel-Bulkley equation, (2.2.9), for 1.48wt% Carbopol

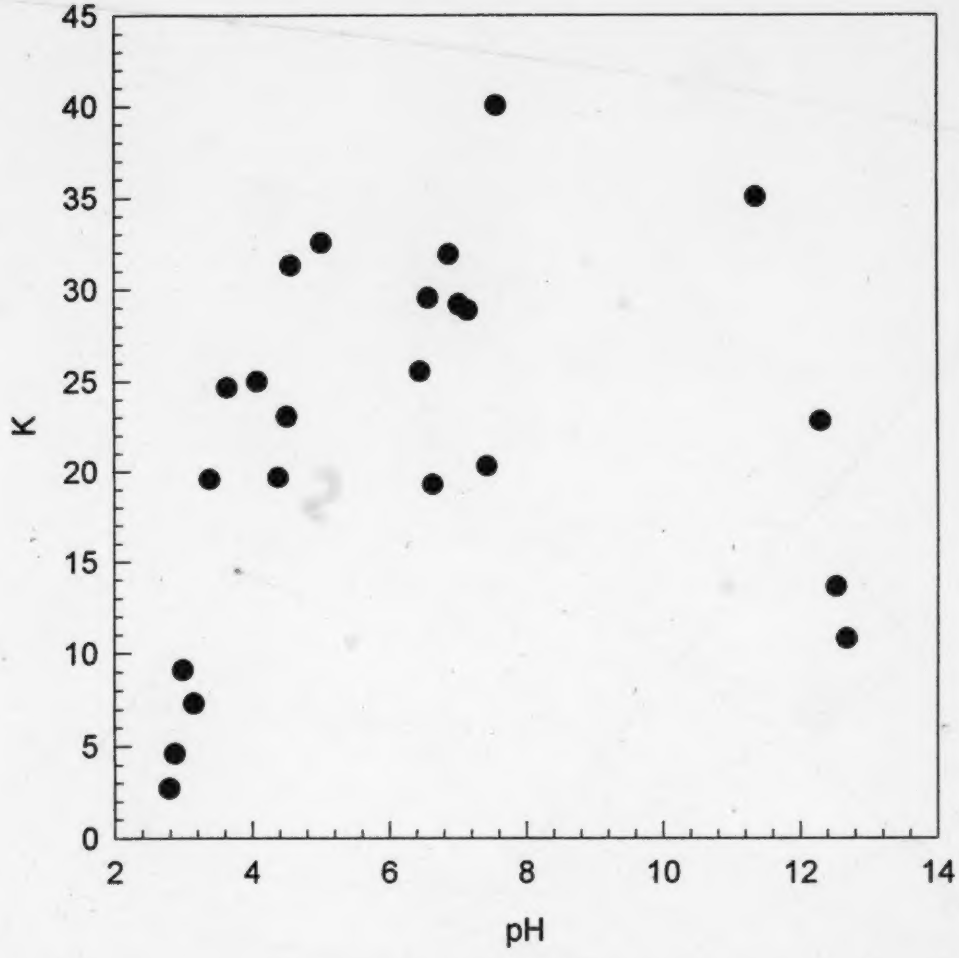

Figure 4.1.4 Variation of the rheological parameter, K, with pH in the Herschel-Bulkley equation, (2.2.9), for 1.48wt% Carbopol

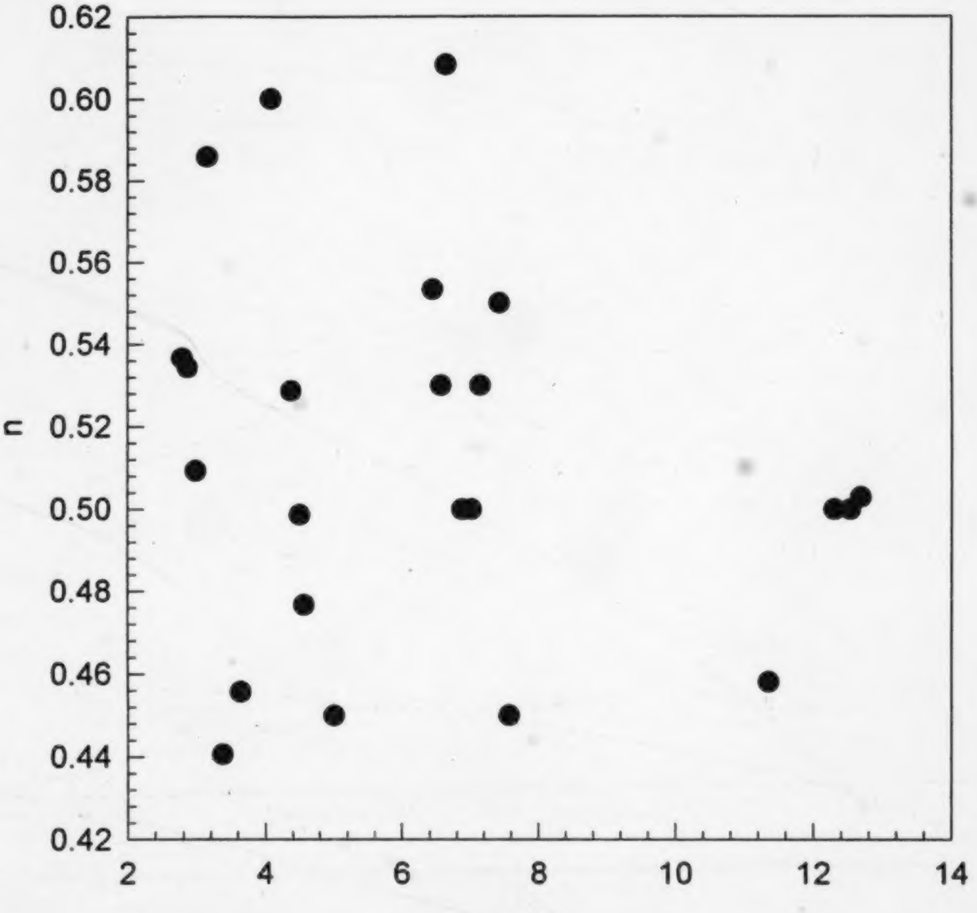

Figure 4.1.5 Variation of the rheological parameter, n, with pH in the Herschel-Bulkley equation, (2.2.9), for 1.48wt% Carbopol

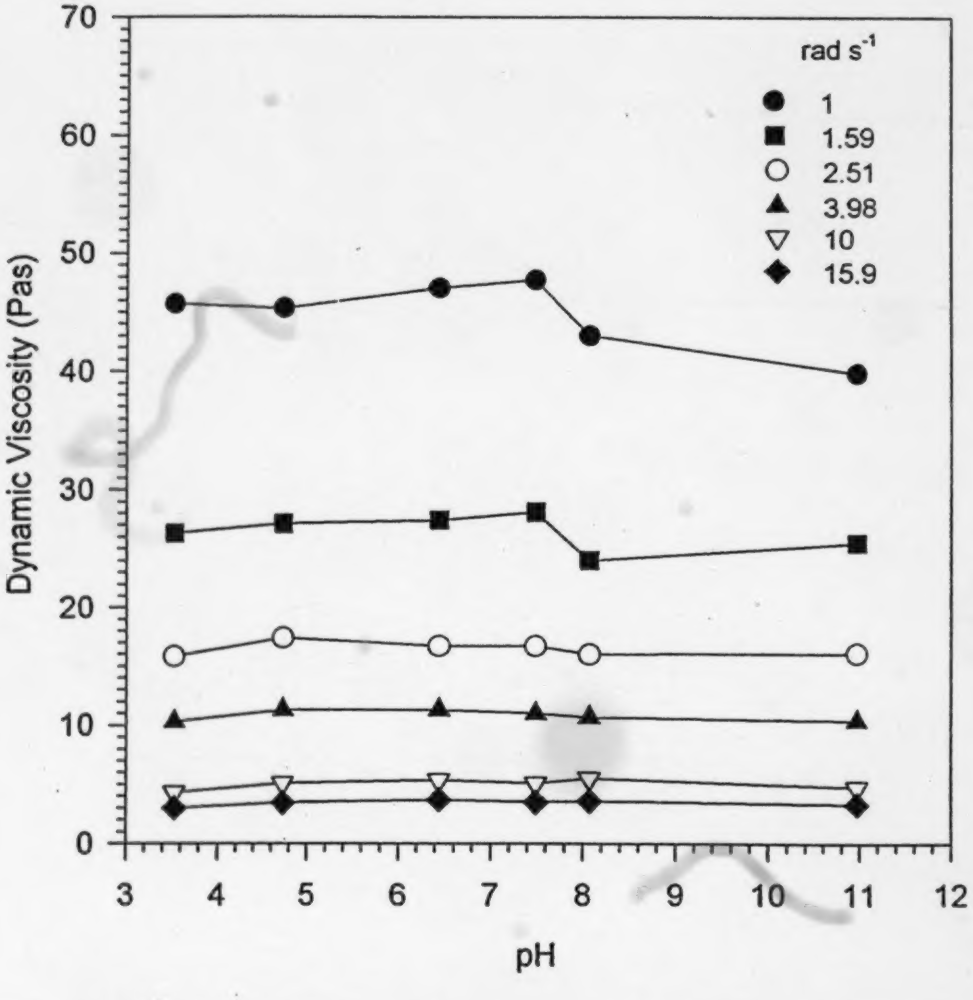

Figure 4.1.6 Dynamic viscosity variation with pH for 1.48wt% Carbopol solutions

4.2 Power Consumption Analysis

4.2.1 Newtonian Polyethylene Glycol Solutions

To provide a reference point, some measurements were made using a Newtonian fluid. The solution used was 45wt% polyethylene glycol. The viscosity of this solution was 6.68 Pas. The torque was measured when mixing these solutions with impellers HR1-B and DHR-1 in both upward and downward pumping modes. These results are given in Appendix C1 and shown in Figure 4.2.1.1. An interesting observation from these results is that there is some small difference in the measured torque for both HR1-B and DHR-1 impellers when the direction of pumping is reversed. For impeller HR1-B, the measured torque on the impeller is slightly higher in upward pumping mode than downward pumping mode in Figure 4.2.1.1. However, for impeller DHR-1, the reverse is true, where the measured torque is higher in downward pumping mode. In any event, these differences in torque with direction of pumping are small enough to have a negligible effect on the power curves that have been developed.

In Section 2.2, the generalised power-flow relationship for Newtonian fluids was given (equation (2.2.5)). The Reynolds number is given by equation (2.2.7) with the Newtonian viscosity, μ replacing the apparent viscosity η_a. In that section, a number of correlations were presented as modified forms of equation (2.2.5) for Newtonian fluids. A comparison of Power number prediction from these correlations with measured Power number is given in Figure 4.2.1.2 for the impeller HR1-B and in Figure 4.2.1.3 for the impeller DHR-1. For all power-flow correlations taken from the literature, there is

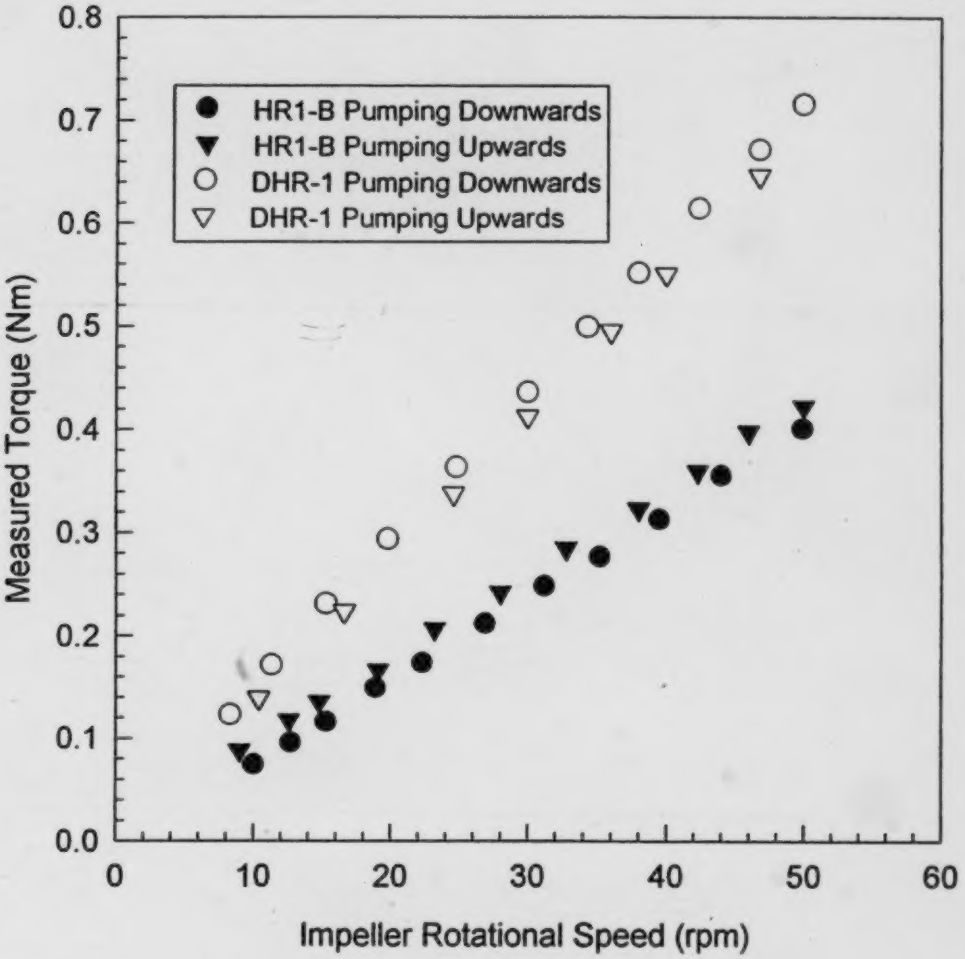

Figure 4.2.1.1 Torque measurements for HR1-B and DHR-1 in 45wt% Polyethylene Glycol solution

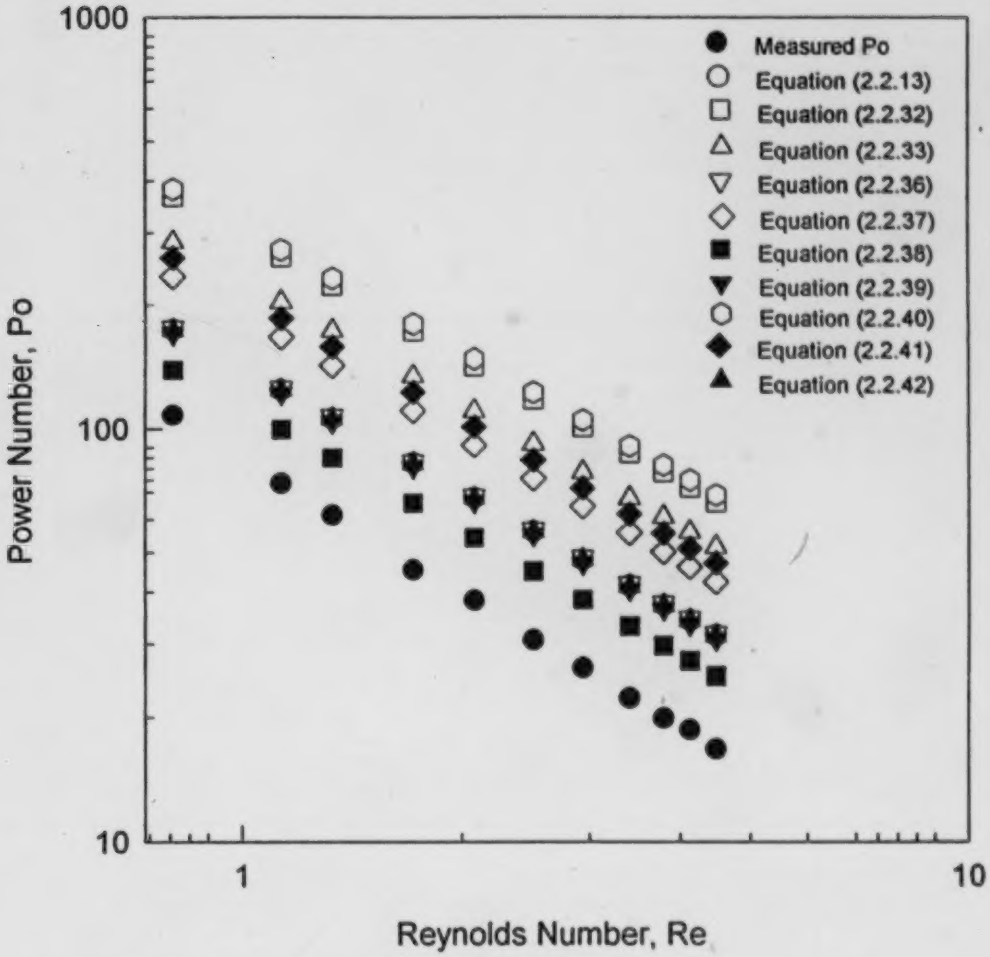

Figure 4.2.1.2 Comparison of measured Power Number and that calculated by the correlations given for 45wt% Polyethylene Glycol solution using HR1-B impeller pumping upwards

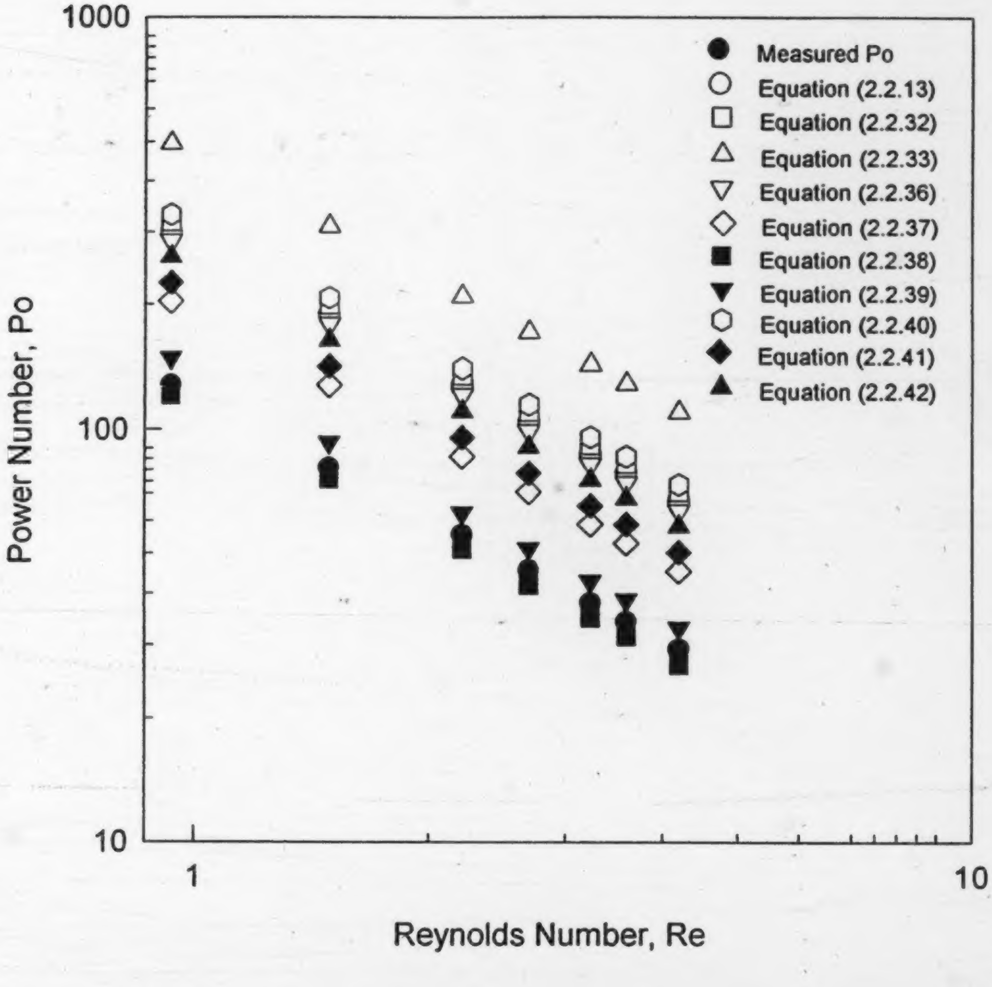

Figure 4.2.1.3 Comparison of measured Power Number and that calculated by the correlations given for 45wt% Polyethylene Glycol solution using DHR-1 impeller pumping upwards

considerable overprediction of Power number for the impeller HR1-B. Equation (2.2.40) from Novak and Rieger, (1975) uses equation (2.2.5) directly. Kp is taken as 296 in equation (2.2.5) following equation (2.2.32), and gives the poorest prediction of power number for HR1-B which is understandable since the correlation is proposed to be better suited for double ribbon impellers, however, prediction is still poor in this case. Kp is generally considered to be a constant in equation (2.2.5) and is dependent on geometry. All of the other correlations essentially predict Kp as a function of the geometry of the mixing system. Some of the geometries used for these various correlations have been presented in Table 2.2.1 and further information regarding other correlations can be found in Käppel, (1979).

It is important to note that the geometry used in this study differs from those used in almost all these correlations in at least one way. D/d in this work is 1.124 and w/D is 0.162. For nine of the correlations the range of w/D and D/d for which the correlation applies falls below that for the geometry of this study. Only the work of Blasinski and Rzyski, (1980) uses a comparable geometric arrangement, although their correlation does not give a good Power number prediction either. The correlation of Schlüter (cited by Käppel, (1979)) most closely approximates the measured Power number from this work. From these findings, it can be concluded that D/d and w/d are important quantities for power-flow prediction. It is suggested from measured values in this study that increased D/d and w/d lead to reduced Po, and hence lower power requirement for a given Re. From the measured Po, Kp is calculated as 83.74 for 45wt% polyethylene glycol solution for the HR1-B impeller using equation (2.2.5). Low end values for Kp have been suggested to be around 100. The correlation of Schlüter again most closely approximates Po for the DHR-1 impeller. In this case, Kp is calculated to be 119.44. The same geometric restrictions apply for the correlations that have been used for DHR-1.

4.2.2 Non-Newtonian Carbopol Solutions

Aqueous solutions containing 1.48wt% Carbopol were investigated in the mixing vessel at pH 2.79 and 11.5. Torque measurements have been made for these solutions with impellers HR1-B and DHR-1 in upward and downward pumping modes and are shown in Figure 4.2.2.1. These results are given in Appendices D1 and D2. Similar results are obtained as was found with the polyethylene glycol solutions; there is a small difference in torque for both the impellers when the pumping direction is reversed, and again it is found that a higher torque is obtained for HR1-B pumping upwards and DHR-1 pumping downwards. In the analysis of the power-flow relationship, only upwards pumping will be presented.

4.2.2.1 The Shear Rate Constant, k_s

In Section 2.2.2.1, a number of correlations were described which made the calculation of k_s in equation (2.2.6) possible. k_s is the parameter which relates rotational speed of the impeller with shear rate in the vessel and has been discussed in Section 2.2.2.1. The correlations used to calculate k_s have been summarised in Table 2.2.2. Each one of these correlations predicts k_s to be a constant, for a given geometry of the mixing system. The value of k_s calculated using these correlations, and the results are given in

Table 4.2.2.1. The correlation of Brito, (1992) provides no meaningful value for k_s since $D/d_e < 1.0$ in equation (2.2.68). Also, it can be seen that the correlation of Kai and Shengyao, (1989) gives values of k_s which are two orders of magnitude less than those reported by other authors. These two correlations were not considered further. The other correlations were used in equation (2.2.6) to calculate shear rates in the mixing vessel.

The calculated shear rates were substituted into the Herschel-Bulkley equation, (2.2.10), to calculate the apparent viscosity of the fluid at given impeller rotational speeds. These results are shown in Figures 4.2.2.3 through 4.2.2.5 for HR1-B and DHR-1 impellers in upward pumping mode using pH 2.79 and pH 11.5 solutions. Calculated values of k_s are used in equation (2.2.6) to calculate shear rate in the mixing vessel at given impeller rotational speeds. Using calculated shear rate values in equation (2.2.9), the apparent viscosity of the fluid at the given impeller rotational speeds can be determined, and from equation (2.2.7) Reynolds numbers in the vessel can be established.

There is no way to measure Reynolds number in the vessel, and hence no physical measurement against which any of the correlations for k_s can be compared. The only available data are that of rheological characterisation in the Couette viscometer. By assuming helical ribbon flow to be the same as Couette flow, some comparison of shear rate can be made. Using Table 3.1 at the given rotational speeds, shear rate on the fluid is known. An apparent viscosity of the fluids at pH 2.79 and 11.5 can now be estimated using Figure 4.1.2 for shear rates corresponding to those of Table 3.1. In other words, for a given rotational speed of the bob of the Couette viscometer , a prediction of the apparent viscosity for any pH can be made using Figure 4.1.2. these findings can be compared to the calculated results shown in Figures 4.2.2.2 through 4.2.2.5 to see which correlation best estimates the measured apparent viscosity of Couette flow. This approach is imprecise and only provides a very general guide as to the best correlation to use in the calculation of k_s, and unfortunately, this is the only method available to do this. Using this approach, the correlation of Kuriyama et al., (1983) given by equation (2.2.55) seems to best approximate the apparent viscosity for fluids of pH 11.5. The close proximity of points in Figure 4.1.2 make it difficult to make a judgement for fluids of pH 2.79. It is suggested that equations (2.2.56) and (2.2.70) might better approximate the apparent viscosity at pH 2.79 than equation (2.2.55) does. From this study, the correlation for k_s given by Shamlou and Edwards, (1985), equation (2.2.54), might give the best representation for calculation of shear rate in the vessel over the full range of pH.

In Figure 4.2.2.5, the effect of calculation of k_s is shown using measured values of Po and values of Re based on the calculated values of k_s, for HR1-B impeller in pH 11.5 solution. It is seen that the correlations of Brito et al.,(1997) and Shamlou and Edwards, (1985) give very comparable values for Re. From rheological measurements, it has been proposed that the correlation of Shamlou and Edwards provides good prediction of k_s. The work of Brito et al., (1997) is based on nine rheologically complex fluids and incorporates the rheological parameter n in the correlation as well as mixer geometry, and therefore might be better suited as a generalised correlation for non-Newtonian k_s prediction.

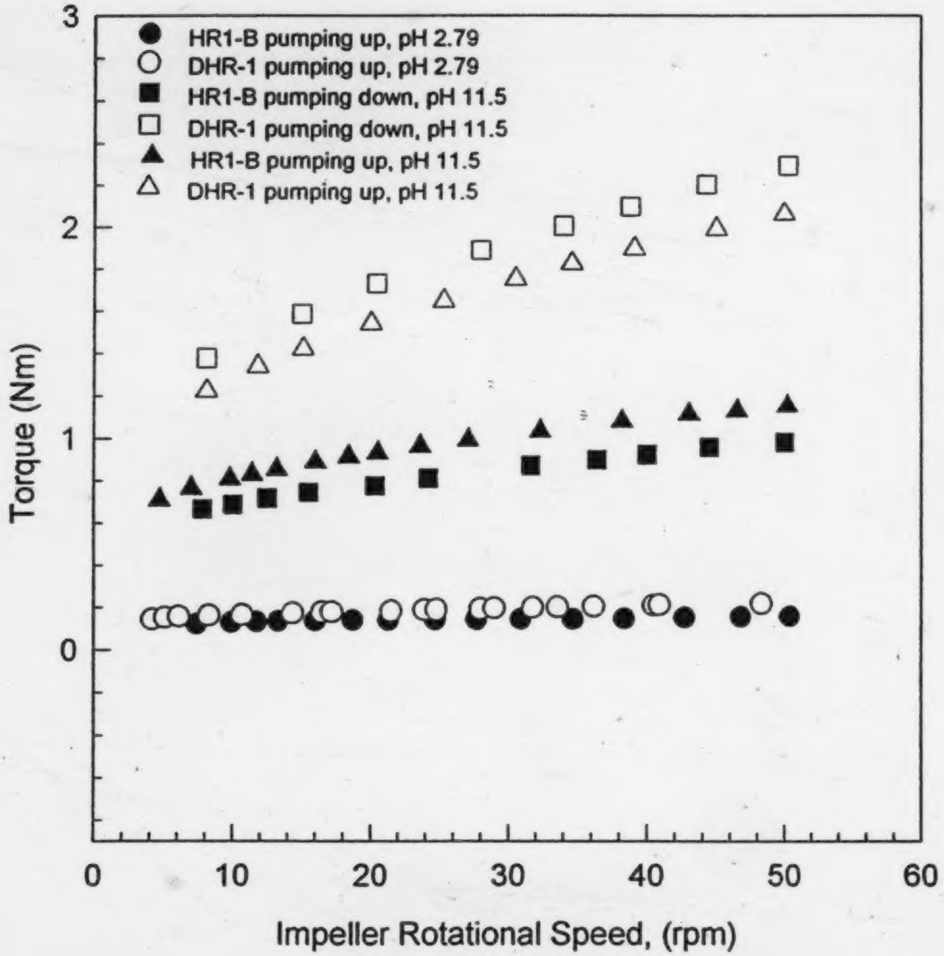

Figure 4.2.2.1 Torque measurements for HR1-B and DHR-1 in 1.48wt% Carbopol Solution at the Given pH

Table 4.2.2.1 **Calculated k_s Values from Correlations for present study at pH 2.79 and 11.5**

Correlation	Equation	Calculated k_s (pH 2.79)	Calculated k_s (pH 11.5)
Misuishi & Miyairi, (1973)	(2.2.54)	35.73	35.73
Kuriyama et al., (1983)	(2.2.55)	53.65	53.65
Takahashi et al., (1984)	(2.2.56)	28.45	28.45
Shamlou & Edwards, (1985)	(2.2.58)	25.07	25.07
Brito, (1992)	(2.2.68)	------	-----
Kai & Shengyao, (1989)	(2.2.69)	0.18	0.14
Brito, (1997)	(2.2.70)	27.31	25.81

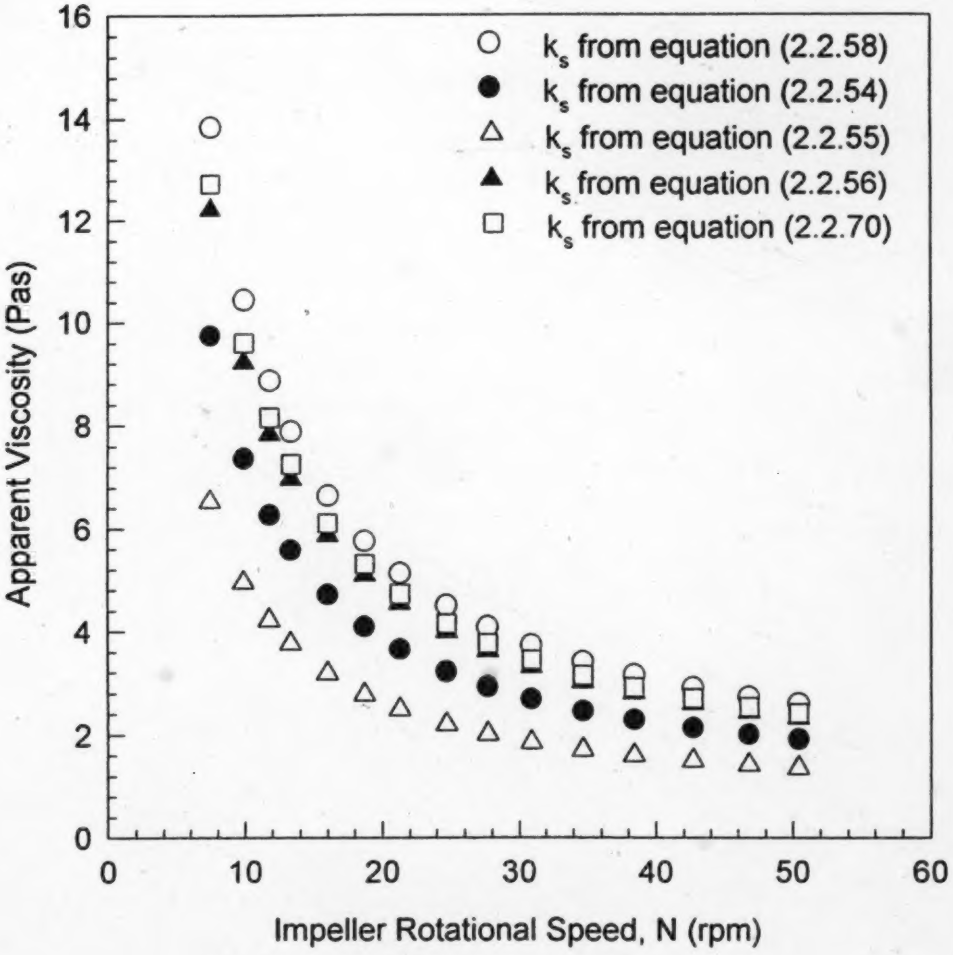

Figure 4.2.2.2 Comparison of apparent viscosity with impeller rotational speed using different correlations to predict k_s for HR1-B impeller pumping upwards in 1.48wt% Carbopol at pH 2.79

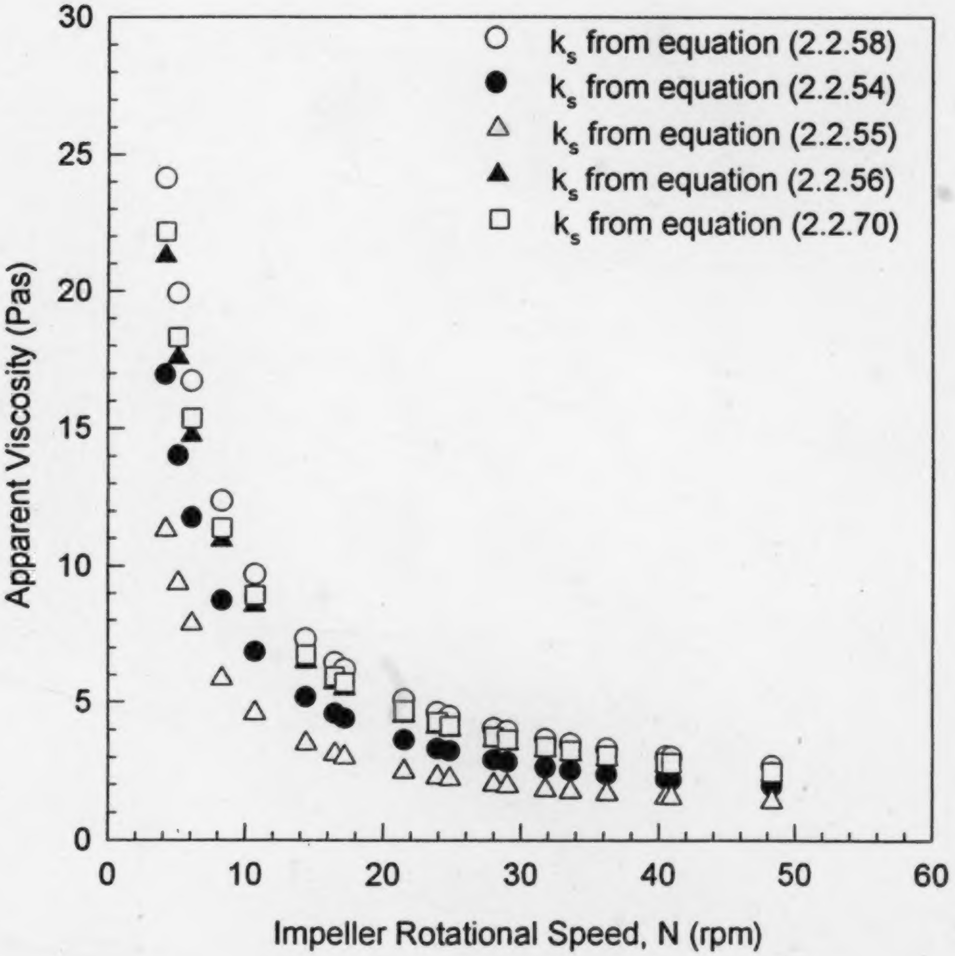

Figure 4.2.2.3 Comparison of apparent viscosity with impeller rotational speed using different correlations to predict k_s for DHR-1 impeller pumping upwards in 1.48wt% Carbopol at pH 2.79

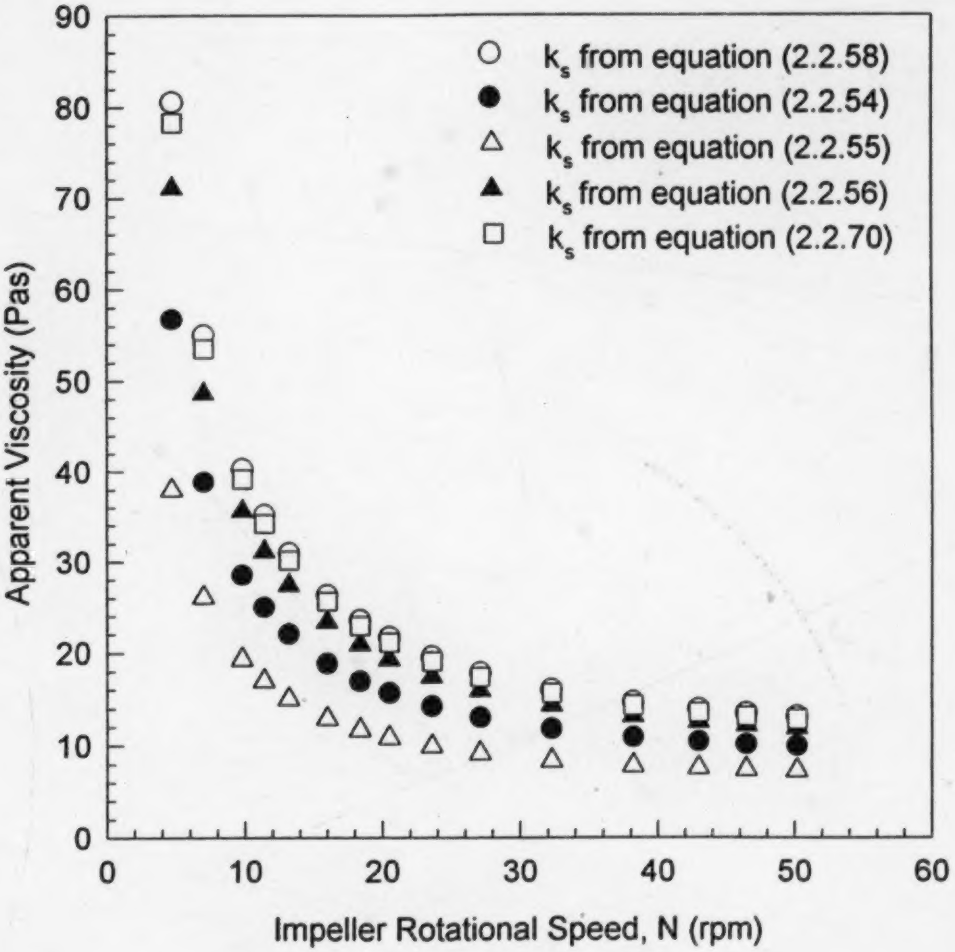

Figure 4.2.2.4 Comparison of apparent viscosity with impeller rotational speed using different correlations to predict k_s for HR1-B impeller pumping upwards in 1.48wt% Carbopol at pH 11.5

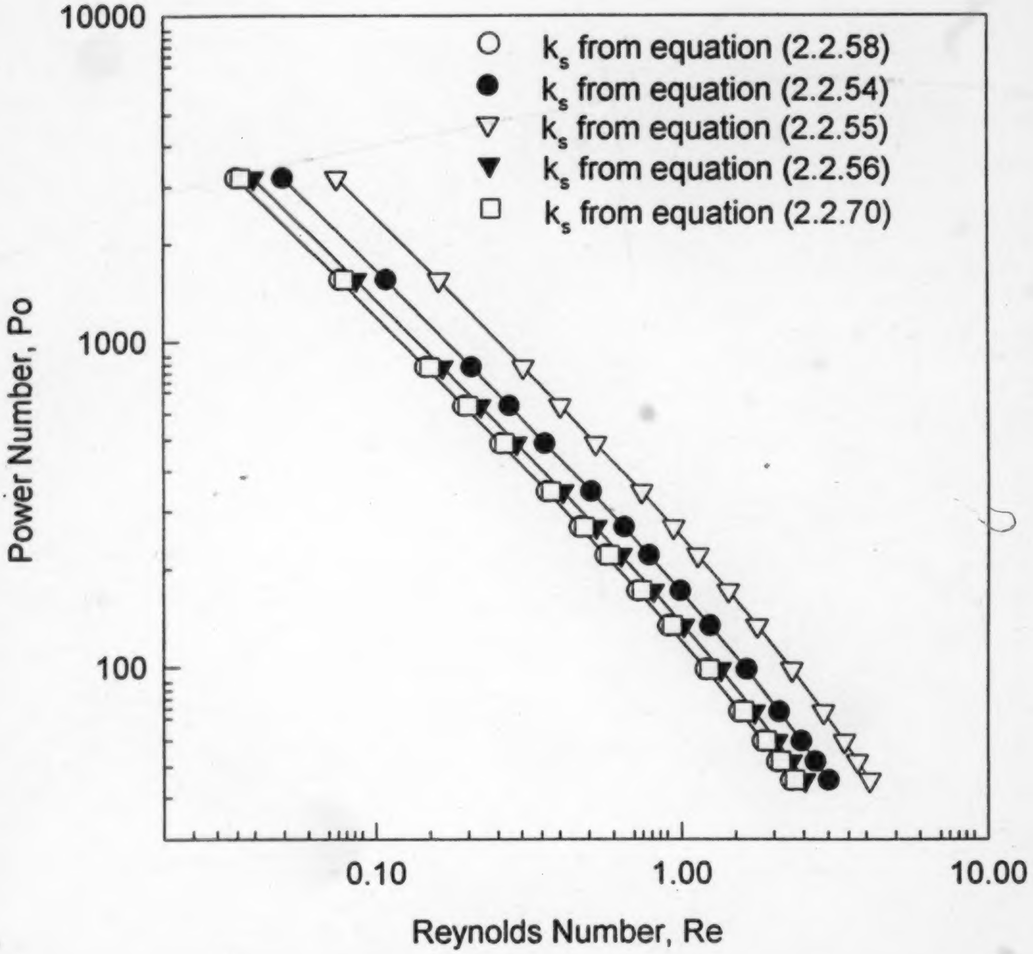

Figure 4.2.2.5 Power curve comparisons using measured Po and predicted Re from various correlations for HR1-B impeller pumping upwards in 1.48wt% Carbopol at pH 2.79

The previous correlations use a constant value for k_s over all rotational speeds in the vessel. These workers based their analyses on Newtonian and shear thinning fluids, and not on yield stress fluids.

Recent work by Rauline, (1998) using Herschel-Bulkley fluids, has suggested a dependence of k_s on impeller rotational speed when mixing these fluids. The analysis was described in Section 2.2.1. A power curve is shown in Figure 4.2.2.6 using measured values of Power number from this study and a Herschel-Bulkley Reynolds number calculated using equation (2.2.26). In Figure 4.2.2.7, the variation of k_s with impeller rotational speed is shown and using equation (2.2.28). A corresponding set of Kp data can be calculated. These are shown in Figure 4.2.2.8. The results presented in Figures 4.2.2.7 and 4.2.2.8 have been calculated as follows: the torque at zero rotational speed is determined from extrapolations of the lines in Figure 4.2.2.1. From a rheological characterisation, τ_y, K and n are known for all pH and the ratio of Kp/k_s can be directly calculated from equation (2.2.28) and the Herschel-Bulkley Reynolds number, Re_{hb}, from equation (2.2.26). For all rotational speeds of the impeller, the Herschel Bulkley number, HB, can be calculated from equation (2.2.25). All of these calculated values can be used in equation (2.2.27) together with measured values of Power number, Po. Rearrangement of equation (2.2.27) gives the variation of k_s with rotational speed, as shown in Figure 4.2.2.7. The ratio of Kp/k_s is known and so the variation of Kp with rotational speed is readily calculated and is shown in Figure 4.2.2.8.

The values of k_s proposed by Hall and Godfrey, (1970) and Shamlou and Edwards, (1985) were 27 and 11.5 respectively (see Section 2.2). In Figure 4.2.2.7, which essentially addresses most of the mixing scenarios of this study, it can be seen that beyond an impeller rotational speed of around 18 rpm, the value of k_s approaches a constant which falls roughly into a range between 10 and 30. The large number of correlations for k_s that are available, coupled with the large number of power-flow relationships that have been reported give rise to many possible combinations to produce a power curve. A number of such combinations have been investigated to see which might produce the closest match of predicted Po and measured Po values. The best match is shown in Figure 4.2.2.9. Interestingly, this is based on a Reynolds number using k_s calculated from the correlation of Shamlou and Edwards, (1985) and the power-flow relationship proposed by Hall and Godfrey, (1970). In conclusion it can be said that for the fluids investigated in this study, the correlation pairing shown in Figure 4.2.2.9 seems to work well, but for Herschel-Bulkley fluids in particular, the analysis of Rauline, (1998) seems to describe more accurately shear rate behaviour and power consumption in the vessel, particularly for very low impeller rotational speeds, always assuming that the Metzner and Otto approach of equation (2.2.6) is valid.

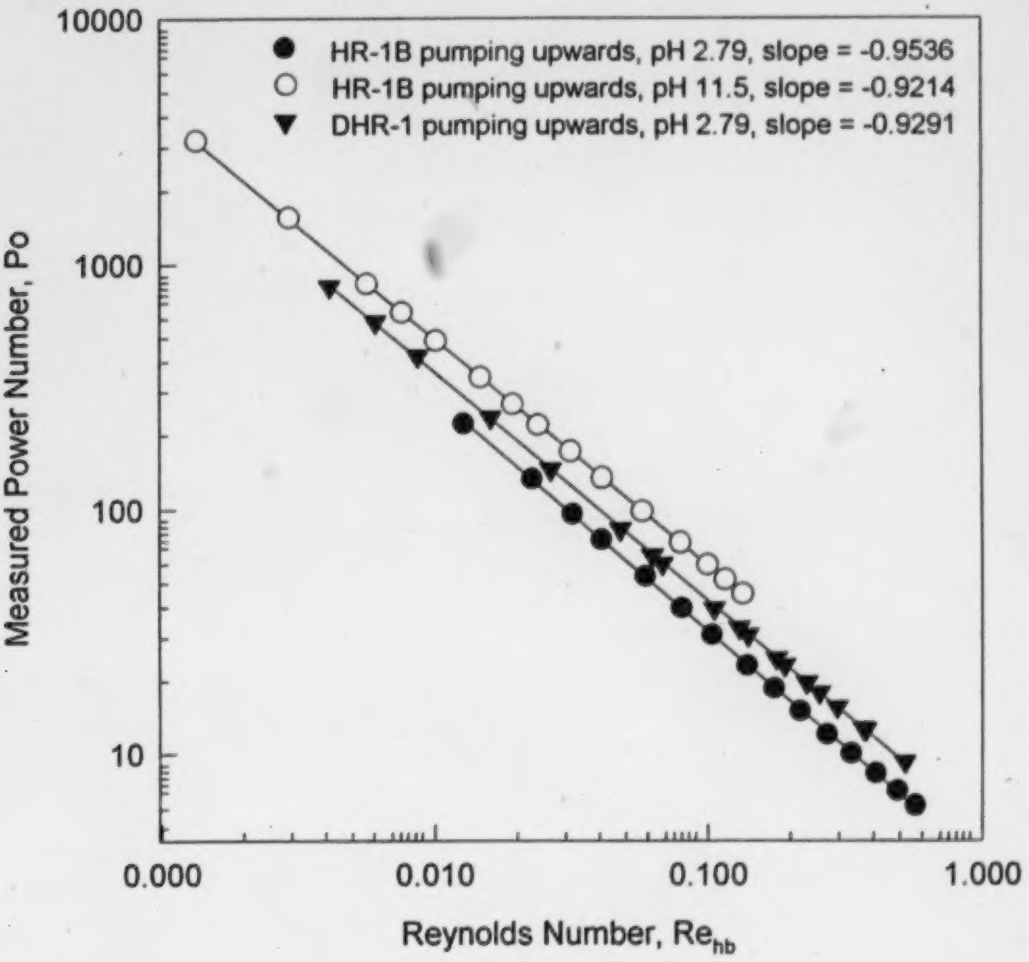

Figure 4.2.2.6 Power curves for three mixing situations based on the Herschel-Bulkley analysis of Rauline, (1998)

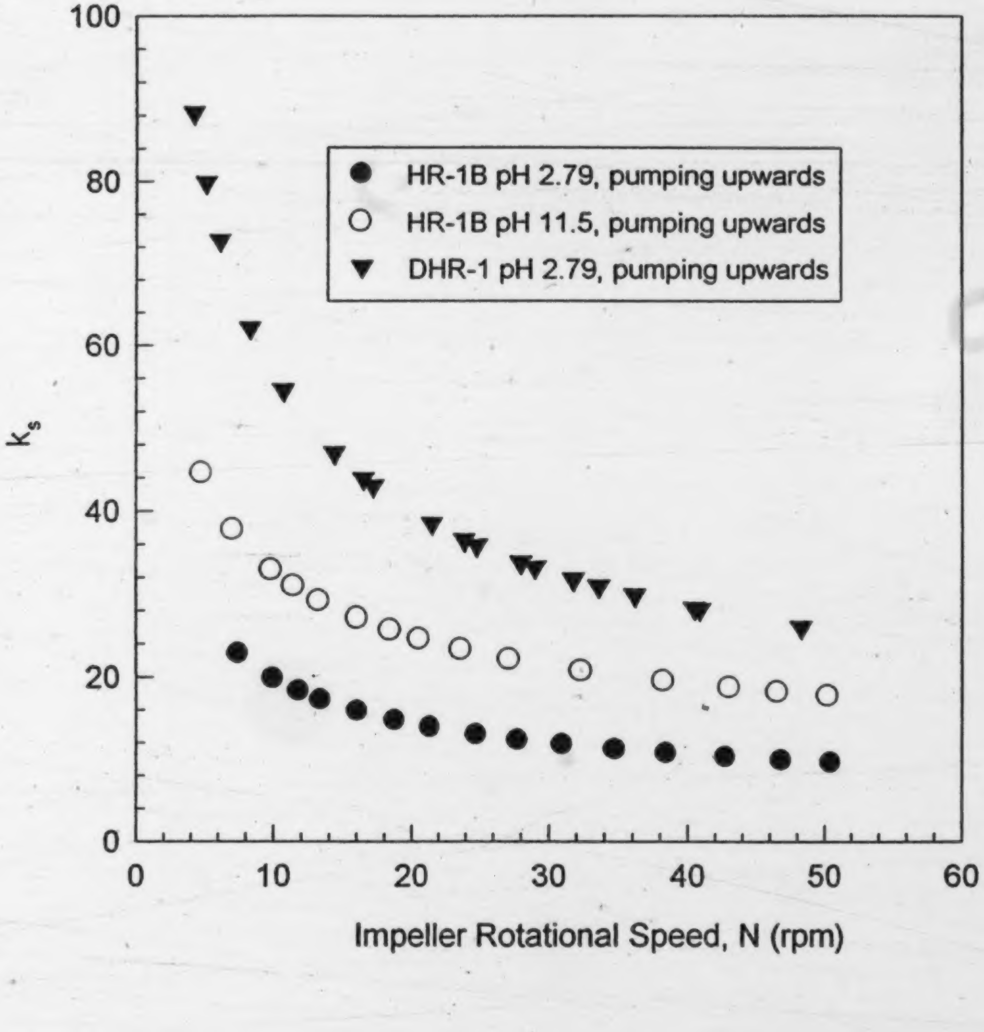

Figure 4.2.2.7 Variation of k_s with N for Herschel-Bulkley fluids from the analysis of Rauline, (1998)

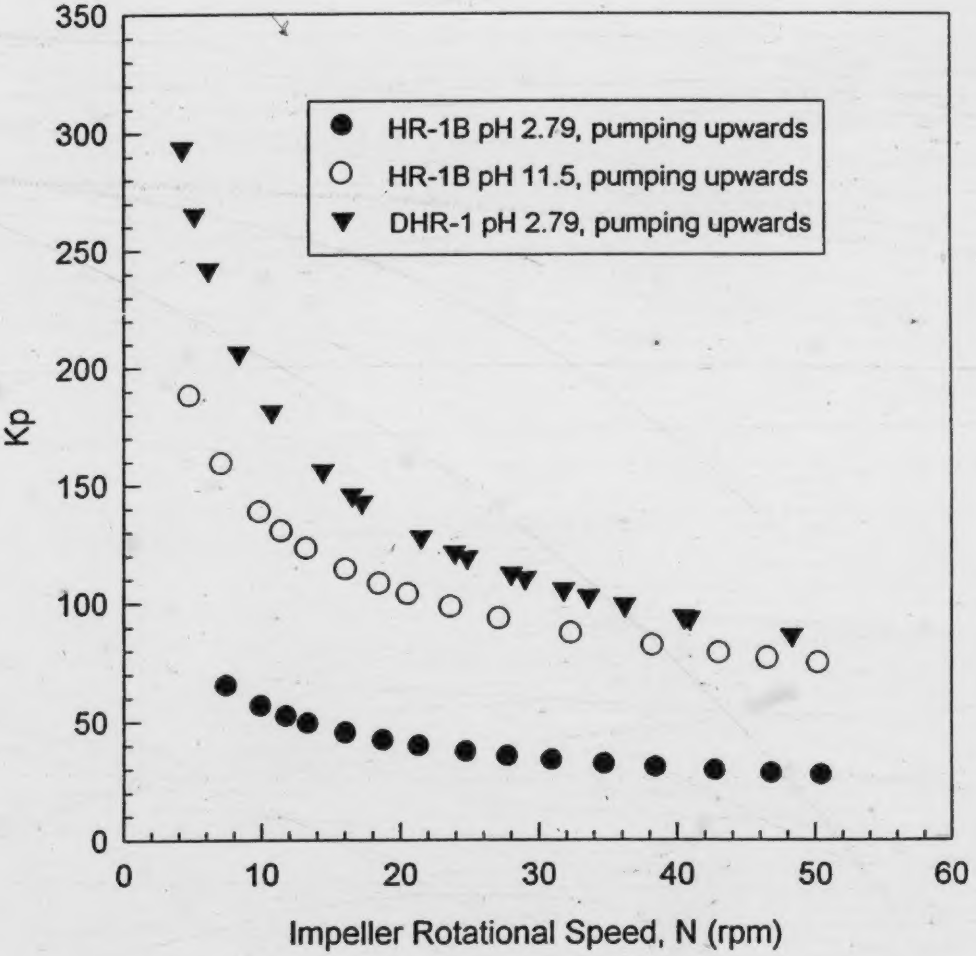

Figure 4.2.2.8 Variation of Kp with N for Herschel-Bulkley fluids from the analysis of Rauline, (1998)

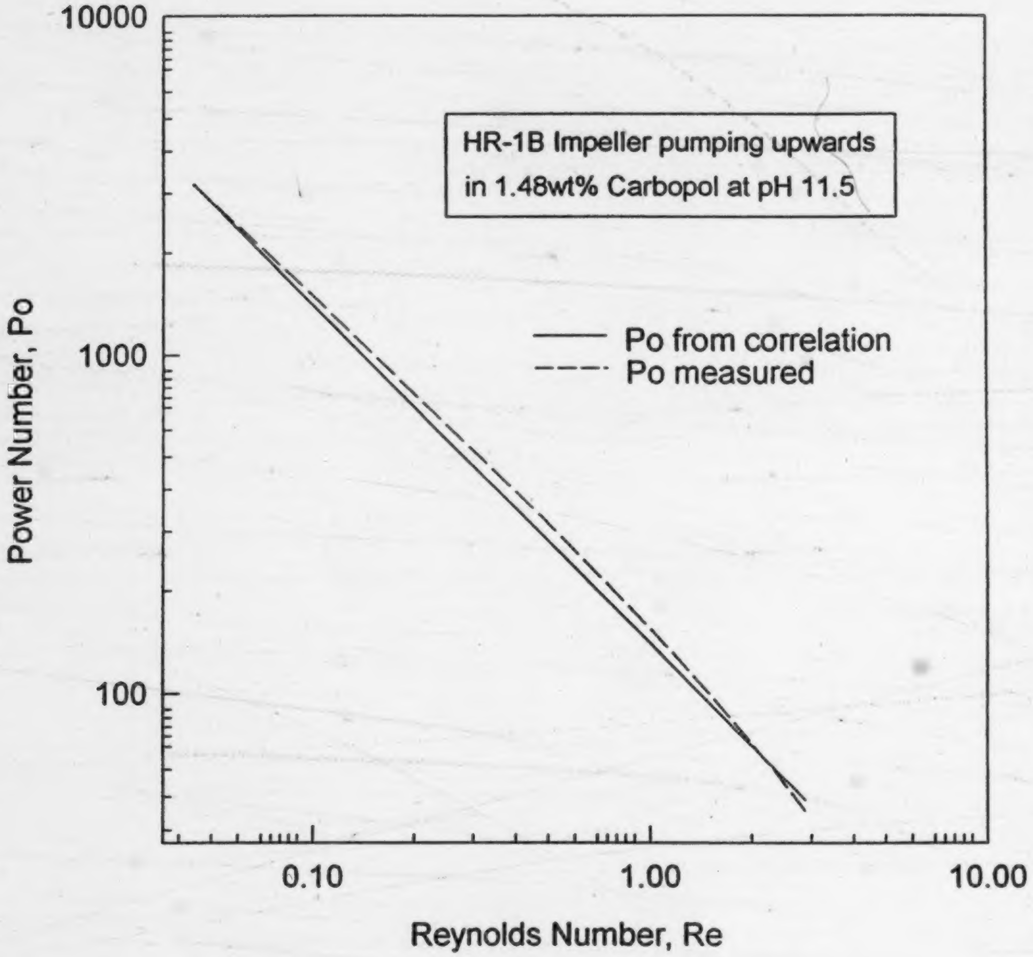

Figure 4.2.2.9 Power-flow correlation of Hall & Godfrey, (1970) and Re calculated using ks from equation (2.2.58)

4.3 Mixing Studies

4.3.1 Thermal Technique

Mixing studies have been performed using the thermal technique. Two thermocouples inserted into the fluid in the vessel monitor temperature changes as mixing proceeds. Sample results of thermograms that have been obtained from experiments are shown in Appendix E.

4.3.1.1 Circulation Time

The thermal technique used to study mixing performance has been described in Sections 2.3 and 3. The correlations related to circulation time calculations in the mixing vessel have been presented in section 2.5. The circulation time, t_c, is taken to be the periodicity of the thermograms that result from experiments using the thermal technique. Measurement of t_c from a thermogram is illustrated in Figure 4.3.1.1.1.

Mixing trials using the thermal technique have been carried out with two impeller types, HR1-B and DHR-1, at three impeller speeds and with Carbopol solutions at two viscosities; a high viscosity fluid (pH 11.5) and a low viscosity fluid (pH 2.79). Ten thermograms have been generated for each one of the mixing situations described above. Average values of circulation time, t_c, have been calculated from these thermograms and are shown in Table 4.3.1.1.1. The thermograms produced from experimental data are very reproducible and the error associated with average t_c values is less than 5%. The dimensionless circulation time, k_c, is defined as the number of revolutions of the impeller

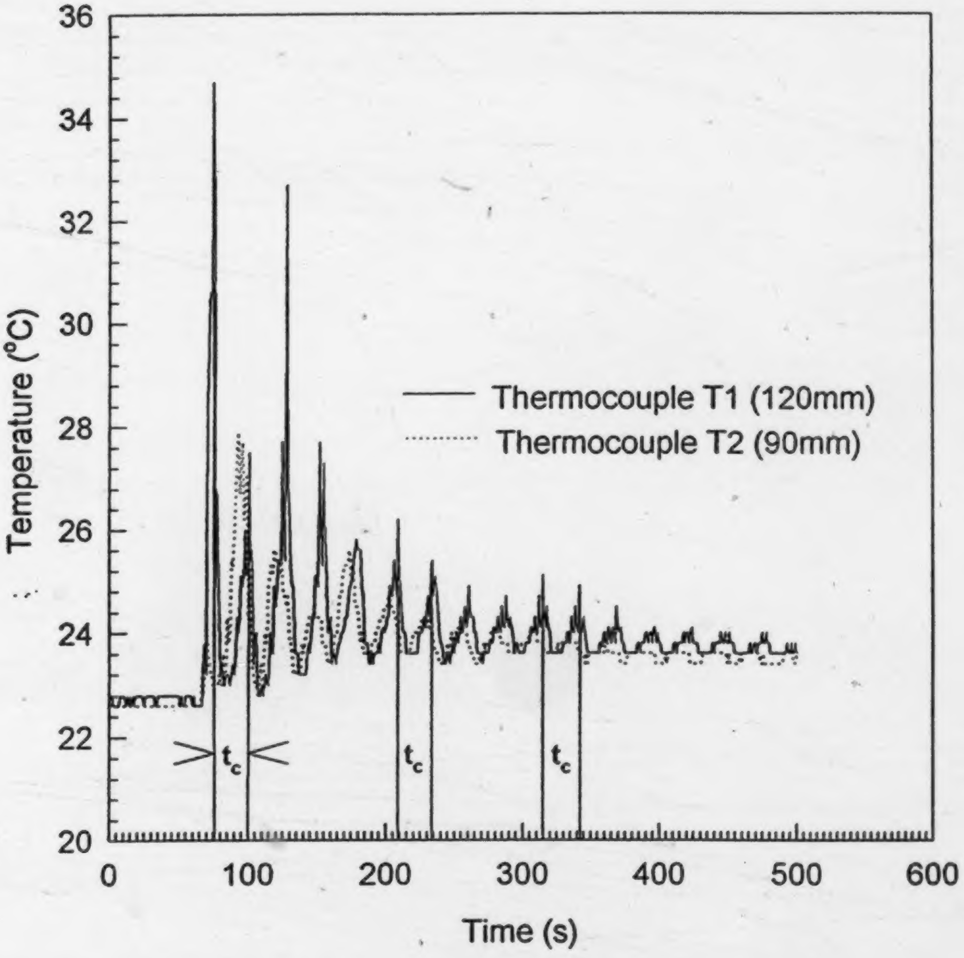

Figure 4.3.1.1.1 HR1-B Pumping Upwards; 20rpm 1.48wt% Carbopol; pH 2.79; Estimation of Circulation Time, t_c

Table 4.3.1.1.1 Average Values of Circulation Time, t_c (s), using 1.48wt% Carbopol

rpm	pH	HR1-B		DHR-1	
		Upwards	Downwards	Upwards	Downwards
10	11.5	35	183	55	66
	2.79	49	51	59	60
15	11.5	29	115	37	40
	2.79	36	31	42	40
20	11.5	18	86	31	29
	2.79	27	25	31	30

to cause one complete circulation of a fluid element in the vessel. Values of k_c can be calculated using equation (2.5.3) and for the present study, k_c values are shown in Table 4.3.1.1.2. These values of k_c use the average values for t_c from Table 4.3.1.1.1 for their calculation by equation (2.5.3). Ryan et al., (1988) have reported values of k_c of 9.5 ± 0.5 for shear thinning fluids with a power law index, n, in the range 0.61 to 0.75. Double flight helical ribbon impellers were used exclusively in their work. The Carbopol solutions used in the present study have $0.44 < n < 0.62$. Referring to Table 4.3.1.1.2, the value of k_c for impeller DHR-1 is observed to vary between 9.2 and 11 for high viscosity (pH 11.5) and low viscosity (2.79) Carbopol solutions, for both upward and downward pumping. These results are in good agreement with the results of Ryan et. al., (1988).

For the impeller HR1-B in upward pumping mode, k_c varies between 8.2 and 9 in low viscosity fluid (pH 2.79) as shown in Table 4.3.1.1.2. This is in reasonable agre[illegible] with the result of Ryan et. al., (1988), however they did not study mixing with a single ribbon impeller. For the impeller HR1-B pumping upwards through high viscosity fluid (pH 11.5), kc varies between 5.8 and 7.5. The order of magnitude of this result is the same as that for Ryan et. al., (1988) but the agreement is not so good. For impeller HR1-B pumping downwards through low viscosity fluid (pH 2.79), k_c varies between 7.75 and 8.5. This is in reasonable agreement with the result of Ryan et. al., (1988). For impeller HR1-B pumping downwards through high viscosity fluid (pH 11.5), k_c varies between 28.67 and 30.5. This result deviates very widely from the result of Ryan et. al., (1988). Furthermore, this is a large deviation from other results for k_c that are obtained for the impeller HR1-B mixing Carbopol solutions. Using the definition of k_c given above, and

Table 4.3.1.1.2 Average Values of k_c using 1.48wt% Carbopol

rpm	pH	HR1-B		DHR-1	
		Upwards	Downwards	Upwards	Downwards
10	11.5	5.8	30.5	9.2	11.0
	2.79	8.2	8.5	9.8	10.0
15	11.5	7.3	28.8	9.25	10.0
	2.79	9.0	7.8	10.5	10.0
20	11.5	6.0	28.7	10.3	9.7
	2.79	9.0	8.3	10.3	10.0

calculated values of k_c from Table 4.3.1.1.2, it can be concluded from this study that downward pumping of impeller HR1-B in high viscosity Carbopol solution (pH 11.5) requires approximately three times more revolutions of the impeller to circulate a fluid element than any of the other mixing trials that have been investigated. For upward pumping of HR1-B an average of 7.5 revolutions cause one complete circulation of a fluid element in the vessel. The impeller DHR-1 requires an average of 9.5 revolutions for one circulation as found by Ryan et al., (1988).

Calculated values of the dimensionless circulation number, Ci, defined in equation (2.5.2), are shown in Table 4.3.1.1.3. These values are based on a working fluid volume of 7.5 litres. Bourne and Butler, (1969) have suggested that Ci is independent of rheology or mixer geometry and has a constant value of 0.046. In the present study, Ci was found to have an average value of 0.041 for impeller HR1-B pumping downwards in high viscosity (pH 11.5) Carbopol solution. For all the other mixing trials that have been investigated, the results of Ci in Table 4.3.1.3 suggest typical values between 2 and 4 times that of Bourne and Butler, (1969). Values for Ci from the present study seem to vary more widely with rheology and direction of pumping for impeller HR1-B. Furthermore, the calculated values for Ci in this study fall outside the range suggested by Carreau et al., (1976). They studied mixing of Newtonian and shear thinning fluids, predominantly with double flight helical ribbon impellers, and found Ci to have values between 0.047 and 0.098. The typical working volume of fluid used in the vessel by these authors was not reported. If it was significantly different from the working volume in this study then this would lead to a discrepancy between the values of Ci reported by Carreau et. al., (1976) and the values of Ci from the present study. The reason for this is that Ci is related to the pumping ability of the impeller. For a good comparison of this, the height of fluid relative to the top of the impeller must alwys be the same, and thus for mixers of similar geometry, the working volumes of fluid must be similar to maintain fluid height ratios relative to the impeller. It is concluded that there is reasonable agreement between calculated values of Ci for DHR-1 in Table 4.3.1.1.3 and those reported by Carreau et. al., (1976).

Values for the circulation number, Ci, are related to the pumping ability of the impeller in the mixing vessel. The values reported for k_c are more meaningful for relating different mixer geometries using helical ribbon impellers. k_c values are suggested to be more appropriate for mixer design and especially for scale-up purposes.

Table 4.3.1.1.3 Values of Circulation Number, Ci, for 1.48wt% Carbopol

rpm	pH	HR1-B		DHR-1	
		Upwards	Downwards	Upwards	Downwards
10	11.5	0.203	0.039	0.129	0.108
	2.79	0.145	0.139	0.121	0.118
15	11.5	0.163	0.041	0.128	0.118
	2.79	0.132	0.153	0.113	0.118
20	11.5	0.197	0.041	0.115	0.122
	2.79	0.132	0.142	0.115	0.118

4.3.1.2 Mixing Time

The correlations related to mixing time calculations have been presented in Section 2.4. A number of techniques are available for determining the mixing time and these are all statistical in nature. Evaluation of the mixing time from a thermogram using the thermal technique is essentially left to personal interpretation because the approach to finally mixed state is asymptotic, and so the definition of the final mixed state can lead to large differences in the estimated mixing time. This principle is illustrated in Figure 4.3.1.2.1. The approach that is chosen in the mixing time estimation will influence the result that is obtained. The approach used to determine mixing times in this study is illustrated in Figure 4.3.1.2.2.

Mixing times using the thermal technique in this study have been difficult to determine for the reasons described above. Average values for t_m determined from ten thermograms for each run are shown in Table 4.3.1.2.1. There is much more variation for values of the mixing time, t_m, than for the circulation time, t_c, but this is largely due to the inaccuracy in estimating the values of t_m shown in Table 4.3.1.2.1. The number of peaks on the thermogram and the damping effect of these peaks are very important for evaluating circulation and mixing times. In Appendix E, the thermograms tend to have more peaks and a more pronounced damping effect when the volume of injection of heated fluid is increased. Hence for larger volume injections, better prediction of circulation, and especially mixing times has been possible. k_m is defined as the number of revolutions required to achieve a specified level of homogeneity in the vessel. An

Figure 4.3.1.2.1 Progress of mixing in terms of arbitrary mixing index (I). The approach to the fully mixed condition is asymptotic and small errors in mixing index (δI) lead to large errors in estimated mixing time (t_c).

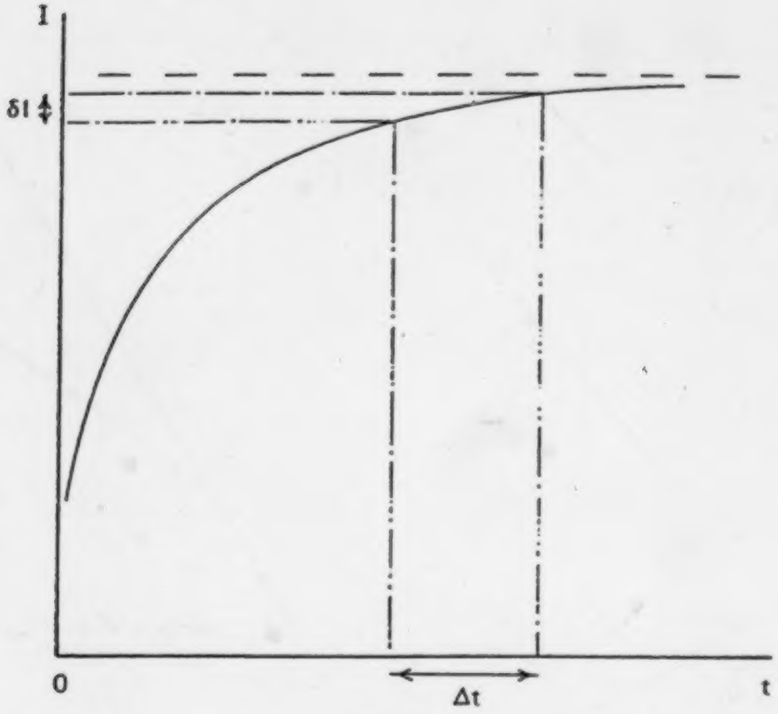

Source: Godfrey, (1985) p.196

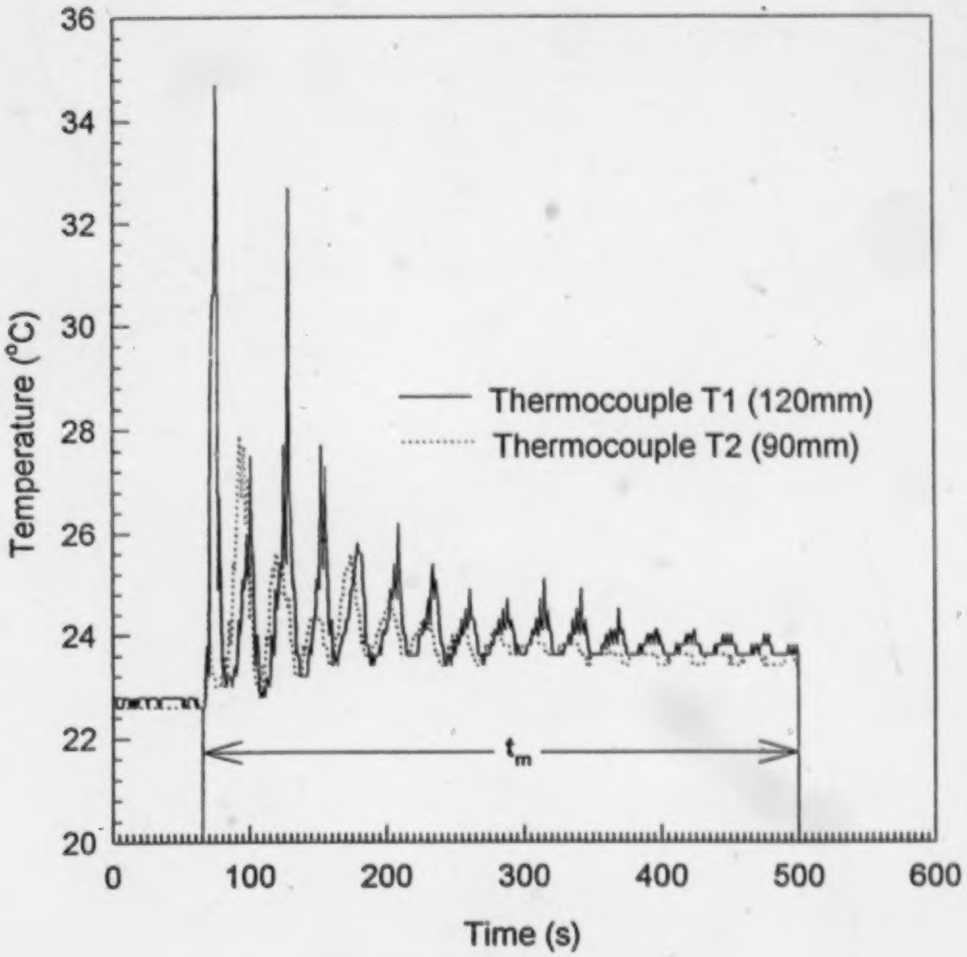

Figure 4.3.1.2.2 HR1-B Pumping Upwards; 20rpm
1.48wt% Carbopol; pH 2.79
Estimation of Mixing Time, t_m

Table 4.3.1.2.1 Average Values of Mixing Time, t_m (s), for 1.48wt% Carbopol

rpm	pH	HR1-B		DHR-1	
		Upwards	Downwards	Upwards	Downwards
10	11.5	480	575	220	170
	2.79	360	400	370	270
15	11.5	400	530	150	150
	2.79	320	285	210	150
20	11.5	150	450	120	100
	2.79	360	365	185	160

assessment of the performance of a mixer configuration is better made by studying values of k_m than by studying values of t_m directly.

Values of k_m from this study are shown in Table 4.3.1.2.2. For the impeller DHR-1 mixing high viscosity fluid (pH 11.5), k_m varies between 28 and 38 for all rotational speeds and pumping in both directions. There is a larger variation when impeller DHR-1 mixes the low viscosity fluid (pH 2.79). In this case, k_m varies between 38 and 62. For the impeller HR1-B mixing high viscosity fluid, k_m varies between 60 and 122 for all rotational speeds and both directions of pumping. The range of k_m for the impeller HR1-B mixing low viscosity fluid is between 50 and 150, again for all rotational speeds and both pumping directions. Nagata et. al., (1972) reported some results using non-Newtonian fluids. They found k_m to be 40 for double ribbon impellers and k_m varying between 100 and 150 for single ribbon impellers, both in upward pumping mode. Given the error associated in estimating t_m in the present study, it can be concluded that the results of this study fall into the range of values reported by Nagata et. al., (1972), for both single and double ribbon impellers.

Zlokarnik, (1967) and Ho and Kwong, (1973) have reported a dependence of k_m on Reynolds number for Newtonian fluids. This dependence has not been investigated in the present study using non-Newtonian fluids because of the large number of ways to approach the definition of the Reynolds number in the mixing vessel, when non-Newtonian fluids are present.

From the definition of the dimensionless mixing time, k_m, previously given, it can be concluded that the value of k_m is as much as 4 times lower for impeller DHR-1 than

Table 4.3.1.2.2 Average Values of k_m for 1.48wt% Carbopol

rpm	pH	HR1-B		DHR-1	
		Upwards	Downwards	Upwards	Downwards
10	11.5	80	95.8	36.7	28.3
	2.79	60	66.7	61.7	45
15	11.5	100	132.5	37.5	37.5
	2.79	80	71.25	52.5	37.5
20	11.5	50	150	40	33.3
	2.79	120	121.7	61.7	53.3

HR1-B in circumstances where the fluid is highly viscous from the calculated values for k_m in Table 4.3.1.2.2.

The thermal technique has proved to be an unsuccessful method to use for assessing mixing and circulation times for Newtonian polyethylene glycol solutions. The response curves of the thermograms using this fluid are poor, with few spikes from which a circulation time can be determined and it is also not possible to obtain a reasonable prediction of mixing time. Two sample thermograms are shown in Appendices F1 and F2 for mixing with 45wt% polyethylene glycol solutions.

4.3.2 Mixing Assessment from Flow Visualisation

From a quantitative analysis, it was shown in Section 4.3.1 that better mixing is achieved using a double ribbon impeller rather than a single ribbon impeller in terms of circulation and mixing time. Flow visualisation using video analysis has been used to confirm the results of the thermal method qualitatively.

Selected images from a complete mixing cycle are presented in Appendices G1 through G4. Four mixing cycles have been studied in this way; high viscosity Carbopol using HR1-B pumping upwards (G1), high viscosity Carbopol using HR1-B pumping downwards (G2), high viscosity Carbopol using DHR-1 pumping upwards (G3) and Polyethylene Glycol using HR1-B pumping upwards (G4). The time indicated alongside the images in these appendices indicates the time that has elapsed since mixing was initiated. The trace of violet dye in the vessel is the point of interest. The finer details of the mixing process have been described in Section 2.1, and some of these phenomena are observed to occur in the images that are presented in Appendix G.

The relative state of the injected ball of crystal violet dye at similar time frames between different mixing cycles provides comparisons on the relative mixing efficiency of these cycles. In addition, by observing the location of the dye in the vessel at any given time frame for a particular mixing cycle, a comparison can be made with the thermogram that has been generated for that cycle. The dye used in the flow visualisation experiments is a substitute for the hot aliquot of fluid used in the thermal method. To provide an example of this, consider the thermogram given by figure E20. In this mixing cycle, one of the thermocouples in the vessel was located directly adjacent to the wall of the vessel at a depth of 124mm. This depth is equivalent to approximately one third of the fluid height down from the surface. There is essentially no response from this thermocouple in figure E20, indicating that virtually no hot fluid reaches the wall of the vessel. Comparisons are now made with the images in Appendix G2. It is confirmed in the flow visualisation that virtually no dye reaches the vessel wall at the depth indicated for the majority of the mixing cycle, which explains why no response is observed with the thermocouple.

It was found from thermal studies that a significantly different mixing efficiency was obtained for impeller HR1-B when the direction of pumping was reversed. Upward pumping of the impeller produced relatively efficient mixing comparable with the performance of the impeller DHR-1. However, downward pumping of HR1-B produced the poorest mixing efficiency with dimensionless circulation times, k_c, as much as five times greater than upward pumping mode (see table 4.3.1.1.2). In the flow visualisation images of Appendices G1 and G2 this phenomena is confirmed. Mixing in upward pumping mode occurs considerably faster than it does in downward pumping mode. In the latter mode of pumping, there is some considerable time before the injected ball of dye is even pulled down into the bulk fluid for mixing to take place. In downward pumping mode, the fluid flow in the vessel is known to be forced down at the walls of the vessel and upwards through the central core between the impeller blades (Bourne and Butler, 1969). The injection point of the dye is shown in figure 3.2.4. It seems apparent that when mixing is initiated and the impeller is pumping downwards, the ball of dye is pulled into the central core between the blades. The up-flow current as the impeller pumps then carries the dye to the surface and it is some time later before the dye is pulled back to the bulk. From the images of Appendix G1, the converse situation seems to be true.

The mixing efficiency of the double ribbon impeller relative to the single ribbon impeller is unquestionably better from the images of Appendix G3. The dye seems to be dispersed almost immediately after mixing is initiated. For an upward pumping impeller we clearly see the helical down-flow current that is generated in the image shown for "time = 5 s". The final mixed state is approached after around 1 minute with impeller DHR-1, however, for HR1-B pumping downwards, the ball of dye essentially remains intact after 1 minute with no mixing occurring at all.

As a reference, flow visualisation with Newtonian Polyethylene Glycol is presented in Appendix G4.

5. Conclusions

Mixing studies have been carried out using aqueous 1.48wt% Carbopol 940 solutions and Polyethylene Glycol solutions in a vessel equipped with single and double flight helical ribbon impellers. The rheology of the Carbopol solutions has been characterised using a steady state Couette flow viscometer and a dynamic disk and plate rheometer. These solutions have been characterised over a wide range of pH and are found to obey a Herschel-Bulkley rheological model; the fluids are shear thinning and possess yield stress.

Power consumption of the impellers for both fluid types have been determined by measuring the torque. Power requirements for the double ribbon impeller are higher than for the single ribbon impeller. A number of correlations have been investigated to determine the shear rates for Carbopol. The classical Metzner-Otto approach seems to work well and is best correlated by Shamlou and Edwards, (1985) and Brito, (1997). These correlations assume a general power law fluid in their prediction of the shear rate constant, k_s. The analysis of Rauline, (1998) has been investigated, again using the Metzner-Otto approach to determine k_s, but assuming a Herschel-Bulkley fluid and not simply a power law fluid. It has been found that the shear rate "constant" actually varies as a function of impeller rotational speed in this case. A number of Power curves have been generated for both the Newtonian polyethylene glycol solutions and for the non-Newtonian Carbopol solutions. The Power curves for the Carbopol solutions are best characterised by the correlation of Hall and Godfrey, (1970) when using Reynolds numbers based on a shear rate constant determined from the correlation of Shamlou and

Edwards, (1985). The power curve resulting from this combination of correlations compares very well with the curve that results using the Herschel-Bulkley analysis of Rauline, (1998).

The mixing performance in the vessel for the Carbopol solutions has been determined by calculating mixing and circulation times using a thermal technique. For high and low viscosity Carbopol fluids, at three speeds of impeller rotation and for both upward and downward pumping of the impeller, the double flight ribbon impeller has been found to take approximately 9.5 revolutions to circulate a fluid element in the vessel. The performance of single ribbon impeller in low viscosity fluid is comparable with the double ribbon in terms of dimensionless circulation time, except for the condition where the single ribbon impeller pumps downwards through high viscosity fluid. In this case, the circulating ability of the impeller is much poorer, requiring an average of 28 impeller rotations for one circulation.

From the response of the thermograms, it is difficult to accurately predict a mixing time in the vessel, irrespective of the impeller used, the speed of rotation, or the direction of pumping. However, making a best estimate, it has been found that the double ribbon impeller takes between 28 and 38 revolutions to reach a specified level of homogeneity irrespective of impeller speed, fluid viscosity or pumping direction. The single ribbon takes between 38 and 62 revolutions to achieve the same level of homogeneity in low viscosity fluid irrespective of rotational speed or pumping direction. The range increases to between 60 and 122 in high viscosity fluid, again irrespective of impeller speed or pumping direction. The results of the thermal technique are improved with larger volumes of injected fluid and the technique works well for studying mixing of Carbopol fluids. The results are very reproducible with only a 5% variation in results obtained for ten similar runs.

The circulation or mixing times for Polyethylene Glycol solutions with either impeller could not be established due to the poor response of the thermograms for these solutions.

The mixing and circulation behaviour for Carbopol solutions from the thermal trials have been confirmed qualitatively using flow visualisation by video analysis. In terms of mixing efficiency, an overall conclusion is that the double ribbon impeller provides the best agitation of the non-Newtonian Carbopol fluids. Upward pumping of the impeller is the optimum mode of operation, and this is especially so if single ribbon impellers are used.

6. Recommendations

A number of opportunities for further research in this project exist. These include:

- Investigating rheology and mixing behaviour with different concentrations of Carbopol
- Performing numerical simulations of the mixing process
- Further investigation into the precise shear rates that occur in the vessel
- Investigating any relationship between mixing and circulation times and Reynolds number in the vessel

The thermal method has worked well for quantitative analysis of the mixing process, however, entrained air bubbles in the Carbopol solutions made it impossible to confirm these results using quantitative colorimetry by spectrophotometer probe. Methods to overcome this kind of problem could be investigated.

The non-Newtonian rheology of the Carbopol microgels is an important area for further investigation. A better understanding of the relationship between the microstructure of the gels and the observed rheology might be achieved by further research in this area.

7. References

Ahmed, S. W.; Latto, B.; Baird, M. H. I.; Mixing of Stratified Liquids; *Chem Eng Des Res*, **63**, May 1985, 157-167

Allen, L. V.; Compounding Gels; http://www.paddocklabs.com/secundum/secart45.html; 12/08/97

Bertrand, F.; Tanguy, P. A.; Brito-de-la-Fuente, E.; A New Perspective for the Mixing of Yield Stress Fluids with Anchor Impellers; *J. Chem. Eng. Jpn.*, **29** (1), 1996, 51-58

Blasinski, H.; Rzyski, E.; Power Requirements of Helical ribbon Mixers; *J. Chem. Eng.*, **19**, 1980, 157-160

Blasinski, H.; Kuncewicz, C.; Heat Transfer During the Mixing of Pseudoplastic Fluids with Ribbon Agitators; *Int. Chem. Eng.*, **21** (4), October 1981, 679-683

Boardman, G., *Nature*, **187**, 1960, 50-56

Bourne, J. R., Butler, H., *AIChE-IChemE Symposium Series:* **89** (10), 1965

Bourne, J. R.; Butler, H.; An Analysis of the Flow Produced by Helical Ribbon Impellers; *Trans. Inst. Chem. Engrs.*, **47**, 1969, T11-T17

Bourne, J. R.; Knoepfli, W.; Riesen, R.; Batch and Continuous Blending of Newtonian Fluids using Helical Ribbon Impellers; *Third European Conference on Mixing,* April 4-6, 1979; Paper A1, 1-18

Brodkey, R. S., The Phenomena of Fluid Motions, Addison-Wesley, Mass., 1967

Brown, G. L.; Garrett, B. S.; Latex Thickening: Interactions Between Aqueous Polymeric Dispersions and Solutions; *J. Appl. Polym. Sci.*, **1** (3), 1959, 283-295

Brito-de-la-Fuente, E.; Leuliet, J. C.; Choplin, L.; Tanguy, P. A.; On the Role of Elasticity on Mixing with a Helical Ribbon Impeller; *Trans IChemE*, **69 Part A**, July 1991, 324-331

Brito-de-la-Fuente, E.; Mixing of Rheological Complex Fluids with Helical Ribbonand Helical Screw Ribbon Impellers; Ph.D. Thesis, University of Laval, Quebec, 1992

Brito-de-la-Fuente, E.; Choplin, L.; Tanguy, P. A.; Mixing with Helical Ribbon Impellers: Effect of Highly Shear Thinning Behaviour and Impeller Geometry; *Trans IChemE*, **75 Part A**, January 1997, 45-52

Calderbank, P. H.; Moo-Young, M. B.; The Power Characteristics of Agitators for the Mixing of Non-Newtonian Fluids; *Trans. Inst. Chem. Engrs.*, **39**, 1961, 337-347

Carnali, J. O.; Naser, M. S.; The Use of Dilute Solution Viscometry to Characterize the Network Properties of Carbopol Microgels; *Colloid Polym Sci.* **270**, 1992, 183-193

Carreau, P. J.; Patterson, I.; Yap, C. Y.; Mixing of Viscoelastic Fluids with Helical Ribbon Agitators I-Mixing Time and Flow Patterns; *Can. J. Chem. Eng.*, **54**, June 1976, 135-142

Chavan, V. V.; Ulbrecht, J.; Power Correlation for Helical Ribbon Impellers in Inelastic Non-Newtonian Fluids; *J. Chem. Eng.*, **3**, 1972, 308-311

Chavan, V. V.; Ford, D. E.; Arumugam, M.; Influence of Fluid Rheology on Circulation, Mixing and Blending; *Can. J. Chem. Eng.*, **53**, December 1975, 628-635

Chavan, V. V.; Close-Clearance Helical Impellers: A Physical Model for Newtonian Liquids at Low Reynolds Numbers; *AIChEJ.*, **29** (2), March 1983, 177-185

Chavan, V. V., Mashelkar, R. A., *Mixing of Viscous Newtonian and Non-Newtonian Fluids* in Advances in Transport Processes, edited by Mujumdar, A. S., Wiley, New York, **Vol. 1**, 1980, 210-252

Cheng, J.; Carreau, P. J.; Mixing in the Transition Flow Regime with Helical Ribbon Agitators; *Can. J. Chem. Eng.*, **72**, June 1994, 418-430

Contraves Rheomat 115 Operating Instructions Manual

Coulson, J. M., Richardson, J. F., Backhurst, J. R., Harker, J. H., Chemical Engineering Volume 1 (Fluid Flow, Heat Transfer and Mass Transfer), Fourth edition, Pergamon Press., 1990

Cox, W. P., Merz, E. H., *J. Polym. Sci.*, **28**, 1958, 619-625

Doraiswamy, D.; Grenville, R. K.; Etchells III, A. W.; Two Score Years of the Metzner-Otto Correlation; *Ind. Eng. Chem. Res.*, **33**, 1994, 2253-2258

Ducla, J. M.; Desplanches, H.; Chevalier, J. L.; Effective Viscosity of Non-Newtonian Fluids in a Mechanically Stirred Tank; *Chem. Eng. Commun.*, **21**, 1983, 29-36

Edwards, M. F., Mixing of Low Viscosity Liquids in Stirred Tanks, in *Mixing in the Process Industries*, edited by Harnby, N., Edwards, M. F., Nienow, A. W., Butterworths, London, 1985, Chapter 8

Edwards, M. F., Laminar Flow and Distributive Mixing, in *Mixing in the Process Industries*, edited by Harnby, N., Edwards, M. F., Nienow, A. W., Butterworths, London, 1985, Chapter 12

Erwin, L., *Polym. Eng. Sci.*, **18**, 1978, 738-743

Fischer, W. H.; Bauer, W. H.; Wiberley, S. E..; Yield Stress and Flow Properties of Carboxypolymethylene-Water Systems; *Trans Soc. Rheol.*, **V**, 1961, 221-235

Ford, D. E., Mashelkar, R. A., Ulbrecht, J., Mixing Times in Newtonian and Non-Newtonian Fluids, *Process Technology International*, **17** (10), 1972, 803-807

Godfrey, J. C., Mixing of High Viscosity Fluids, in *Mixing in the Process Industries*, edited by Harnby, N., Edwards, M. F., Nienow, A. W., Butterworths, London, 1985, Chapter 11

Godleski, E. S.; Smith, J. C.; Power Requirements and Blend Times in the Agitation of Pseudoplastic Fluids; *AIChEJ.*, **8** (5), 615-620

Gray, J. B.; Batch Mixing of Viscous Liquids; *Chem. Eng. Prog.*, **59** (3), March 1963, 55-59

Hall, K. R.; Godfrey, J. C.; Power Consumption by Helical Ribbon Impellers; *Trans. Instn. Chem. Engrs.*, **48**, 1970, T201-T208

Hayes, R. E.; Afacan, A.; Boulanger, B.; Tanguy, P. A.; Experimental Study of Reactive Mixing in a Laminar Flow Batch Reactor; *Trans IChemE*, **76 Part A**, January 1998, 73-81

Hiby, J. W.; Definition and Measurement of the Degree of Mixing in Liquid Mixtures; *Int. Chem. Eng.*, **21** (2), 197-204

Ho, F.; Kwong, A.; A Guide to Designing Special Agitators; *Chem. Eng.*, July 1973, 94-104

Hoogendoorn, C. J.; Den Hartog, A. P.; Model Studies on Mixers in the Viscous Flow Regime; *Chem. Eng. Sci.*, **22**, 1967, 1689-1699

Kai, W., Shengyao, Y., Heat Transfer and Power Consumption of Non-Newtonian Fluids in Agitated Vessels, *Chem. Eng. Sci.*, **44** (1), 1989, 33-40

Käppel, M., Development and Application of a Method for Measuring Mixture Quality of Miscible Liquids. III. Application of the New Method for Highly Viscous Newtonian Liquids, *Int. Chem. Eng.*, **19** (4), October 1979, 571-590

Ketz, Jr., R. J.; Prud'homme, R. K.; Graessley, W. W.; Rheology of Concentrated Microgel Solutions; *Rheol. Acta.*, **27**, 1988, 531-539

King, R., Mechanical Aspects of Mixing, in *Mixing in the Process Industries*, edited by Harnby, N., Edwards, M. F., Nienow, A. W., Butterworths, London, 1985, Chapter 14

Kuriyama, M.; Ohta, M.; Yanagawa, K.; Arai, K.; Saito, S; Heat Transfer and temperature Distributions in an Agitated Tank Equipped with Helical Ribbon Impeller; *J. Chem. Eng. Jpn.*, **14** (4), 1981, 323-330

Kuriyama, M.; Arai, K.; Saito, S; Mechanism of Heat Transfer to Pseudoplastic Fluids in an Agitated Tank with Helical Ribbon Impeller; *J. Chem. Eng. Jpn.*, **16** (6), 1983, 489-494

Maruyama, T.; Suzuki, S.; Mizushina, T.; Pipeline Mixing Between Two Fluid Streams Meeting at a T-Junction; *Int. Chem. Eng.*, **21** (2), April 1981, 205-212

McCabe, W. L., Smith, J. C., Harriott, P., Unit Operations of Chemical Engineering, Fourth Edition, McGraw Hill Inc., New York, 1985

Metzner, A. B.; Otto, R. E.; Agitation of Non-Newtonian Fluids; *AIChEJ.*, **3** (1), 1957, 3-10

Metzner, A. B.; Feehs, R. H.; Ramos, H. L.; Otto, R. E.; Tuthill, J. D.; Agitation of Viscous Newtonian and Non-Newtonian Fluids; *AIChEJ.*, 7 (1), 1961, 3-9

Middleman, S., Fundamentals of Polymer Processing, McGraw Hill Inc., New York, 1977

Moes, A., Nouveaux Agents Epaississants dans la Formulation des Suspensions, *Il Farmaco*, **27** (3), 1991, 130-146

Nagata, S., Yanagimoto, M., Yokoyama, T., A Study of Mixing of High Viscosity Liquids, *J. Chem. Eng. Jpn.*, **21**, 1957, 278-283

Nagata, S.; Nishikawa, M.; Tada, H.; Hirabayashi, H.; Gotoh, S.; Power Consumption of Mixing Impellers in Bingham Plastic Liquids; *J. Chem. Eng. Jpn.*, **3** (2), 1970, 237-243

Nagata, S.; Nishikawa, M.; Tada, H.; Gotoh, S.; Power Consumption of Mixing Impellers in Pseudoplastic Liquids; *J. Chem. Eng. Jpn.*, **4** (1), 1971, 72-76

Nagata, S.; Nishikawa, M.; Katsube, T.; Takaish, K.; Mixing of Highly Viscous Non-Newtonian Liquids; *Int. Chem. Eng.*, **12** (1), January 1972, 175-182

Nienow, A. W., Introduction to mixing Problems, in *Mixing in the Process Industries*, edited by Harnby, N., Edwards, M. F., Nienow, A. W., Butterworths, London, 1985, Chapter 1

Nienow, A. W.; Elson, T. P.; Aspects of Mixing in Rheologically Complex Fluids; *Chem. Eng. Res. Des.*, **66**, January 1988, 5-15

Novak, V.; Rieger, F.; Homogenization Efficiency of Helical Ribbon and Anchor Agitators; *J. Chem. Eng.*, **9**, 1975, 63-70

Parker, N. H., Mixing, *Chem. Eng.*, **71** (12), 1964, 165-169

Patterson, W. I.; Carreau, P. J.; Yap, C. Y.; Mixing with Helical Ribbon Agiatators. Part II. Newtonian Fluids; *AIChEJ.*, **25** (3), May 1979, 508-516

Ogawa, K., Ito, S., A Definition of Quality of Mixedness, *J. Chem. Eng. Jpn.*, **8** (2), 1975, 148-151

Ottino, J. M., Macosko, C. W., *Chem. Eng. Sci.*, **35**, 1979, 1454

Penney, W. Roy; Bell, K. J.; Close Clearance Agitators. Part I. Power Requirements; *Ind. Eng. Chem.*, **59** (4), April 1967, 40-46

Rauline, D., Agitation de Fluides Seuil et de Fluides Thixotropes, M.Sc. Thesis, Ecole Polytechnique, Montreal, June 1998

Ravissot, G., Resines Solubles en Milieu Aqueux, company litreature of Polyplastic S. A., Cedex, France, September, 1989

Rieger, F.; Novak, V.; Power Consumption of Agitators in Highly Viscous Non-Newtonian Liquids; *Trans. Instn. Chem. Engrs.*, **51**, 1973, 105-111

Rieger, F.; Novak, V.; Havelkova, D; Homogenization Efficiency of Helical Ribbon Agitators; *J. Chem. Eng.*, **33**, 1986, 143-150

Ryan, D. F.; Janssen, L. P. B. M.; van Dierendonck, L. L.; Circulation Time Prediction in the Scale-Up of Polymerization Reactors with Helical Ribbon Agitators; *Chem. Eng. Sci.*, **43** (8), 1988, 1961-1966

Sawinski, J., Havas, G., Deak, A., Power requirements of Anchor and Helical Ribbon Impeller for the Case of Agitating Newtonian and Pseudoplastic Liquids, *Chem. Eng. Sci.*, **31**, 1976, 507-509

Shamlou, P. A.; Edwards, M. F.; Power Consumption of Helical Ribbon Mixers in Viscous Newtonian and Non-Newtonian Fluids; *Chem. Eng. Sci.*, **40** (9), 1985, 1773-1781

Skelland, A. H. P., Mixing and Agitation of Non-Newtonian Fluids, in *Handbook of Fluids in Motion*, edited by N. P. Cheremisinoff and R. Gupta, Ann Arbor Science, Ann Arbor, Michigan, 1983, Chapter 7

Smith, J. M. Industrial Needs for Mixing Research, *Trans IChemE*, **68 Part A**, January 1990, 3-6

Spencer, R. S., Wiley, R. M., *J. Coll. Sci.*, **6**, 133

Takahashi, K., Arai, K., Saito, S., Power Correlation for Anchor and Helical Ribbon Impellers in Highly Viscous Liquids, *J. Chem. Eng. Jpn.*, **13** (2), 1980, 147-150

Takahashi, K., Saskai, M., Arai, K., Saito, S., Effects of Geometrical variables of Helical Ribbon Impellers on Mixing of Highly Viscous Newtonian Liquids, *J. Chem. Eng. Jpn.*, **15** (3), 1982, 217-223

Takahashi, K., Yokota, T., Konno, H., Power Consumption of Helical Ribbon Agitators in Highly Viscous Pseudoplastic Liquids, *J. Chem. Eng. Jpn.*, **17** (6), 1984, 657-659

Takahashi, K., Takahata, Y., Yokota, T.., Konno, H., Mixing of Two Miscible Highly Viscous Newtonian Liquids in a Helical Ribbon Agitator, *J. Chem. Eng. Jpn.*, **18** (2) 159-162

Takahashi, K., Yokota, T., Konno, H., Mixing of Pseudoplastic Liquid in a Vessel Equipped with a Variety of Helical Ribbon Impellers, *J. Chem. Eng. Jpn.*, **21** (2), 1988, 63-79

Takahashi, K., Iwaki, M., Yokota, T., Konno, H., Circulation Time for Pseudoplastic Liquids in a Vessel Equipped with a Variety of Helical Ribbon Impellers, *J. Chem. Eng. Jpn.*, **22** (4), 1989, 413-417

Tanguy, P. A., Thibault, F., Brito-de-la-Fuente, E., A New Investigation of the Metzner-Otto Concept for Anchor Mixing Impellers, *Can. J. Chem. Eng.*, **74**, April 1996, 222-228

Tanguy, P. A., Thibault, F., Brito-de-la-Fuente, E., Espinosa-Solares, T., Tecante, A., Mixing Performance Induced by Coaxial Flat Blade-Helical Ribbon Impellers Rotating at Different Speeds, *Chem. Eng. Sci.*, **52** (11), 1997, 1733-1741

Tatterson, G. B., Fluid Mixing and Gas Dispersion in Agitated Tanks, McGraw Hill, Inc., New York, 1991, Chapter 3, Chapter 5.

Taylor, N. W., Bagley, E. B., Dispersions or Solutions? A Mechanism for Certain Thickening Agents, *J. Appl. Polym. Sci.*, **18**, 1974, 2747-2761

Taylor, N. W., Bagley, E. B., Tailoring Closely Packed Gel-Particle Systems for Use as Thickening Agents, *J. Appl. Polym. Sci.*, **21**, 1977, 113-122

Ulbrecht, J. J., Carreau, P., Mixing of Viscous Non-Newtonian Liquids, in *Mixing of Liquids by Mechanical Agitation*, edited by J. J. Ulbrecht, G. R. Patterson, Gordon and Breach Science, New York, **Vol. 1**, 1985, 93-137

de la Villeon, J., Bertrand, F., Tanguy, P. A., Labrie, R., Bousquet, J., Lebouvier, D., Numerical Investigation of Mixing Efficiency of Helical Ribbons, *AIChEJ.*, **44** (4), April 1998, 972-977

Wu, J., Thompson, M. C., Non-Newtonian Shear Thinning Flows Past a Flat Plate, *J.Non-Newtonian Fluid Mech.*, **66**, 1996, 127-144

White, F. M., Viscous Fluid Flow, McGraw Hill Inc., New York, 1974

Yap, C. Y., Patterson, W. I., Carreau, P. J., Mixing with Helical Ribbon Agitators III Non-Newtonian Fluids, *AIChEJ.*, **25** (3), May 1979, 516-521

Zlokarnik, M., Eignung von Rührern zum Homogenisieren von Flussigkeitsgemischen, *Chemie-Ing-Techn.* **39**, 1967, 539-548

Appendix A1: Sample Titration Calculation for 1.48wt% Carbopol

In figure 3.1.1, a titration curve for volumetric additions of 23wt% NaOH to 1.48wt% Carbopol solutions was shown. This was based on measured values of pH using a pH meter, as described in Section 3. The rheological behaviour of the Carbopol gels has been shown to be unusual and has been suggested to be due to the chemical microstructure of the gels (see Section 2.7). A sample calculation is provided here to show that reaction of the acidic gels with a basic solution does not follow a conventional mole balance calculation. In this calculation, an addition of 0.0189 ml. 23wt% NaOH to 1.48wt% Carbopol of pH 2.79 is considered. The results of several calculations to generate a titration curve are shown in figure A2.

Carbopol pH: 2.79

$\text{pH} = -\log[\text{H}^+] \Rightarrow [\text{H}^+] = 1 \times 10^{-2.79} = 1.6218 \times 10^{-3}\ \text{mol l}^{-1}$

Carbopol sample is 100ml. $\Rightarrow$ mols $[\text{H}^+]$ = **1.6218×10^{-4} mol l^{-1}**

NaOH: 23wt%

30g NaOH in 100g water

$\Rightarrow$ 30g $[\text{OH}^-]$ in 100ml. water

$\Rightarrow$ mols $[\text{OH}^-] = 30/40 = 7.5\ \text{mol l}^{-1}$

Appendix A1 cont.

Volume addition: 0.0189 ml.

$\Rightarrow$ **mols [OH$^-$] = 1.4175 x 10^{-4} mols**

Neutralisation:

1.6218 x 10^{-4} [H$^+$] - 1.4175 x 10^{-4} [OH$^-$] = **2.043 x 10^{-5} mol [H$^+$]**

Total volume: 100ml. + 0.0189ml. = 100.0189ml.

Concentration [H$^+$]: 2.043 x 10^{-5} mol / 100.0189ml. = **2.0426 x10^{-4} mol l^{-1}**

pH of resulting solution: -log (2.0426 x 10^{-4}) = **3.699**

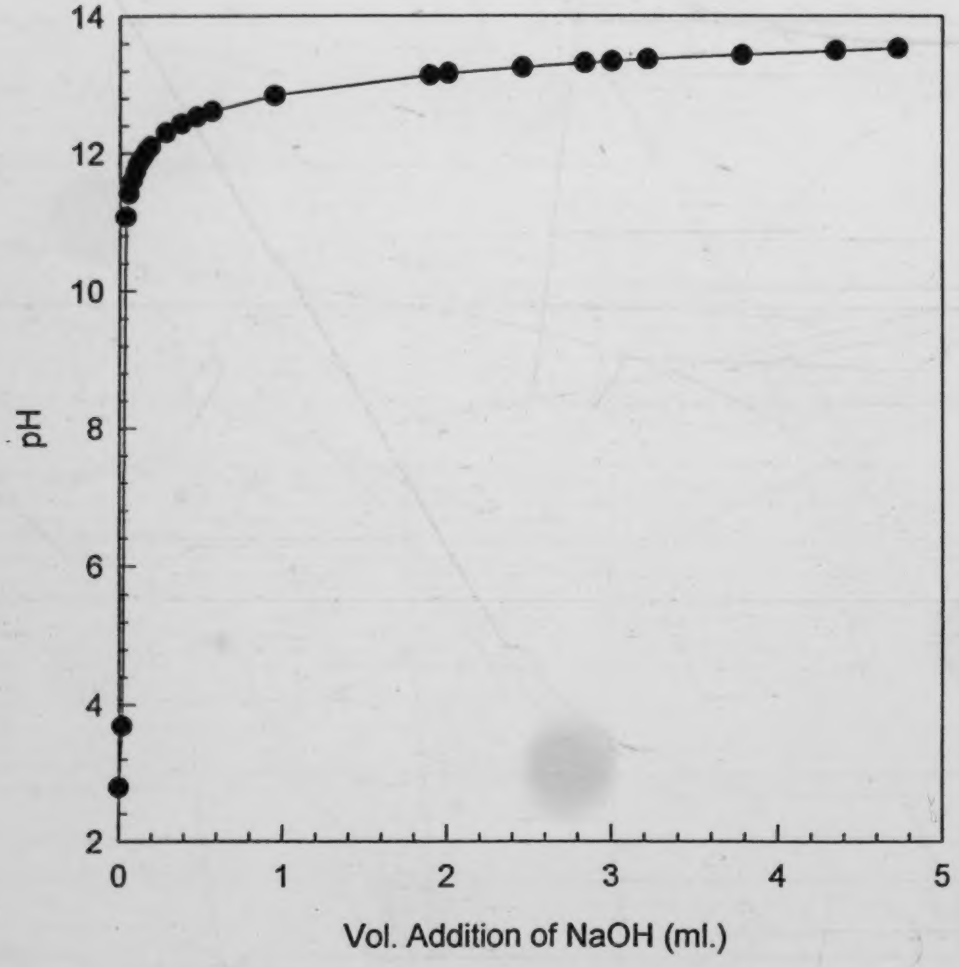

Figure A2 Variation of pH with volumetric additions of 23wt% NaOH based on mole balance calculations

Appendix B1: Shear Stress (Pa) - Shear Rate Data for 1.48wt% Carbopol Solutions

γ	8.01	11.40	16.34	23.21	33.16	47.44	67.78	96.73	137.82	194.52
pH	τ									
2.79	39.9	42.2	43.4	46.8	49.1	53.1	58.2	63.9	69.6	77.6
2.87	79.9	82.2	85.6	90.1	95.8	101.5	109.5	118.7	128.9	142.6
2.99	125.5	127.8	135.8	143.8	152.9	163.2	175.7	191.7	209.9	231.6
3.15	232.8	239.6	248.7	257.9	269.3	278.4	295.5	313.8	338.9	373.1
3.38	267.0	278.4	283.0	294.4	308.1	325.2	344.6	367.4	392.5	414.2
3.64	291.0	304.6	318.3	334.3	352.6	370.8	397.1	424.5	461.0	504.3
4.08	316.1	333.2	357.1	433.6	467.8	524.9	587.6	639.0	701.7	770.2
4.38	303.5	321.8	338.9	354.9	368.5	399.4	431.3	467.8	513.5	569.4
4.51	303.5	312.6	328.6	343.4	369.7	393.6	427.9	462.1	505.5	553.4
4.57	309.2	320.6	340.0	364.0	389.1	418.7	457.5	499.8	551.1	607.0
5.01	306.9	325.2	346.9	374.2	406.2	419.9	439.3	476.9		
6.45	295.5	309.2	330.9	357.1	391.4	430.2	478.1	530.6		
6.57	295.5	317.2	338.9	368.5	403.9	441.6	488.3	532.8		
6.64	270.4	293.2	308.1	335.5	368.5	405.1	450.7	519.2		
6.88	309.2	332.0	360.6	382.2	394.8	434.7	481.5	548.8		
7.02	304.6	318.3	332.0	353.7	378.8	414.2	462.1	511.2		
7.15	286.4	300.1	322.9	374.2	402.8	443.8	462.1	510.0		
7.43	230.5	245.3	264.1	265.3	310.4	340.0	373.1	417.0		
7.57	286.4	286.4	286.4	286.4	286.4	286.4	286.4	286.4		
11.36	245.3	259.0	278.4	301.2	327.5	359.4	397.1	435.9		
12.3	212.2	237.3	248.7	264.7	285.3	310.9	341.2	376.0		
12.53	164.3	173.4	183.7	196.3	211.1	227.1	237.3	257.9		
12.68	108.4	114.1	120.9	130.1	140.3	152.9	167.7	184.8		

Appendix B2: Apparent Viscosity (Pas) - Shear Rate Data for 1.48wt% Carbopol Solutions

γ	8.01	11.40	16.34	23.21	33.16	47.44	67.78	96.73	137.82	194.52
pH	η									
2.79	4.99	3.70	2.65	2.02	1.48	1.12	0.86	0.66	0.51	0.40
2.87	9.97	7.20	5.24	3.88	2.89	2.14	1.62	1.75	0.94	0.73
2.99	15.67	11.21	8.31	6.19	4.61	3.44	2.59	2.83	1.52	1.19
3.15	29.07	21.01	15.22	11.11	8.12	5.67	4.36	4.63	2.46	1.92
3.38	33.34	24.41	17.32	12.68	9.29	6.86	5.08	5.42	2.85	2.13
3.64	36.34	26.71	19.48	14.40	10.63	7.82	5.86	6.26	3.34	2.59
4.08	39.47	29.22	21.86	18.68	14.11	11.06	8.67	9.43	5.09	3.96
4.38	42.32	31.12	22.56	17.20	13.01	9.86	6.36	6.90	3.73	2.93
4.51	41.04	30.12	22.63	16.96	12.90	9.74	6.31	6.82	3.67	2.84
4.57	42.46	31.92	23.81	18.04	13.80	10.54	6.75	7.37	4.00	3.12
5.01	43.32	32.82	24.86	18.09	13.25	10.05	6.48	7.04		
6.45	41.32	31.32	23.95	18.53	14.42	11.18	7.05	7.83		
6.57	36.91	27.81	20.74	15.88	12.18	9.31	7.21	7.86		
6.64	33.77	25.71	19.00	14.45	11.11	8.54	6.65	7.66		
6.88	38.62	29.11	22.07	16.47	11.91	9.16	7.10	8.10		
7.02	38.05	27.91	20.32	15.24	11.42	8.73	6.82	7.54		
7.15	35.77	26.31	19.76	16.12	12.15	9.36	6.82	7.52		
7.43	32.99	25.01	19.00	14.65	11.25	8.79	5.50	6.15		
7.57	35.77	25.41	18.86	14.40	11.15	8.49	4.23	4.23		
11.36	34.77	26.41	20.04	15.48	11.97	9.19	5.86	6.43		
12.3	31.06	23.21	17.46	13.39	10.29	7.93	5.03	5.55		
12.53	22.94	17.21	12.92	9.78	7.16	5.44	3.50	3.80		
12.68	15.10	11.41	8.59	6.59	5.06	3.90	2.47	2.73		

Appendix B3: Least Squares Regression Data to fit the Herschel-Bulkley Equation

pH 6.57

γ	τexp	τcalc	error	(error)^2	Ty	209.84488
8.0071878	295.519	298.77037	-0.011002	0.000121	K	29.524454
11.404177	317.198	317.10191	0.0003029	9.177E-08	n	0.53
16.337898	338.877	339.61534	-0.002179	4.747E-06	error sum	7.81E-04
23.212757	368.543	366.16578	0.0064503	4.161E-05		
33.161081	403.914	398.69405	0.0129234	0.000167		
47.436522	441.567	438.15317	0.0077312	5.977E-05		
67.778014	488.348	485.68597	0.0054511	2.971E-05		
96.733299	532.847	542.91614	-0.018897	0.0003571		
137.82069				0.0007811		
194.51805						

pH 6.64

γ	τexp	τcalc	error	(error)^2	Ty	204.32427
8.0071878	270.417	272.72464	-0.008534	7.282E-05	K	19.300338
11.404177	293.237	289.1383	0.0139774	0.0001954	n	0.6081967
16.337898	308.07	309.86664	-0.005832	3.401E-05	error sum	4.78E-04
23.212757	335.454	335.00014	0.001353	1.831E-06		
33.161081	368.543	366.65706	0.0051173	2.619E-05		
47.436522	405.055	406.14752	-0.002697	7.275E-06		
67.778014	450.695	455.06627	-0.009699	9.407E-05		
96.733299	519.155	515.62896	0.0067919	4.613E-05		
137.82069				0.0004777		
194.51805						

pH 6.88

γ	τexp	τcalc	error	(error)^2	Ty	222.56083
8.0071878	309.211	312.83539	-0.011721	0.0001374	K	31.902549
11.404177	332.031	330.29596	0.0052255	2.731E-05	n	0.5
16.337898	360.556	351.51146	0.025085	0.0006293	error sum	2.76E-03
23.212757	382.235	376.2661	0.0156158	0.0002439		
33.161081	394.786	406.27376	-0.029099	0.0008467		
47.436522	434.721	442.28701	-0.017404	0.0003029		
67.778014	481.502	485.20624	-0.007693	5.918E-05		
96.733299	548.821	536.33225	0.0227556	0.0005178		
137.82069				0.0027645		
194.51805						

pH 7.02

γ	τexp	τcalc	error	(error)^2	Ty	217.17789
8.0071878	304.647	299.74058	0.0161053	0.0002594	K	29.177214
11.404177	318.339	315.70955	0.0082599	6.823E-05	n	0.5
16.337898	332.031	335.11266	-0.009281	8.614E-05	error sum	1.21E-03
23.212757	353.71	357.7526	-0.011429	0.0001306		
33.161081	378.812	385.1968	-0.016855	0.0002841		
47.436522	414.183	418.13355	-0.009538	9.098E-05		
67.778014	462.105	457.38632	0.0102113	0.0001043		
96.733299	511.168	504.14481	0.0137395	0.0001888		
137.82069				0.0012125		
194.51805						

pH 7.15

γ	τexp	τcalc	error	(error)^2	Ty	192.8076
8.0071878	266.391	268.96821	-0.009069	8.224E-05	K	33.989717
11.404177	300.083	307.59111	-0.02502	0.000626	n	0.5
16.337898	322.903	330.1946	-0.022581	0.0005099	error sum	7.80E-03
23.212757	374.248	356.56876	0.0472394	0.0022316		
33.161081	402.773	388.53962	0.0353385	0.0012488		
47.436522	443.849	426.90697	0.0381662	0.0014567		
67.778014	462.105	472.63611	-0.022789	0.0005194		
96.733299	510.027	527.10696	-0.033488	0.0011215		
137.82069				0.007796		
194.51805						

pH 7.43

γ	τexp	τcalc	error	(error)^2	Ty	168.64737
8.0071878	230.482	232.42704	-0.008439	7.122E-05	K	20.312729
11.404177	245.315	246.12091	-0.003285	1.079E-05	n	0.55
16.337898	264.1415	263.05915	0.0040976	1.679E-05	error sum	3.05E-04
23.212757	285.25	283.17703	0.0072672	5.281E-05		
33.161081	310.352	307.99964	0.0075797	5.745E-05		
47.436522	340.018	338.32724	0.0049726	2.473E-05		
67.778014	373.107	375.12221	-0.005401	2.917E-05		
96.733299	417.0355	419.74064	-0.006487	4.208E-05		
137.82069				0.000305		
194.51805						

Appendix B3: Least Squares Regression Data to fit the Herschel-Bulkley Equation

pH 4.08

γ	τexp	τcalc	error	(error)^2	Ty	239.7807
8.007188	316.057	326.8702	-0.03421	0.001171	K	24.99642
11.40418	333.172	347.456	-0.04287	0.001838	n	0.6
16.3379	357.133	373.3773	-0.04549	0.002069	error sum	2.62E-02
23.21276	433.58	404.7161	0.066571	0.004432		
33.16108	467.81	444.0744	0.050738	0.002574		
47.43652	524.86	493.0284	0.060648	0.003678		
67.77801	587.615	553.4927	0.058069	0.003372		
96.7333	638.96	628.1308	0.016948	0.000287		
137.8207	701.715	720.0297	-0.0261	0.000681		
194.518	770.175	830.3267	-0.0781	0.0061		
				0.026202		

pH 4.38

γ	τexp	τcalc	error	(error)^2	Ty	246.3327
8.007188	303.506	307.4186	-0.01289	0.000166	K	19.67444
11.40418	321.762	319.5637	0.006832	4.67E-05	n	0.528603
16.3379	338.877	334.4719	0.012999	0.000169	error sum	6.50E-04
23.21276	354.851	352.0447	0.007908	6.25E-05		
33.16108	368.543	373.5633	-0.01362	0.000186		
47.43652	399.35	399.654	-0.00076	5.79E-07		
67.77801	431.296	431.0672	0.000535	2.86E-07		
96.7333	467.81	468.8705	-0.00227	5.14E-06		
137.8207	513.45	514.2518	-0.00156	2.44E-06		
194.518	569.359	567.3781	0.003479	1.21E-05		
				0.00065		

pH 4.51

γ	τexp	τcalc	error	(error)^2	Ty	236.2607
8.007188	303.506	301.2943	0.007287	5.31E-05	K	23.05056
11.40418	312.634	313.8336	-0.00384	1.47E-05	n	0.498579
16.3379	328.608	329.0623	-0.00138	1.91E-06	error sum	2.45E-04
23.21276	343.441	346.8223	-0.00985	9.69E-05		
33.16108	369.684	368.3401	0.003635	1.32E-05		
47.43652	393.645	394.1513	-0.00129	1.65E-06		
67.77801	427.875	424.8965	0.006961	4.85E-05		
96.7333	462.105	461.5021	0.001305	1.7E-06		
137.8207	505.463	504.9801	0.000955	9.13E-07		
194.518	553.385	555.3477	-0.00355	1.26E-05		
				0.000245		

pH 4.57

γ	τexp	τcalc	error	(error)^2	Ty	222.9105
8.007188	309.211	307.2158	0.006453	4.16E-05	K	31.27937
11.40418	320.621	322.6926	-0.00646	4.17E-05	n	0.476598
16.3379	340.018	341.3413	-0.00389	1.51E-05	error sum	1.31E-04
23.21276	363.979	362.921	0.002907	8.45E-06		
33.16108	389.081	388.864	0.000558	3.11E-07		
47.43652	418.747	419.7399	-0.00237	5.62E-06		
67.77801	457.541	456.2301	0.002865	8.21E-06		
96.7333	499.758	499.3369	0.000843	7.1E-07		
137.8207	551.103	550.1388	0.00175	3.06E-06		
194.518	607.012	608.5412	-0.00252	6.35E-06		
				0.000131		

pH 5.01

γ	τexp	τcalc	error	(error)^2	Ty	231.5087
8.007188	306.929	314.427	-0.02443	0.000597	K	32.51505
11.40418	325.185	328.7304	-0.0109	0.000119	n	0.45
16.3379	346.864	345.8025	0.00306	9.37E-06	error sum	4.01E-03
23.21276	374.248	365.372	0.023717	0.000562		
33.16108	406.196	388.6779	0.043127	0.00186		
47.43652	419.888	416.1527	0.008896	7.91E-05		
67.77801	439.285	448.3163	-0.02056	0.000423		
96.7333	476.938	485.9535	-0.0189	0.000357		
137.8207				0.004007		
194.518						

pH 6.45

γ	τexp	τcalc	error	(error)^2	Ty	212.7222
8.007188	295.519	293.4502	0.007001	4.9E-05	K	25.53398
11.40418	309.211	310.8978	-0.00546	2.98E-05	n	0.553311
16.3379	330.89	332.5047	-0.00488	2.38E-05	error sum	1.80E-04
23.21276	357.133	358.1979	-0.00298	8.89E-06		
33.16106	391.363	389.9367	0.003644	1.33E-05		
47.43652	430.157	428.7603	0.003247	1.05E-05		
67.77801	478.079	475.9188	0.004518	2.04E-05		
96.7333	530.565	533.1718	-0.00491	2.41E-05		
137.8207				0.00018		
194.518						

Appendix B3: Least Squares Regression Data to fit the Herschel-Bulkley Equation

pH 7.57

γ	τexp	τcalc	error	(error)^2	Ty	174.1854
8.007188	266.391	276.294	0.035256	0.001243	K	40.04023
11.40418	289.814	293.9077	-0.01413	0.0002	n	0.45
16.3379	306.07	314.931	-0.02227	0.000496	error sum	2.30E-03
23.21276	334.313	339.0295	-0.01411	0.000199		
33.16108	369.684	367.7293	0.005288	2.8E-05		
47.43652	402.773	401.5628	0.003005	9.03E-06		
67.77801	440.426	441.1702	-0.00169	2.85E-06		
96.7333	492.912	487.5181	0.010943	0.00012		
137.8207				0.002297		
194.518						

pH 11.36

γ	τexp	τcalc	error	(error)^2	Ty	153.2824
8.007188	245.315	244.1502	0.004748	2.25E-05	K	35.03609
11.40418	259.007	260.1309	-0.00434	1.88E-05	n	0.458111
16.3379	278.404	279.2604	-0.00306	9.46E-06	error sum	1.03E-04
23.21276	301.224	301.2513	-9.1E-05	8.23E-09		
33.16108	327.467	327.5164	-0.00015	2.27E-08		
47.43652	359.415	358.5696	0.002352	5.53E-06		
67.77801	397.068	395.0278	0.005138	2.64E-05		
96.7333	435.862	437.814	-0.00448	2.01E-05		
137.8207				0.000103		
194.518						

pH 12.3

γ	τexp	τcalc	error	(error)^2	Ty	154.223
8.007188	212.226	218.6348	-0.0302	0.000912	K	22.7628
11.40418	237.328	231.0931	0.026271	0.00069	n	0.5
16.3379	248.738	246.2306	0.01008	0.000102	error sum	1.75E-03
23.21276	264.712	263.8933	0.003093	9.57E-06		
33.16108	285.25	285.3041	-0.00019	3.59E-08		
47.43652	310.9225	310.9999	-0.00025	6.2E-08		
67.77801	341.159	341.6232	-0.00136	1.85E-06		
96.7333	375.9595	378.1022	-0.0057	3.25E-05		
137.8207				0.001748		
194.518						

pH 12.53

γ	τexp	τcalc	error	(error)^2	Ty	128.4827
8.007188	164.304	166.9794	-0.01628	0.000265	K	13.60452
11.40418	173.432	174.4253	-0.00573	3.28E-05	n	0.5
16.3379	183.701	183.4724	0.001244	1.55E-06	error sum	1.77E-03
23.21276	196.252	194.0288	0.011328	0.000128		
33.16108	211.085	206.8253	0.02018	0.000407		
47.43652	227.059	222.1827	0.021476	0.000461		
67.77801	237.328	240.4852	-0.0133	0.000177		
96.7333	257.866	262.2874	-0.01715	0.000294		
137.8207				0.001767		
194.518						

pH 12.68

γ	τexp	τcalc	error	(error)^2	Ty	86.63429
8.007188	108.395	109.0977	-0.00648	4.2E-05	K	6.44744
11.40418	114.1	114.4075	-0.00269	7.26E-06	n	0.6
16.3379	120.946	121.0935	-0.00122	1.49E-06	error sum	3.02E-04
23.21276	130.074	129.1768	0.006897	4.76E-05		
33.16108	140.343	139.3287	0.007227	5.22E-05		
47.43652	152.894	151.9556	0.006137	3.77E-05		
67.77801	167.727	167.5514	0.001047	1.1E-06		
96.7333	184.842	186.8032	-0.01061	0.000113		
137.8207				0.000302		
194.518						

Appendix C1: Measured Torque and Power Data for 45wt% PEG Solution using HR1-B and DHR-1

HR1-B pumping downwards

rpm	readout	torque ++	Power	Po
10	49.34	0.075	0.078	74.131
12.7	49.15	0.096	0.128	59.193
15.3	48.97	0.116	0.186	49.421
18.9	48.68	0.149	0.295	41.505
22.3	48.46	0.174	0.406	34.783
26.9	48.12	0.212	0.598	29.182
31.2	47.8	0.249	0.812	25.385
35.2	47.55	0.277	1.020	22.209
39.5	47.23	0.313	1.295	19.941
44	46.85	0.356	1.640	18.275
49.9	46.45	0.401	2.096	16.013

HR1-B pumping upwards

rpm	readout	torque	Power	Po
9	50.78	0.088	0.083	108.160
12.6	51.04	0.118	0.155	73.578
14.8	51.2	0.136	0.210	61.534
19.1	51.47	0.166	0.332	45.259
23.2	51.83	0.207	0.502	38.188
28	52.14	0.242	0.709	30.659
32.8	52.52	0.285	0.978	26.309
38	52.86	0.323	1.286	22.246
42.3	53.18	0.359	1.592	19.962
46	53.52	0.398	1.916	18.685
50	53.74	0.423	2.213	16.803

DHR-1 pumping downwards

rpm	readout	torque	Power	Po
8.3	51.09	0.123	0.107	177.716
11.3	51.52	0.172	0.203	133.703
15.3	52.05	0.232	0.371	98.362
19.8	52.6	0.294	0.609	74.490
24.8	53.22	0.364	0.945	58.804
30	53.86	0.436	1.370	48.173
34.3	54.42	0.499	1.794	42.198
38	54.88	0.551	2.194	37.958
42.4	55.44	0.615	2.729	33.988
46.8	55.95	0.672	3.295	30.513
50	56.34	0.716	3.751	28.484

DHR-1 pumping upwards

rpm	readout	torque	Power	Po
10.4	48.77	0.139	0.151	127.730
16.6	48.02	0.224	0.389	80.706
24.6	47.01	0.338	0.870	55.495
30	46.35	0.412	1.296	45.552
36	45.62	0.495	1.866	37.960
40	45.13	0.550	2.305	34.187
46.8	44.28	0.646	3.167	29.333

Measured Torque (Nm) ++

Appendix D1: Measured Torque and Power Data for 1.48wt% Carbopol Solution using HR1-B and DHR-1

HR1-B pumping upwards

pH 2.79

rpm	rps	readout	torque	Power	Po
7.4	0.123	51.09	0.123	0.095	223.572
9.9	0.165	51.16	0.131	0.136	132.936
11.75	0.196	51.18	0.133	0.164	95.998
13.3	0.222	51.19	0.134	0.187	75.561
16	0.267	51.22	0.138	0.231	53.527
18.7	0.312	51.24	0.140	0.274	39.828
21.3	0.355	51.25	0.141	0.315	30.946
24.7	0.412	51.26	0.142	0.368	23.197
27.7	0.462	51.275	0.144	0.418	18.664
30.9	0.515	51.28	0.145	0.468	15.057
34.7	0.578	51.295	0.146	0.532	12.080
38.4	0.640	51.32	0.149	0.600	10.055
42.7	0.712	51.36	0.154	0.687	8.378
46.8	0.780	51.38	0.156	0.764	7.077
50.4	0.840	51.4	0.158	0.835	6.190

Measured Torque (Nm) ++

DHR-1 pumping upwards

pH 2.79

rpm	rps	readout	torque	Power	Po
4.2	0.070	48.72	0.145	0.064	815.017
5.1	0.085	48.65	0.153	0.081	582.973
6.1	0.102	48.6	0.158	0.101	422.594
8.3	0.138	48.55	0.164	0.142	236.411
10.7	0.178	48.52	0.167	0.187	145.194
14.4	0.240	48.46	0.174	0.262	83.416
16.5	0.275	48.42	0.179	0.308	65.185
17.2	0.287	48.41	0.180	0.324	60.366
21.5	0.358	48.37	0.184	0.415	39.606
23.9	0.398	48.32	0.190	0.475	33.035
24.8	0.413	48.31	0.191	0.496	30.863
28	0.467	48.27	0.195	0.573	24.785
29	0.483	48.26	0.197	0.597	23.239
31.8	0.530	48.22	0.201	0.670	19.771
33.6	0.560	48.2	0.203	0.716	17.908
36.2	0.603	48.18	0.206	0.780	15.599
40.5	0.675	48.14	0.210	0.891	12.737
40.9	0.682	48.12	0.212	0.910	12.623
48.3	0.805	48.07	0.218	1.103	9.292

Appendix D2: Measured Torque and Power Data for 1.48wt% Carbopol Solution using HR1-B and DHR-1

HR1-B pumping downwards
pH 11.5

rpm	rps	readout	torque ++	Power	Po
7.8	0.130	44.1	0.667	0.544	1089.226
10	0.167	43.92	0.687	0.719	682.903
12.5	0.208	43.65	0.717	0.939	456.467
15.5	0.258	43.41	0.745	1.209	308.090
20.3	0.338	43.14	0.775	1.648	186.977
24.2	0.403	42.82	0.811	2.056	137.705
31.6	0.527	42.3	0.870	2.879	86.611
36.4	0.607	42.05	0.898	3.424	67.394
40	0.667	41.83	0.923	3.867	57.353
44.5	0.742	41.52	0.958	4.465	48.098
50	0.833	41.33	0.980	5.129	38.952

HR1-B pumping upwards
pH 11.5

rpm	rps	readout	torque	Power	Po
4.7	0.078	56.28	0.710	0.349	3193.149
7	0.117	56.78	0.766	0.562	1554.135
9.8	0.163	57.15	0.808	0.829	836.198
11.4	0.190	57.35	0.830	0.991	635.233
13.2	0.220	57.55	0.853	1.179	486.692
16	0.267	57.88	0.890	1.492	345.734
18.4	0.307	58.09	0.914	1.761	268.391
20.5	0.342	58.25	0.932	2.001	220.496
23.6	0.393	58.52	0.963	2.379	171.819
27.1	0.452	58.78	0.992	2.815	134.280
32.3	0.538	59.15	1.034	3.497	98.508
38.2	0.637	59.55	1.079	4.316	73.508
43	0.717	59.85	1.113	5.011	59.835
46.5	0.775	60	1.130	5.502	51.946
50.2	0.837	60.2	1.152	6.058	45.462

DHR-1 pumping downwards
pH 11.5

rpm	rps	readout	torque	Power	Po
10.4	0.17333333	48.77	0.139	0.151	127.730
16.6	0.27666667	48.02	0.224	0.389	80.706
24.6	0.41	47.01	0.338	0.870	55.495
30	0.5	46.35	0.412	1.296	45.552
36	0.6	45.62	0.495	1.866	37.960
40	0.66666667	45.13	0.550	2.305	34.187
46.8	0.78	44.28	0.646	3.167	29.333

DHR-1 pumping upwards
pH11.5

rpm	rps	readout	torque	Power	Po
8.1	0.135	39.18	1.222	1.037	1852.305
11.8	0.197	38.16	1.338	1.653	955.087
15.1	0.252	37.43	1.420	2.246	619.208
20	0.333	36.37	1.540	3.225	382.729
25.3	0.422	35.41	1.648	4.367	256.017
30.5	0.508	34.5	1.751	5.593	187.149
34.6	0.577	33.84	1.826	6.616	151.616
39.1	0.652	33.21	1.897	7.767	123.354
45	0.750	32.38	1.991	9.381	97.732
50	0.833	31.75	2.062	10.796	81.993

Measured Torque (Nm) ++

Appendix E: Mixing Trials by Thermal Method

pH 2.79 1.48wt% Carbopol Solution								
Impeller:	HR1-B				DHR-1			
Pumping:	Up		Down		Up		Down	
Injection Vol.:	56ml.	200ml.	56ml.	200ml.	56ml.	200ml.	56ml.	200ml.
10rpm		E1			E7	E8	E9	
15rpm	E2**	E3	E4		E10	E11	E12	
20rpm		E5		E6	E13	E15	E14	
pH 11.5 1.48wt% Carbopol Solution								
Impeller:	HR1-B				DHR-1			
Pumping:	Up		Down		Up		Down	
Injection Vol.:	56ml.	200ml.	56ml.	200ml.	56ml.	200ml.	56ml.	200ml.
10rpm	E16		E17	E18	E25	E26	E27	
15rpm	E19		E20	E21		E28		E29
20rpm	E22		E23	E24	E30	E31	E32	

** Indicates Figure #

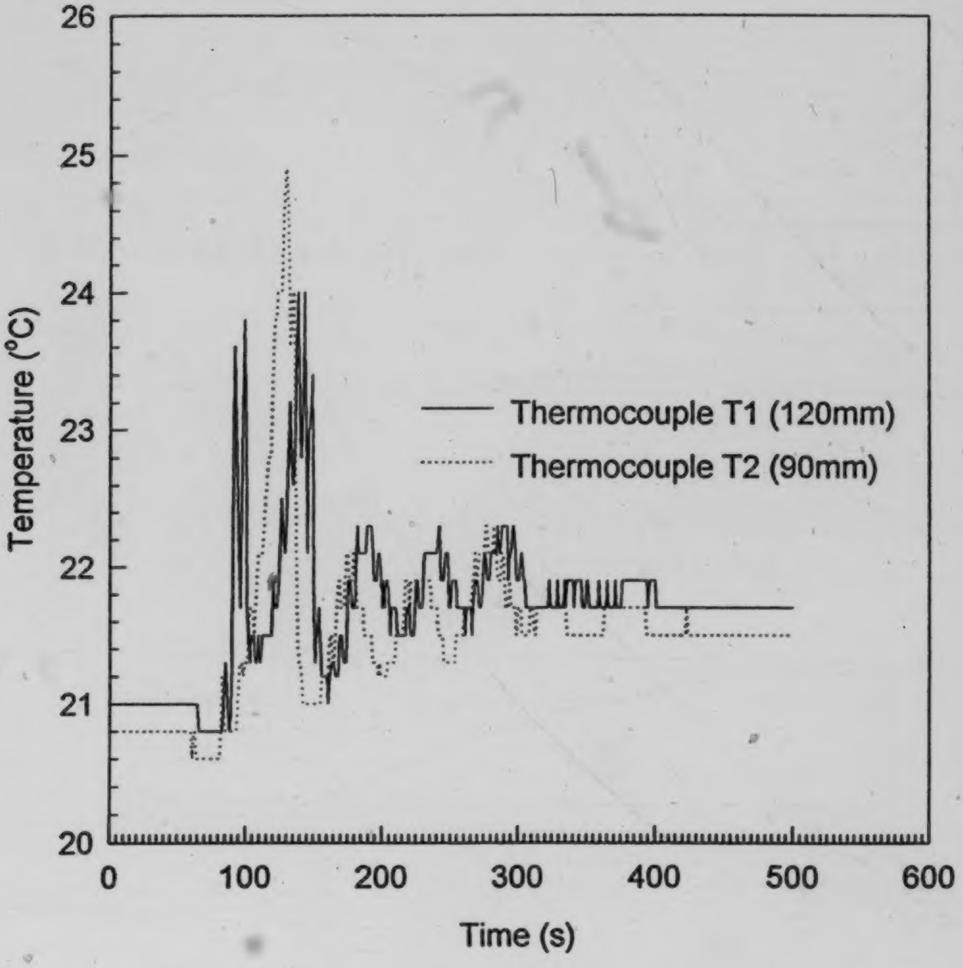

Figure E1 HR1-B Pumping Upwards; 10rpm
1.48wt% Carbopol; pH 2.79

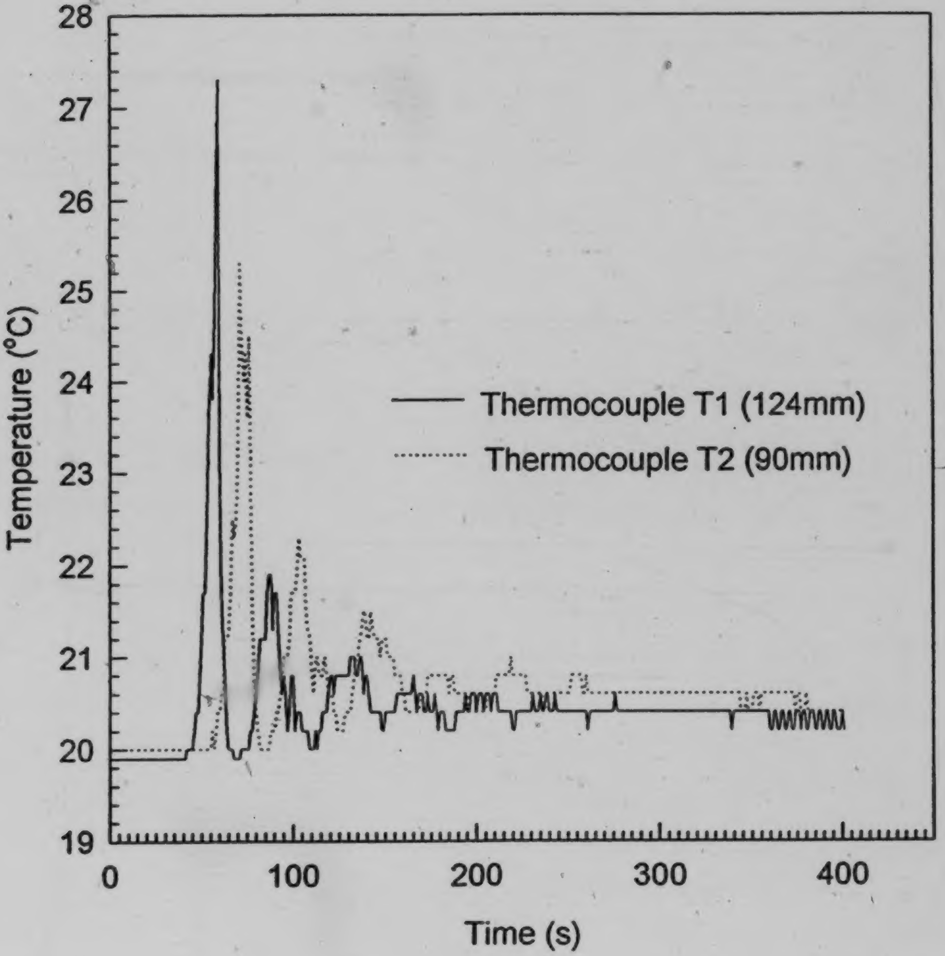

Figure E2 HR1-B Pumping Upwards; 15rpm
1.48wt% Carbopol; pH 2.79

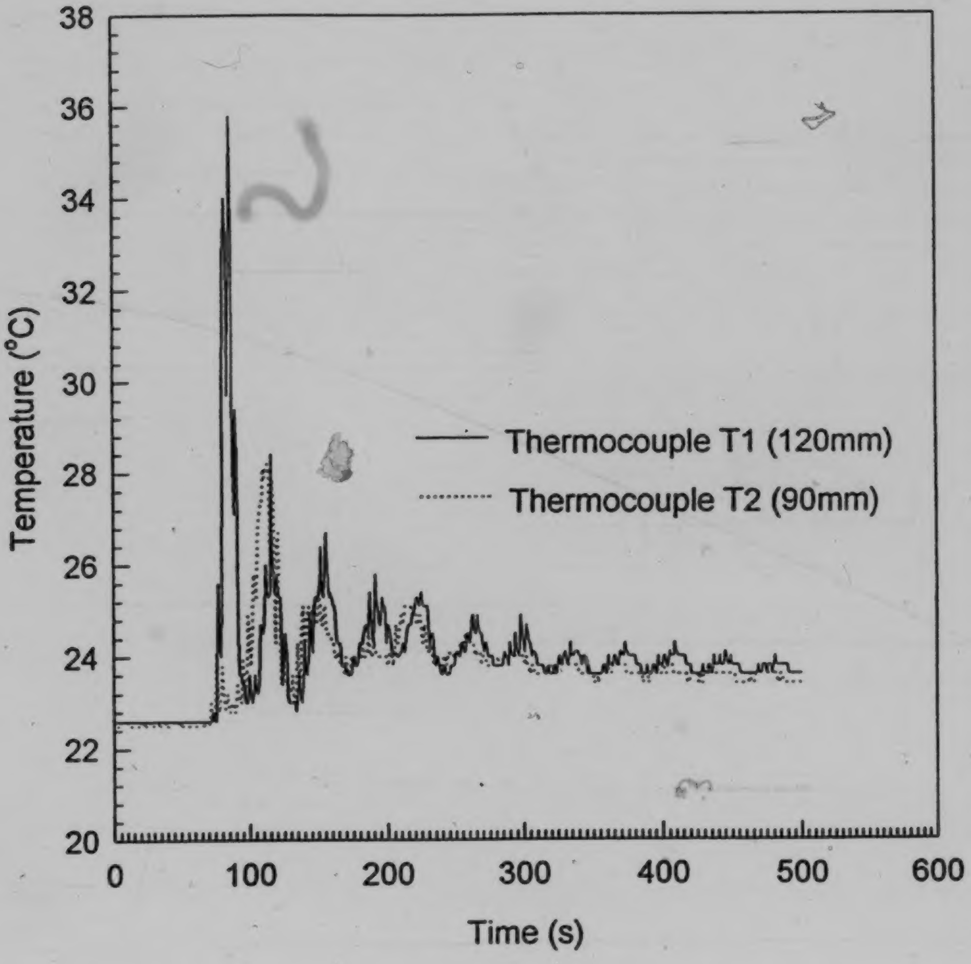

Figure E3 HR1-B Pumping Upwards; 15rpm
1.48wt% Carbopol; pH 2.79

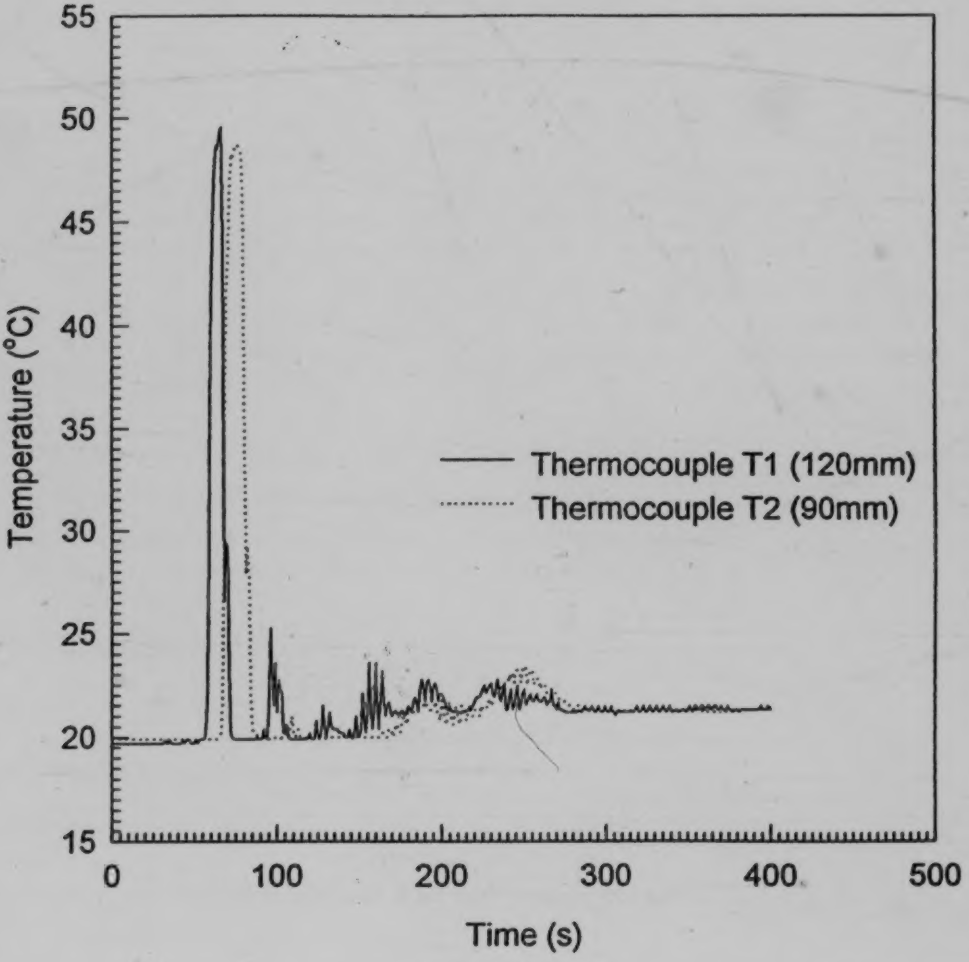

Figure E4 HR1-B Pumping Downwards; 15rpm
1.48wt% Carbopol; pH 2.79

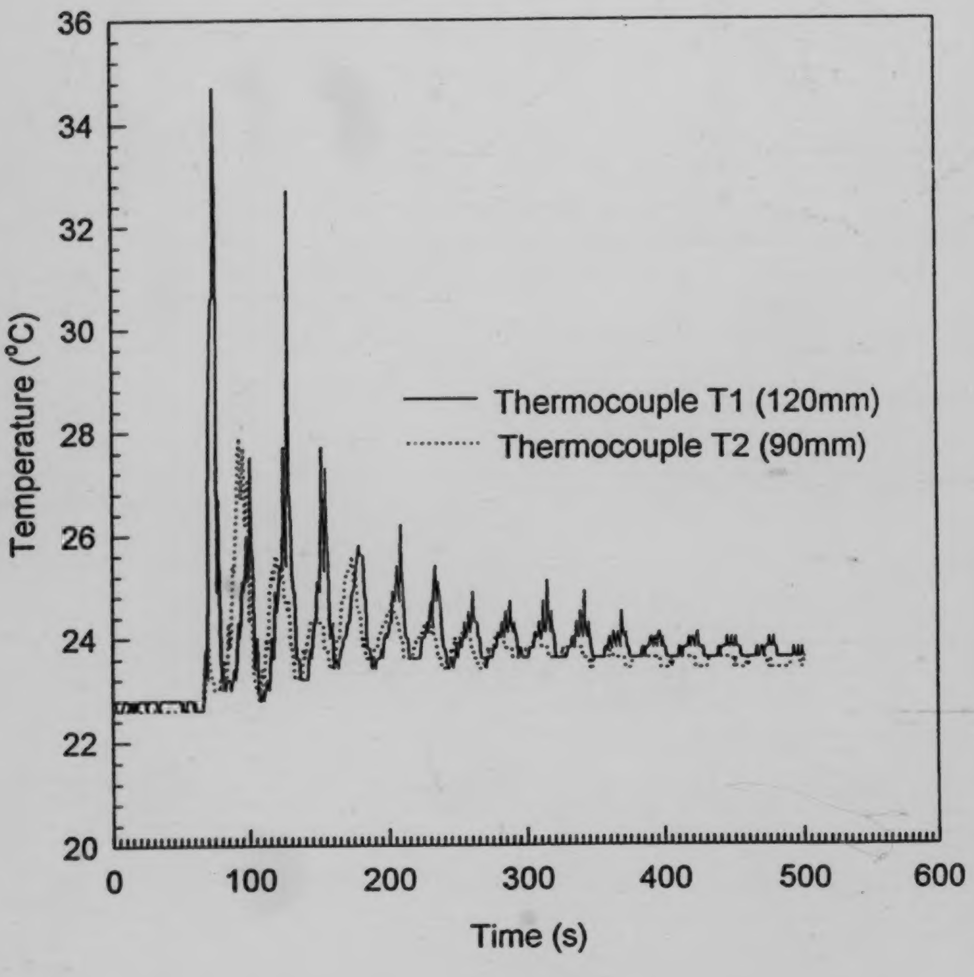

Figure E5 HR1-B Pumping Upwards; 20rpm
1.48wt% Carbopol; pH 2.79

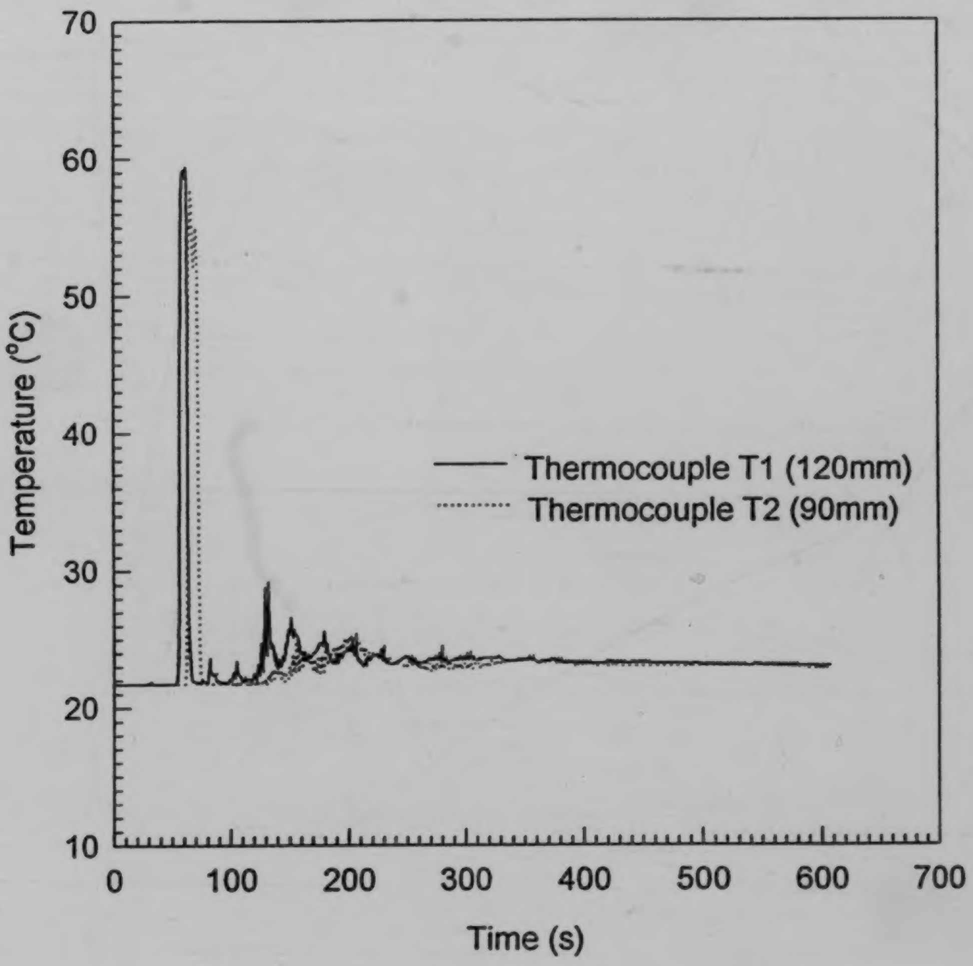

Figure E6 HR1-B Pumping Downwards; 20rpm
1.48wt% Carbopol; pH 2.79

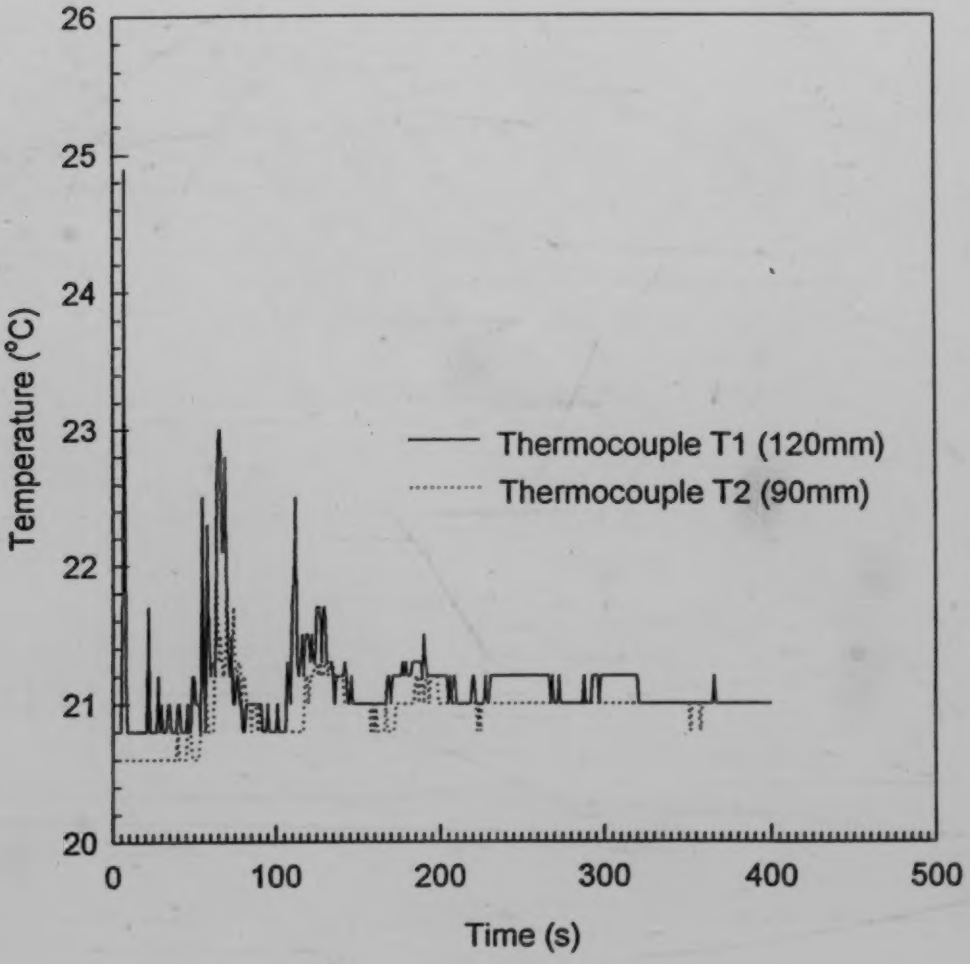

Figure E7 DHR-1 Pumping Upwards; 10rpm
1.48wt% Carbopol; pH 2.79

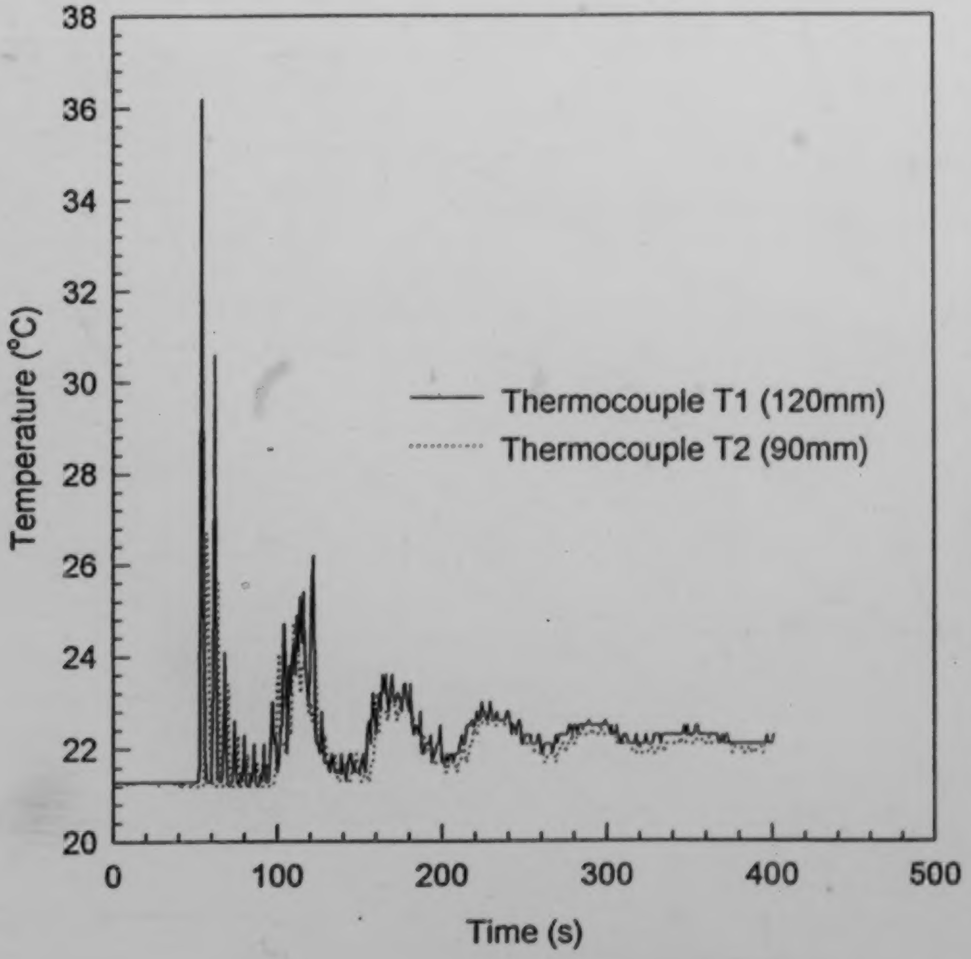

Figure E8 DHR-1 Pumping Upwards; 10rpm
1.48wt% Carbopol; pH 2.79

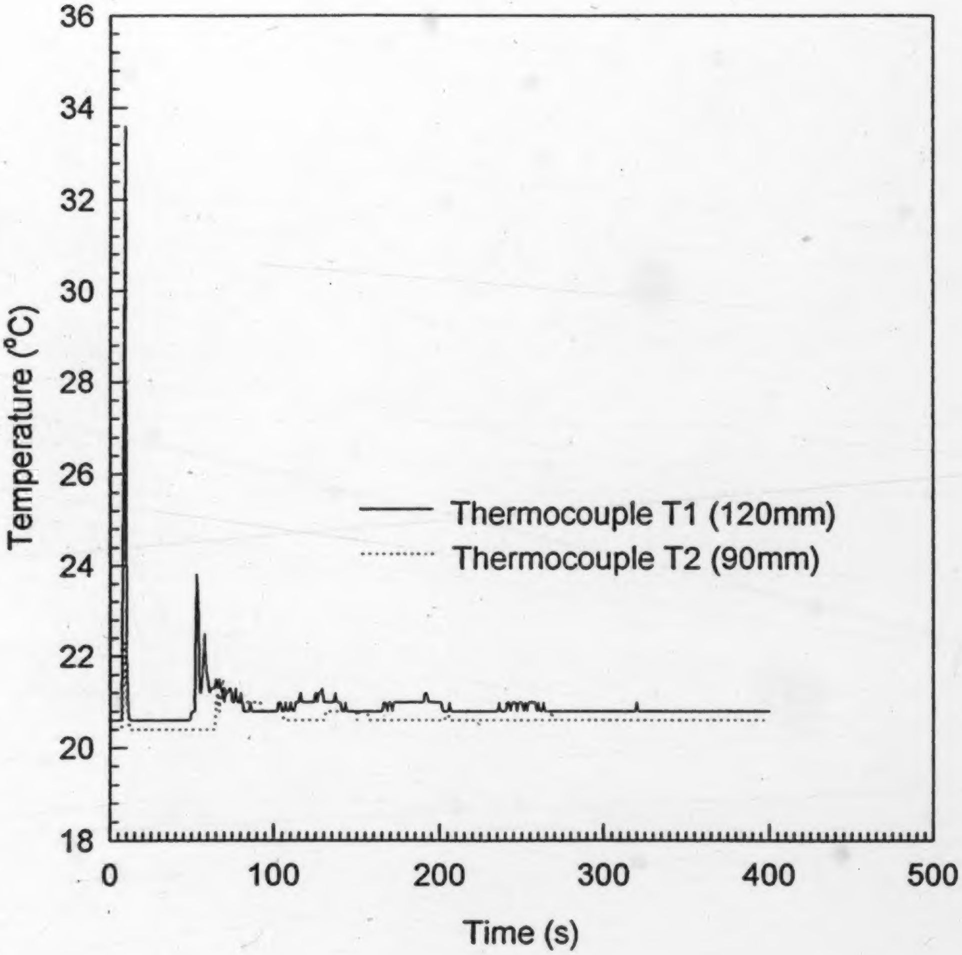

Figure E9 DHR-1 Pumping Downwards; 10rpm
1.48wt% Carbopol; pH 2.79

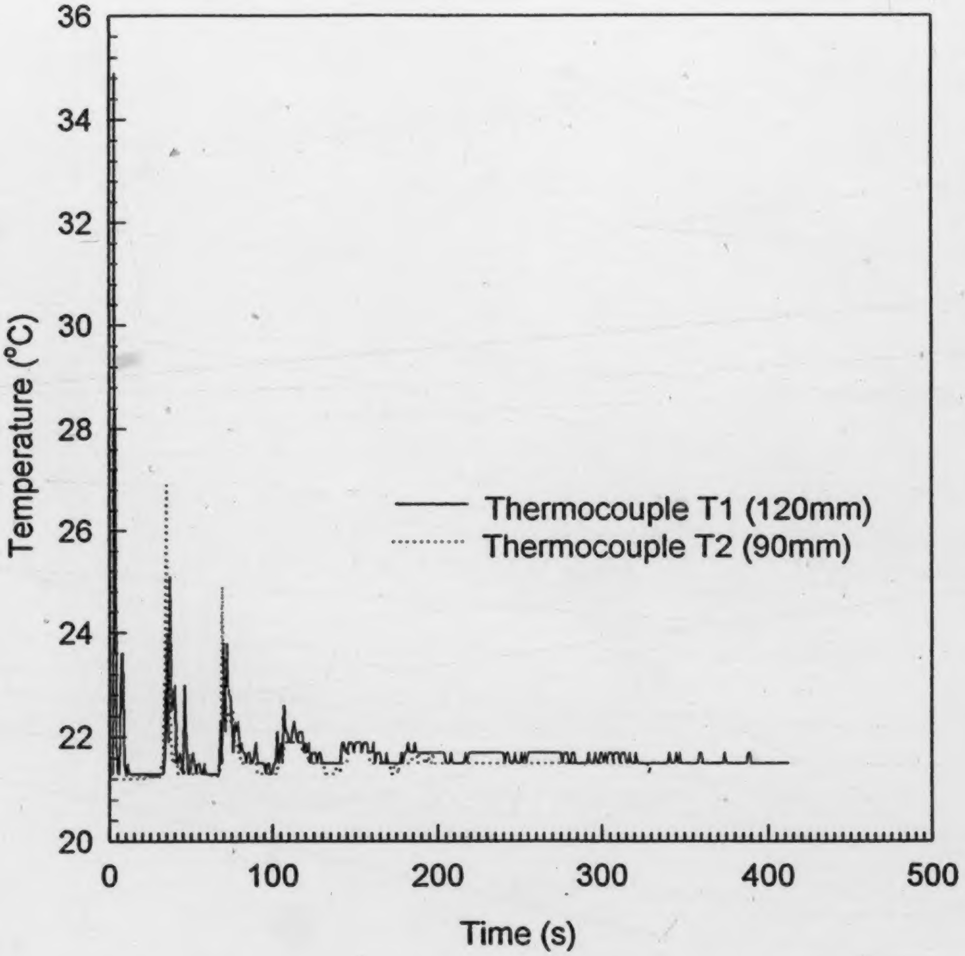

Figure E10 DHR-1 Pumping Upwards; 15rpm
1.48wt% Carbopol; pH 2.79

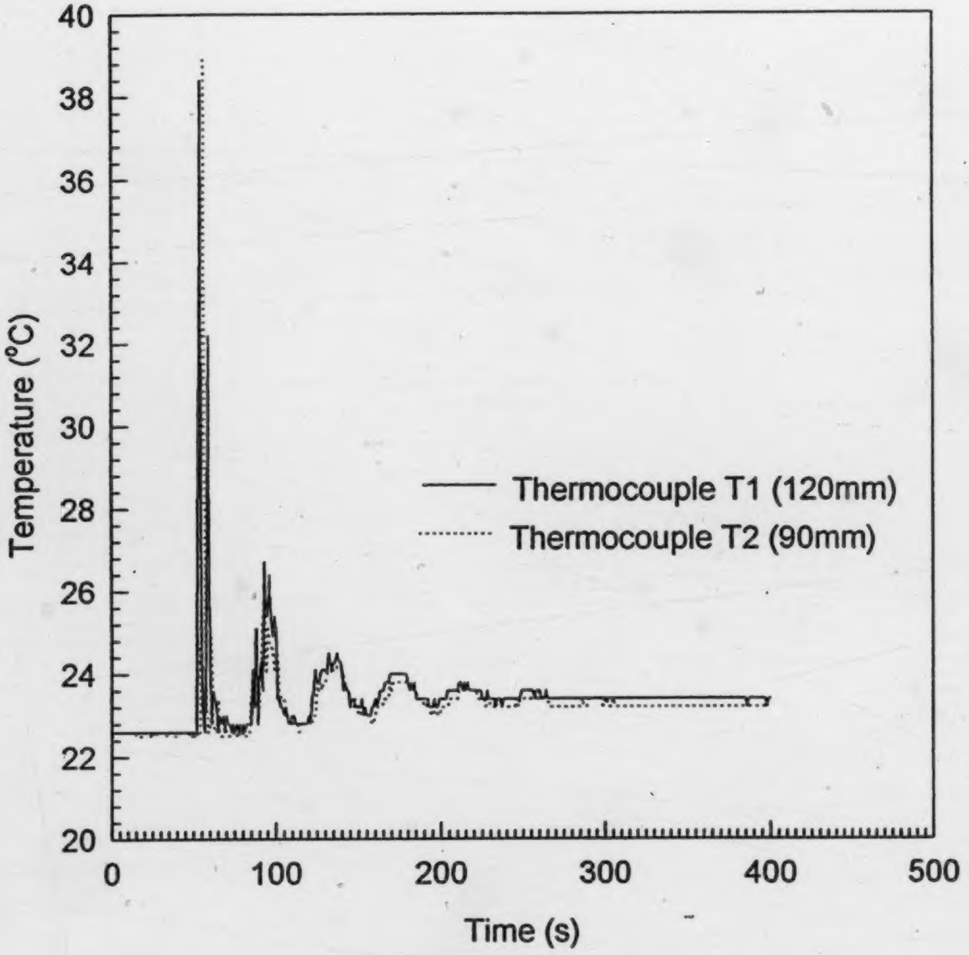

Figure E11 DHR-1 Pumping Upwards; 15rpm
1.48wt% Carbopol; pH 2.79

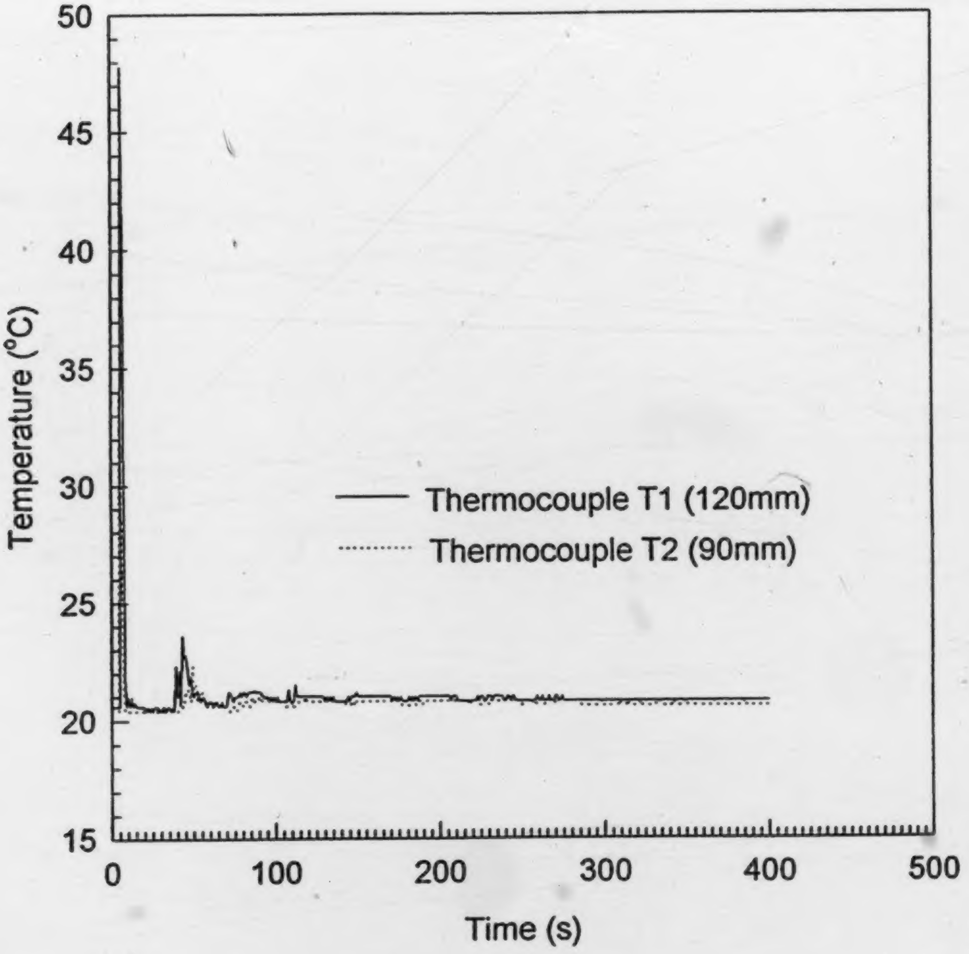

Figure E12 DHR-1 Pumping Downwards; 15rpm
1.48wt% Carbopol; pH 2.79

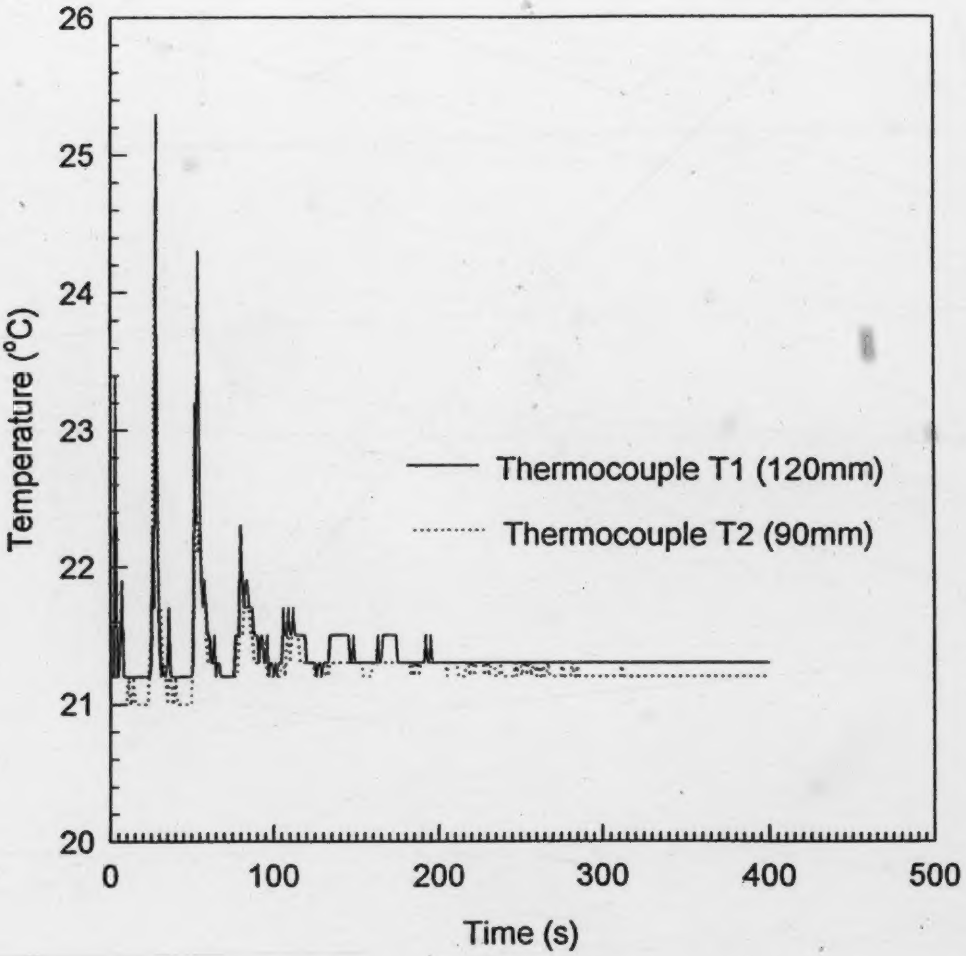

Figure E13 DHR-1 Pumping Upwards; 20rpm
1.48wt% Carbopol; pH 2.79

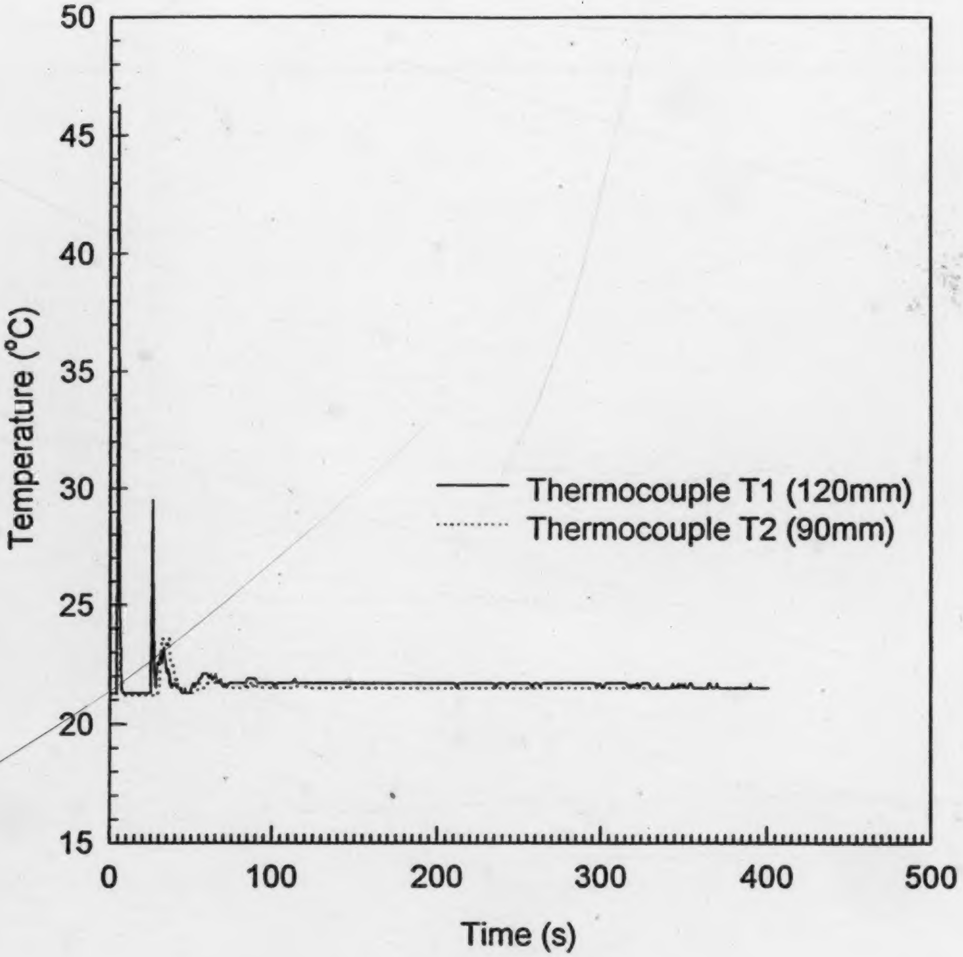

Figure E14 DHR-1 Pumping Downwards; 20rpm 1.48wt% Carbopol; pH 2.79

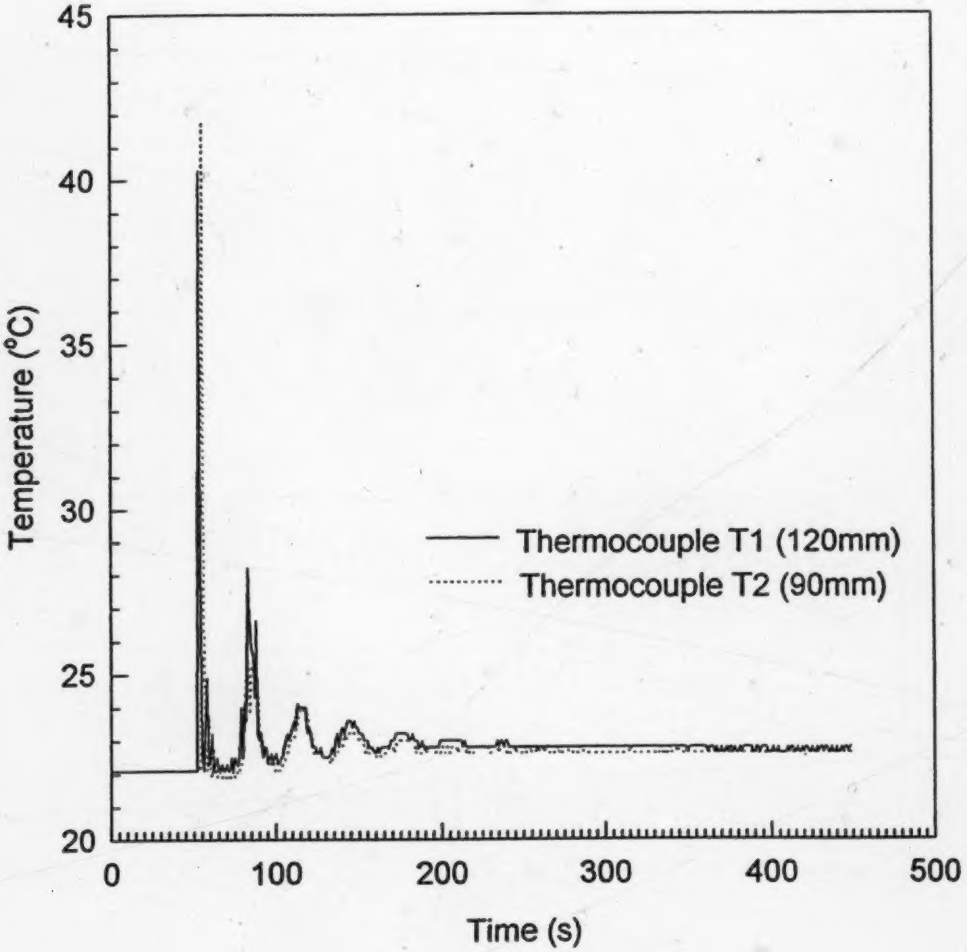

Figure E15 DHR-1 Pumping Upwards; 20rpm
1.48wt% Carbopol; pH 2.79

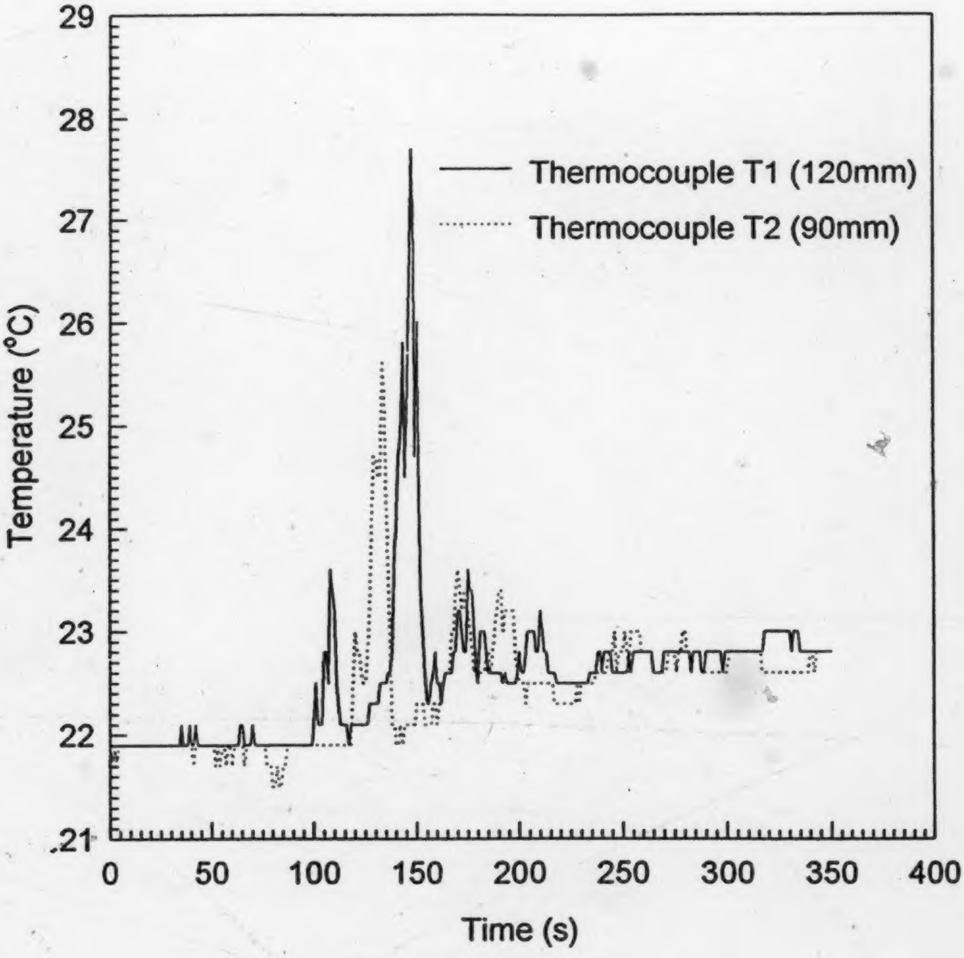

Figure E16 HR1-B Pumping Upwards; 10rpm 1.48wt% Carbopol; pH 11.5

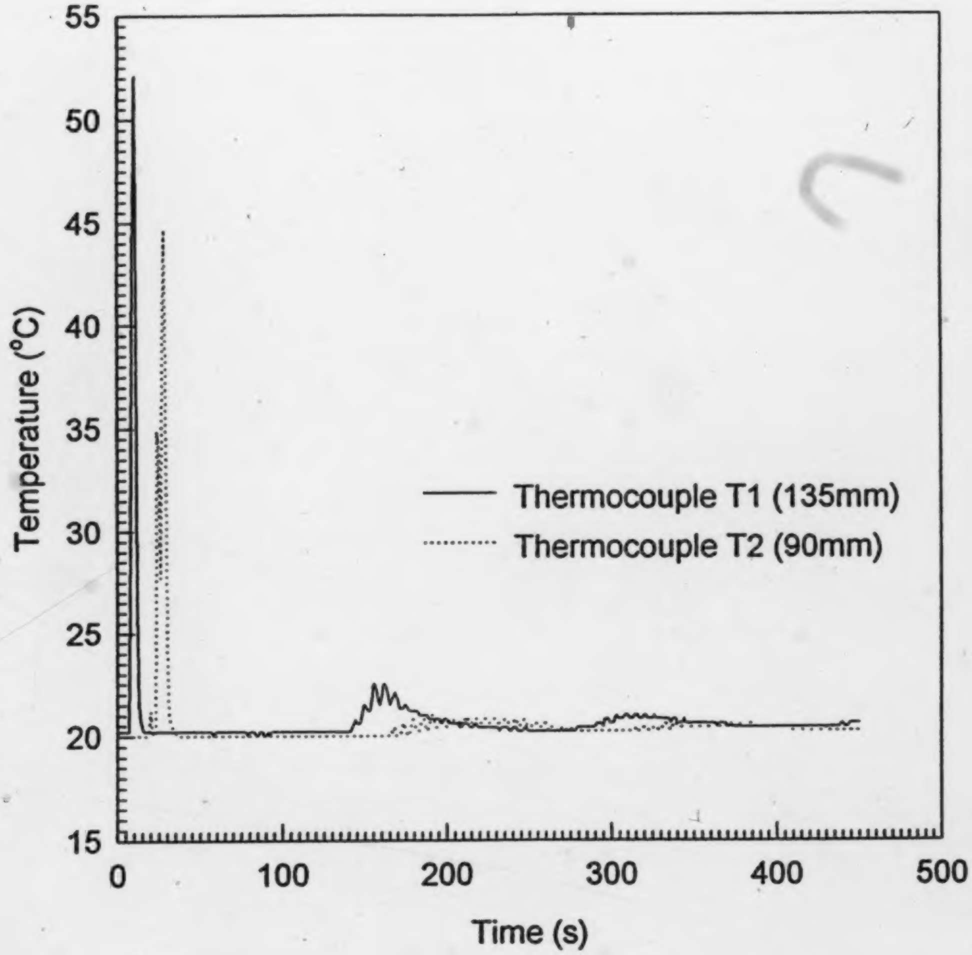

Figure E17 HR1-B Pumping Downwards; 10rpm
1.48wt% Carbopol; pH 11.5

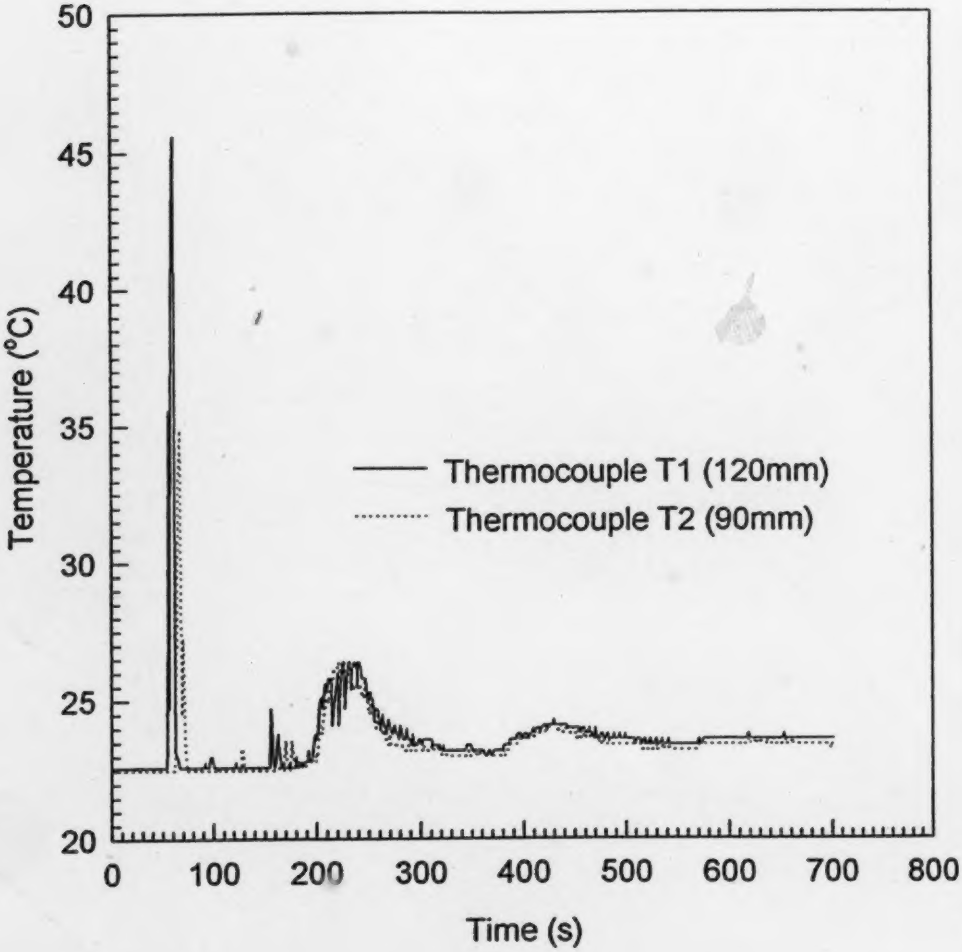

Figure E18 HR1-B Pumping Downwards; 10rpm
1.48wt% Carbopol; pH 11.5

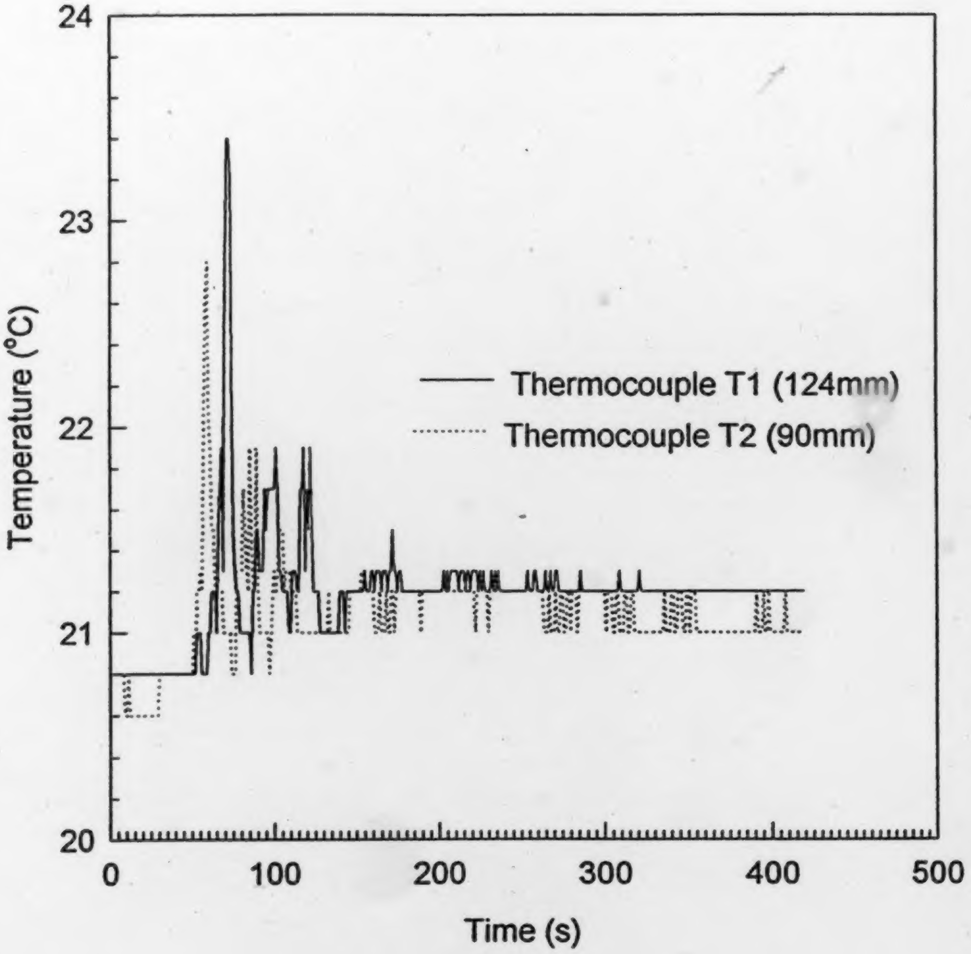

Figure E19 HR1-B Pumping Upwards; 15rpm
1.48wt% Carbopol; pH 11.5

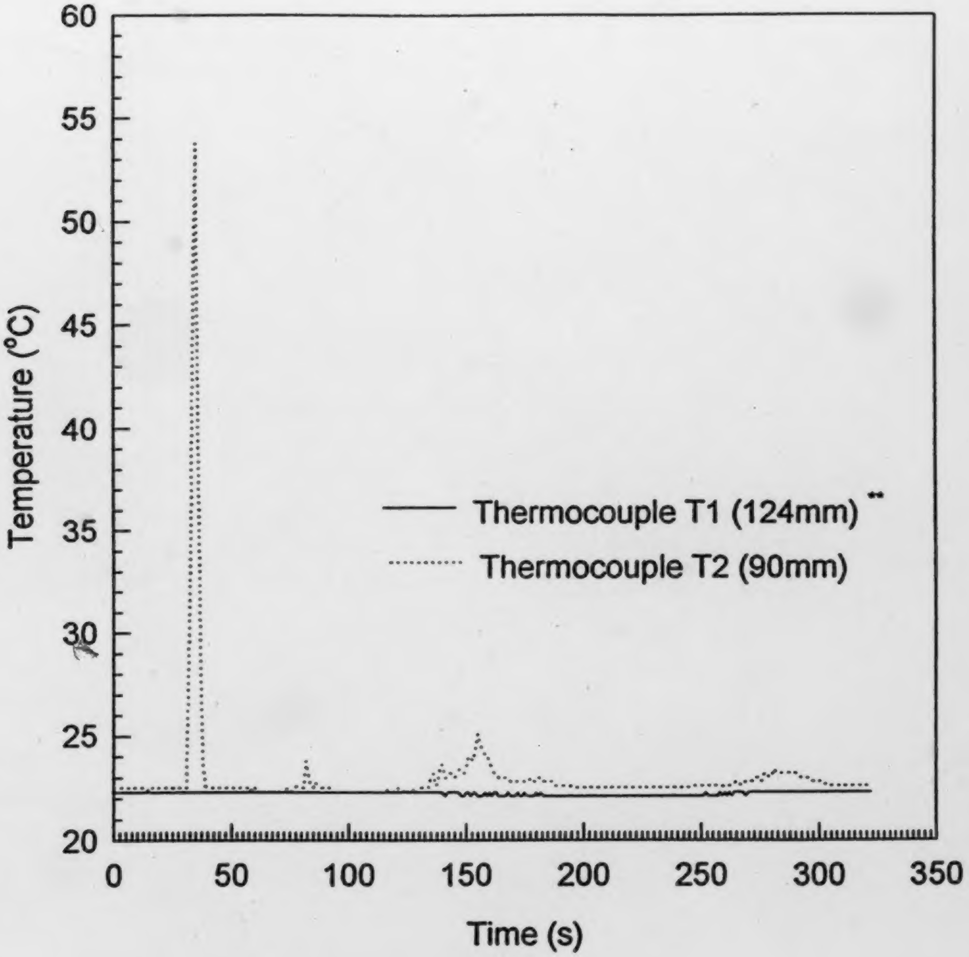

** Thermocouple located at the vessel wall

Figure E20 HR1-B Pumping Downwards; 15rpm
1.48wt% Carbopol; pH 11.5

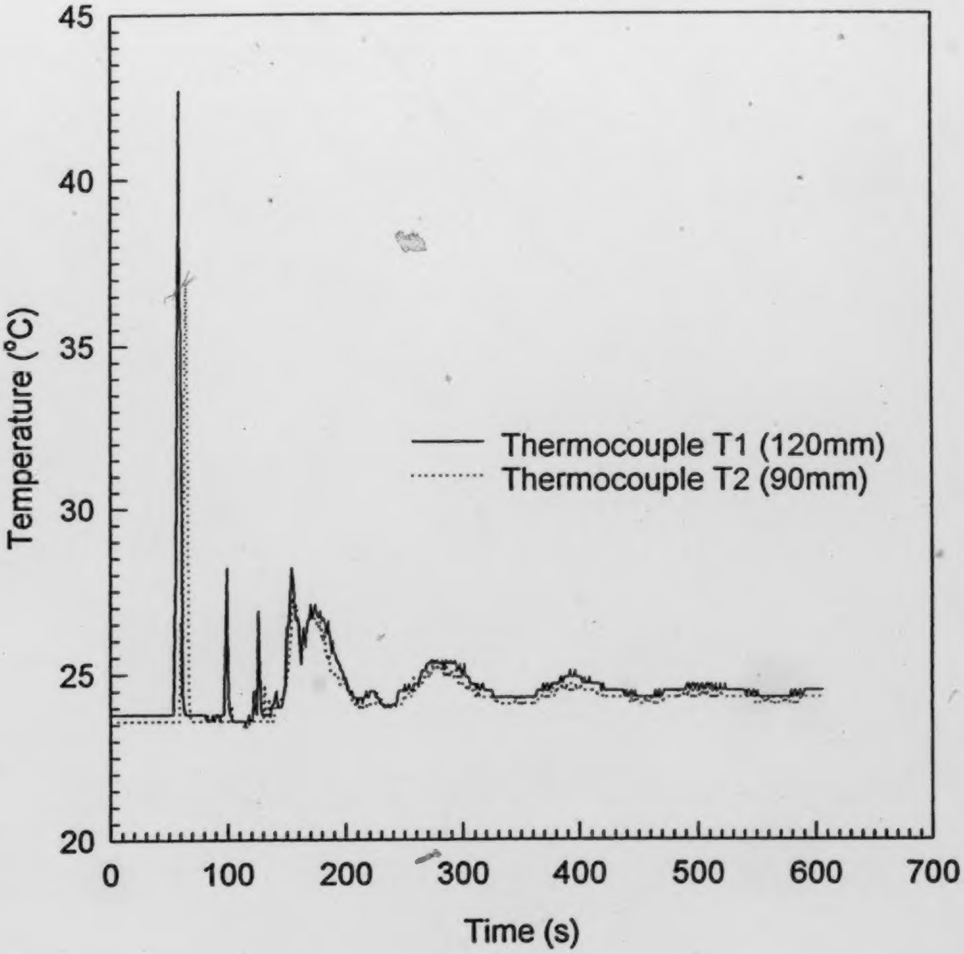

Figure E21 HR1-B Pumping Downwards; 15rpm
1.48wt% Carbopol; pH 11.5

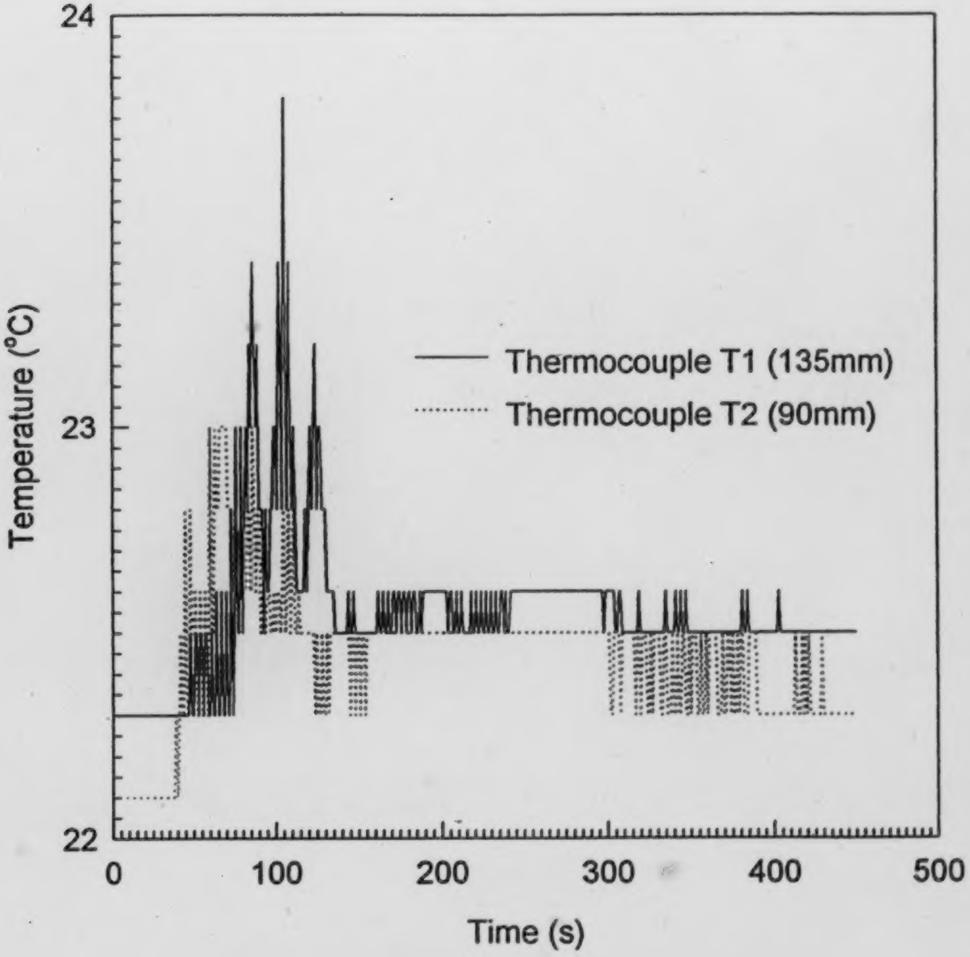

Figure E22 HR1-B Pumping Upwards; 20rpm
1.48wt% Carbopol; pH 11.5

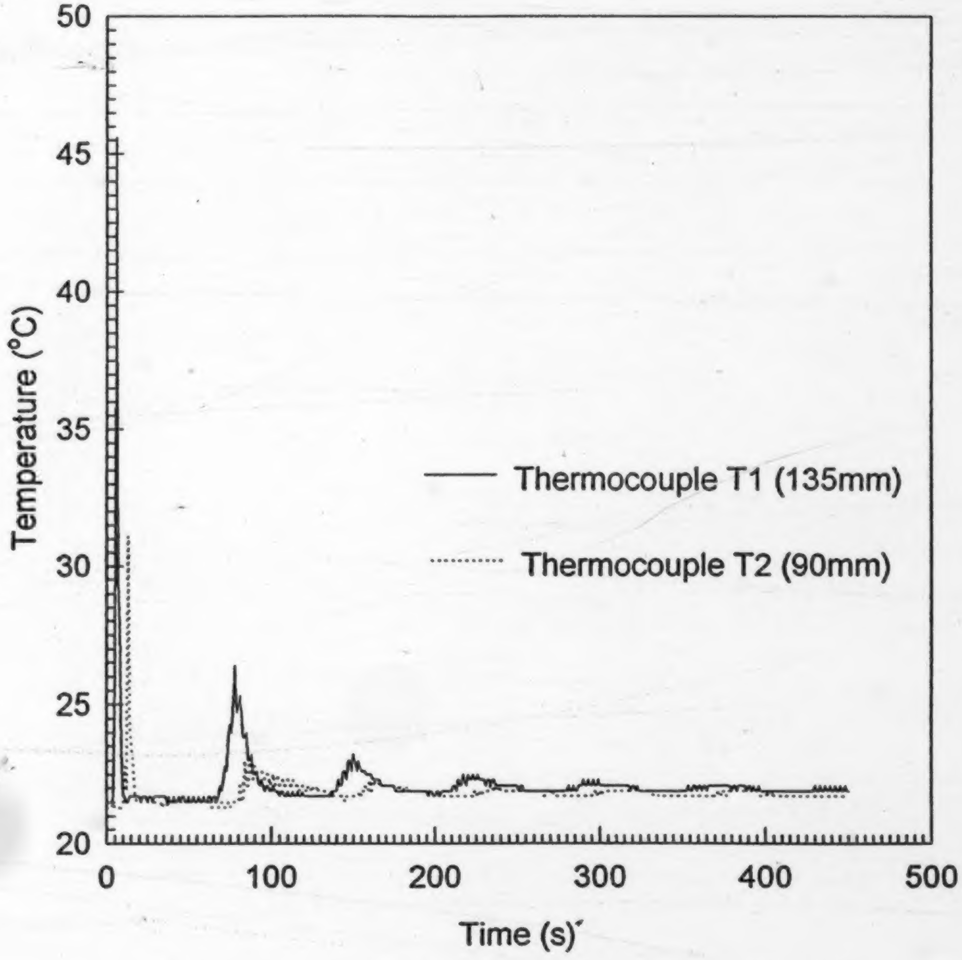

Figure E23 HR1-B Pumping Downwards; 20rpm
1.48wt% Carbopol; pH 11.5

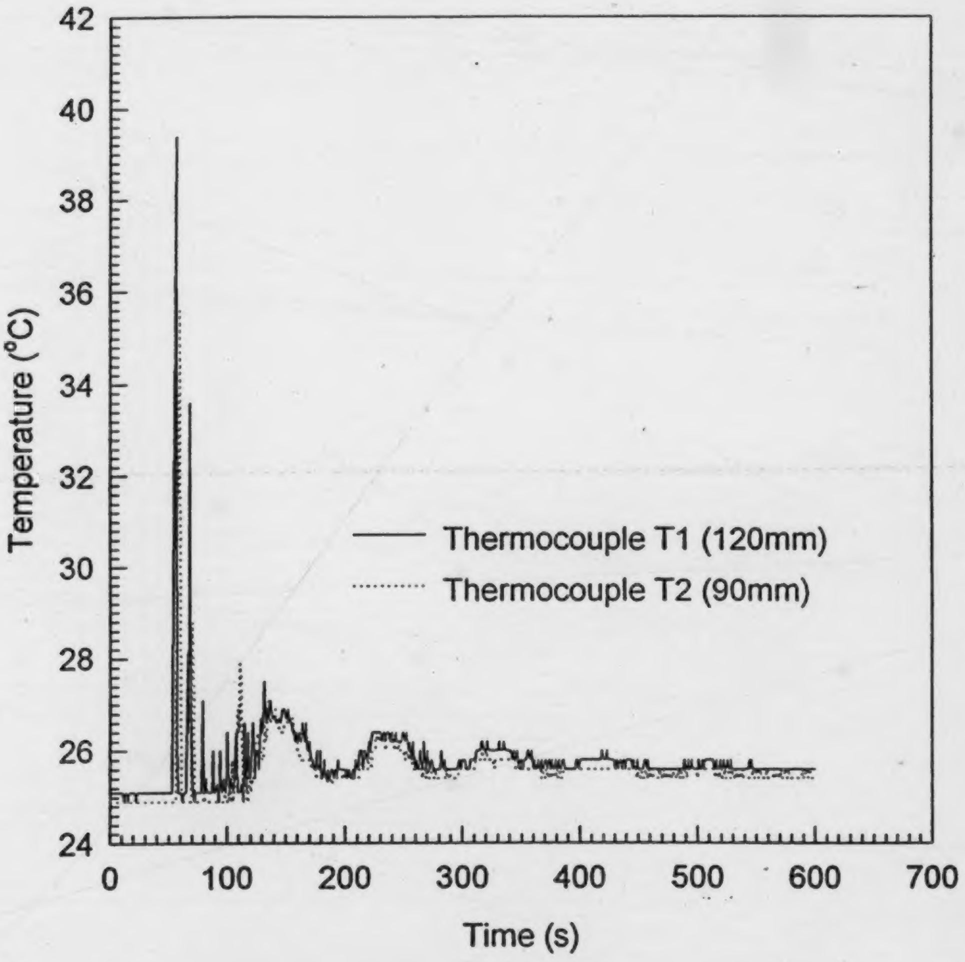

Figure E24 HR1-B Pumping Downwards; 20rpm
1.48 wt% Carbopol; pH 11.5

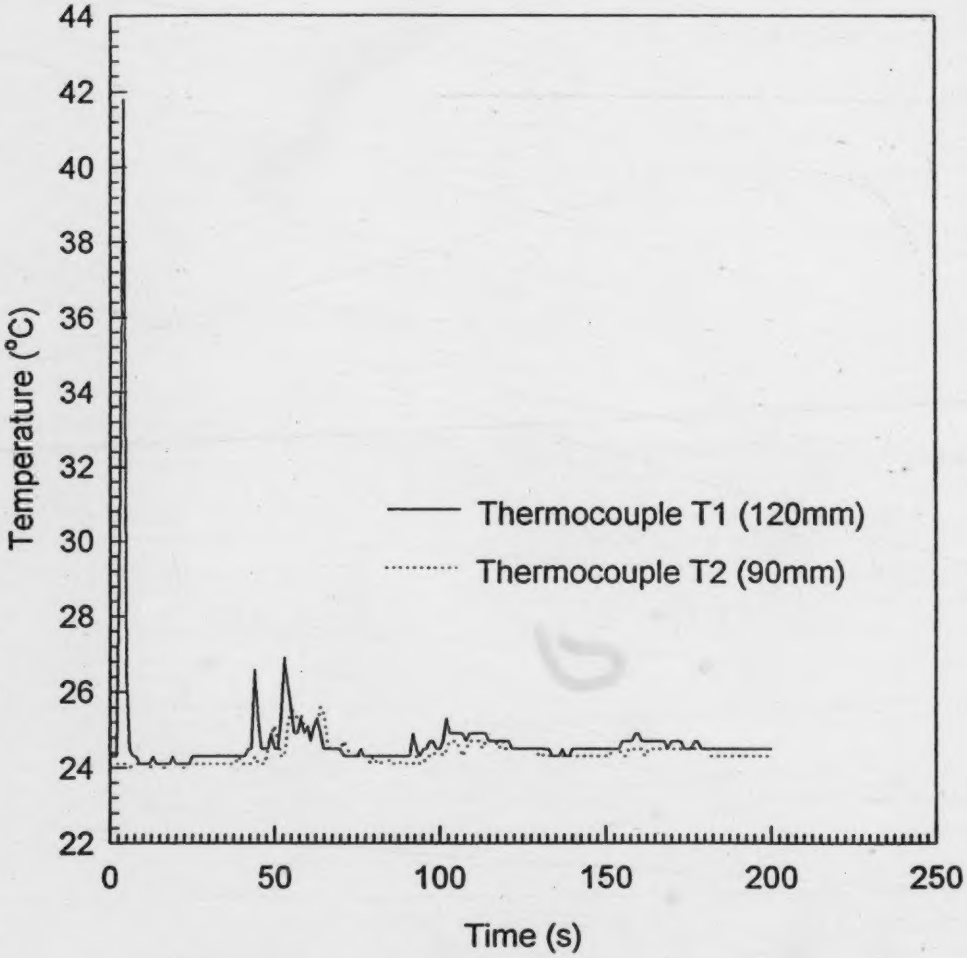

Figure E25 DHR-1 Pumping Upwards; 10rpm
1.48wt% Carbopol; pH 11.5

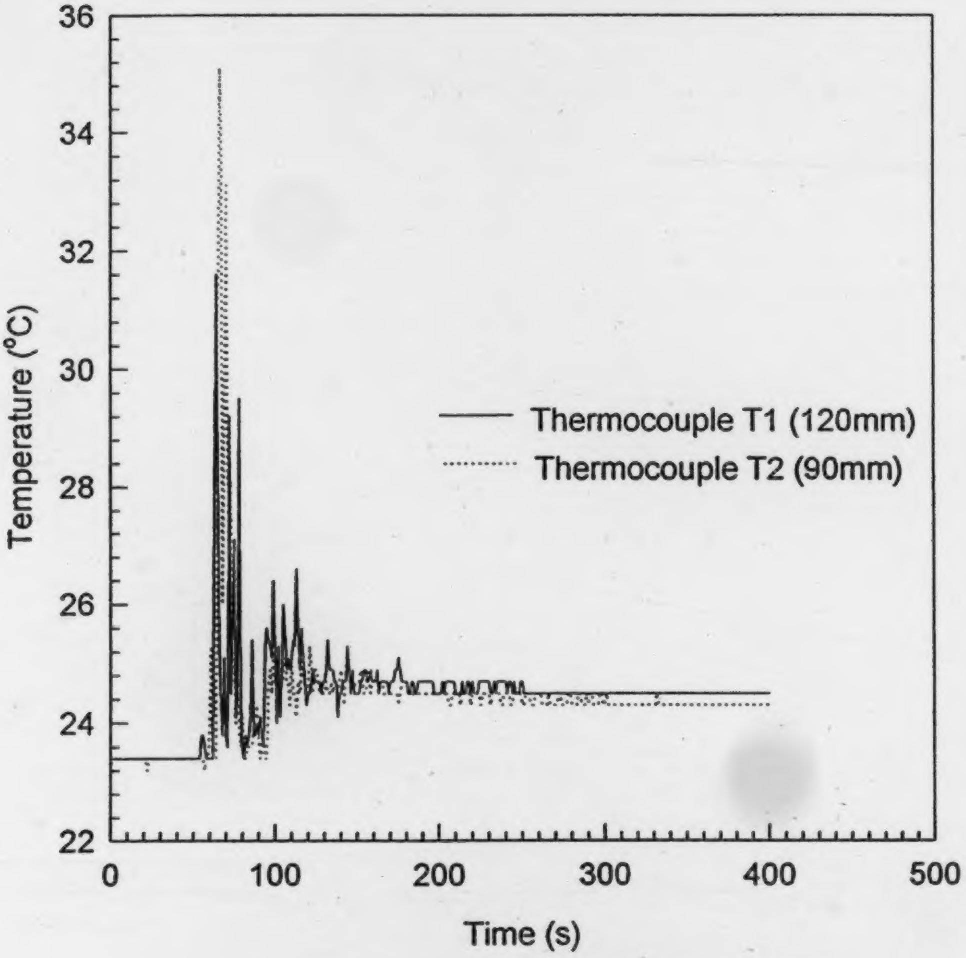

Figure E26 DHR-1 Pumping Upwards; 10rpm
1.48wt% Carbopol; pH 11.5

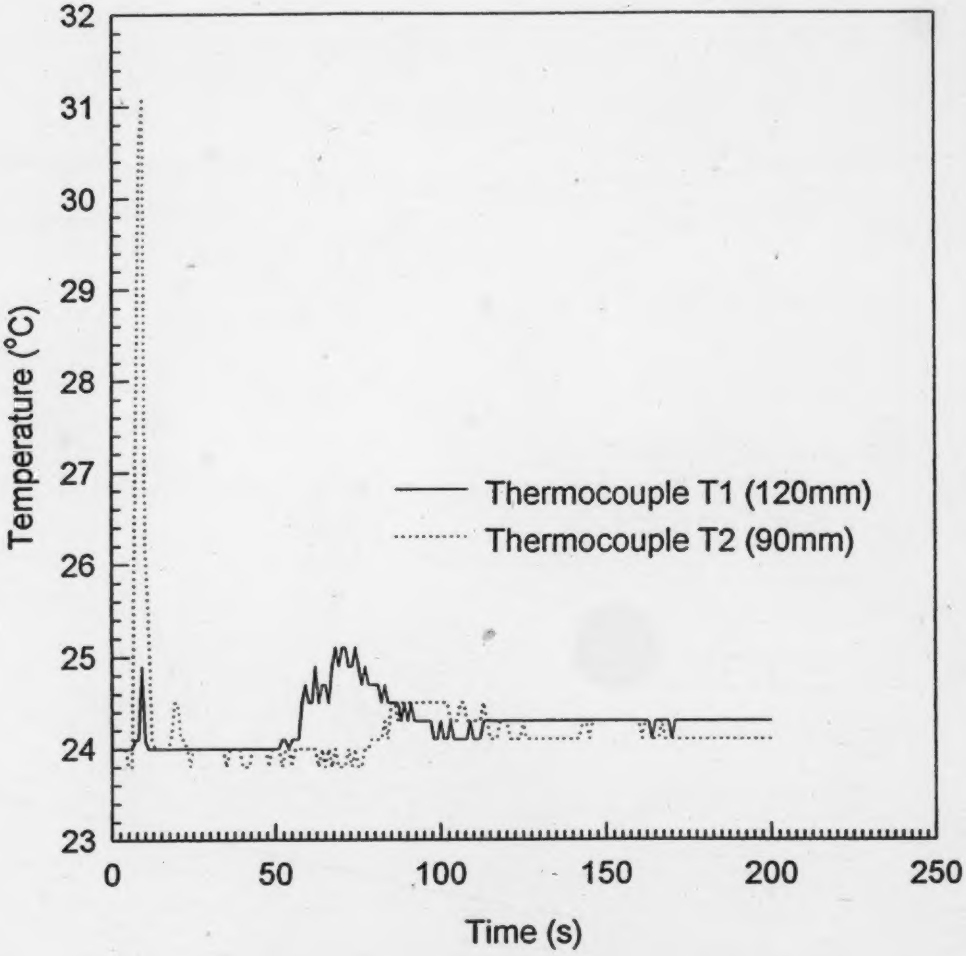

Figure E27 DHR-1 Pumping Downwards; 10rpm
1.48wt% Carbopol; pH 11.5

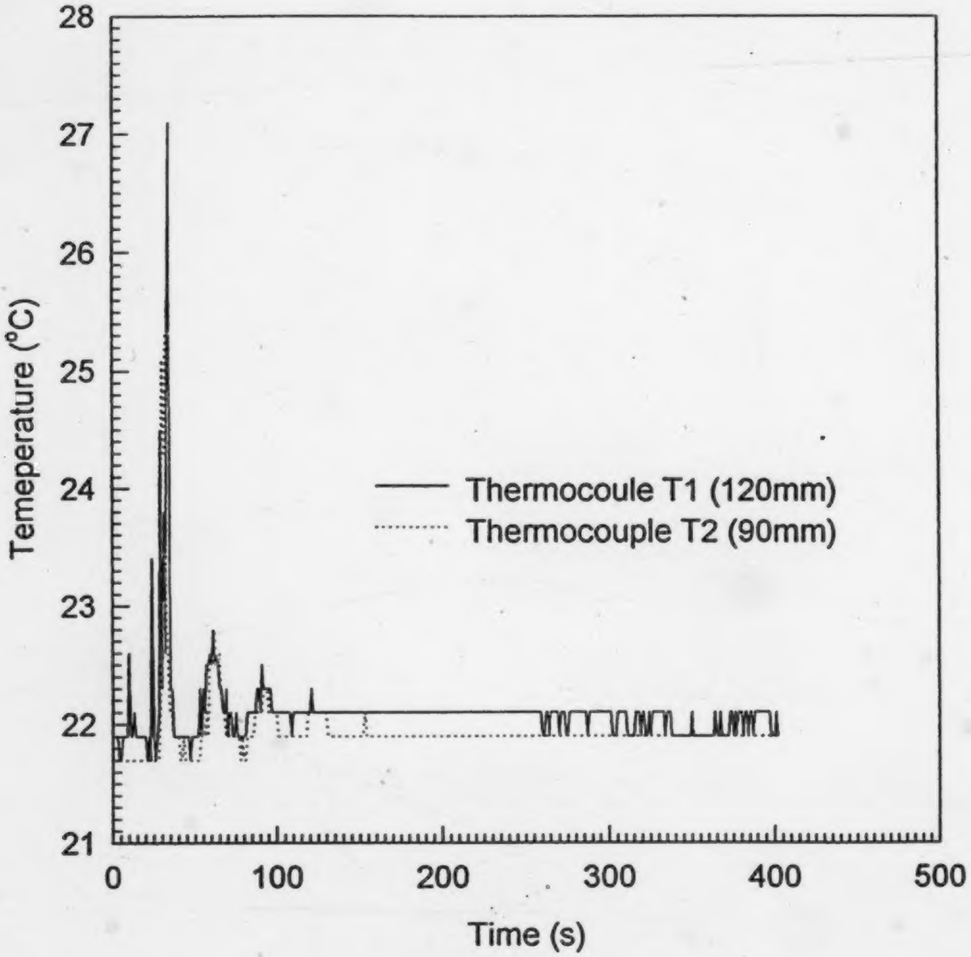

Figure E28 DHR-1 Pumping Upwards; 15rpm
1.48wt% Carbopol; pH 11.5

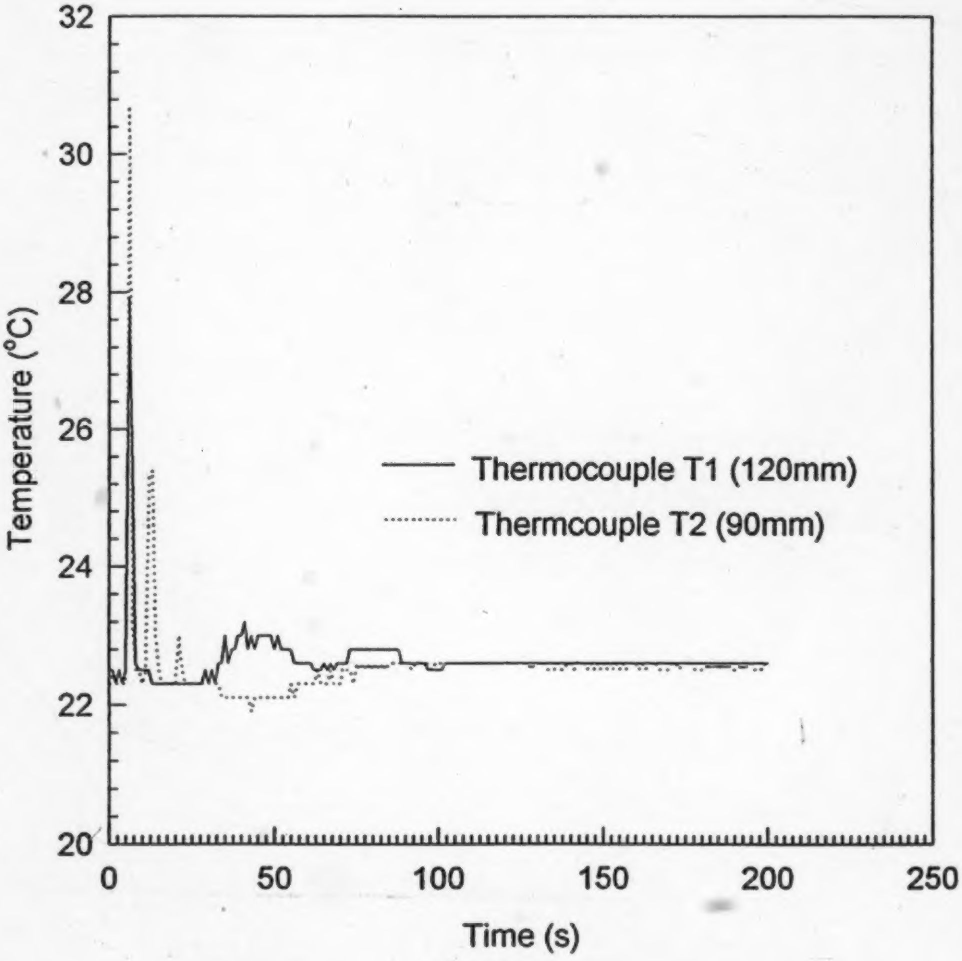

Figure E29 DHR-1 Pumping Downwards; 15rpm 1.48wt% Carbopol; pH 11.5

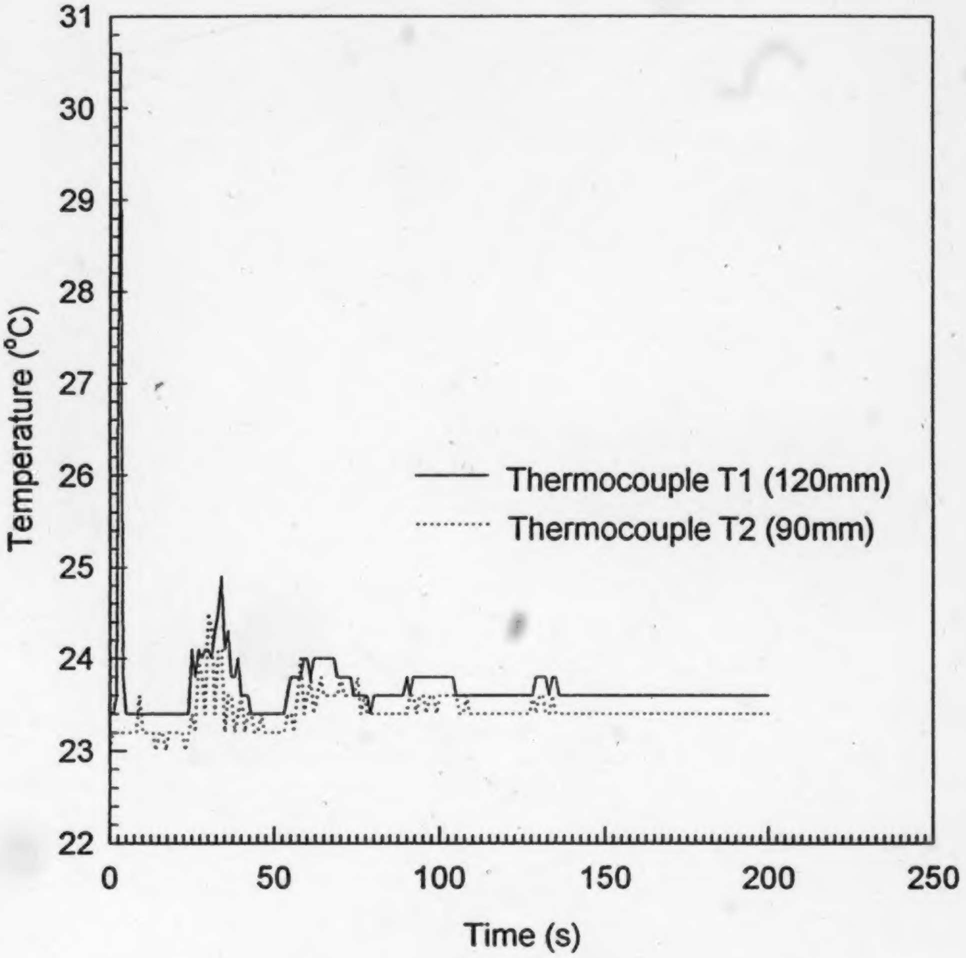

Figure E30 DHR-1 Pumping Upwards; 20rpm
1.48wt% Carbopol; pH 11.5

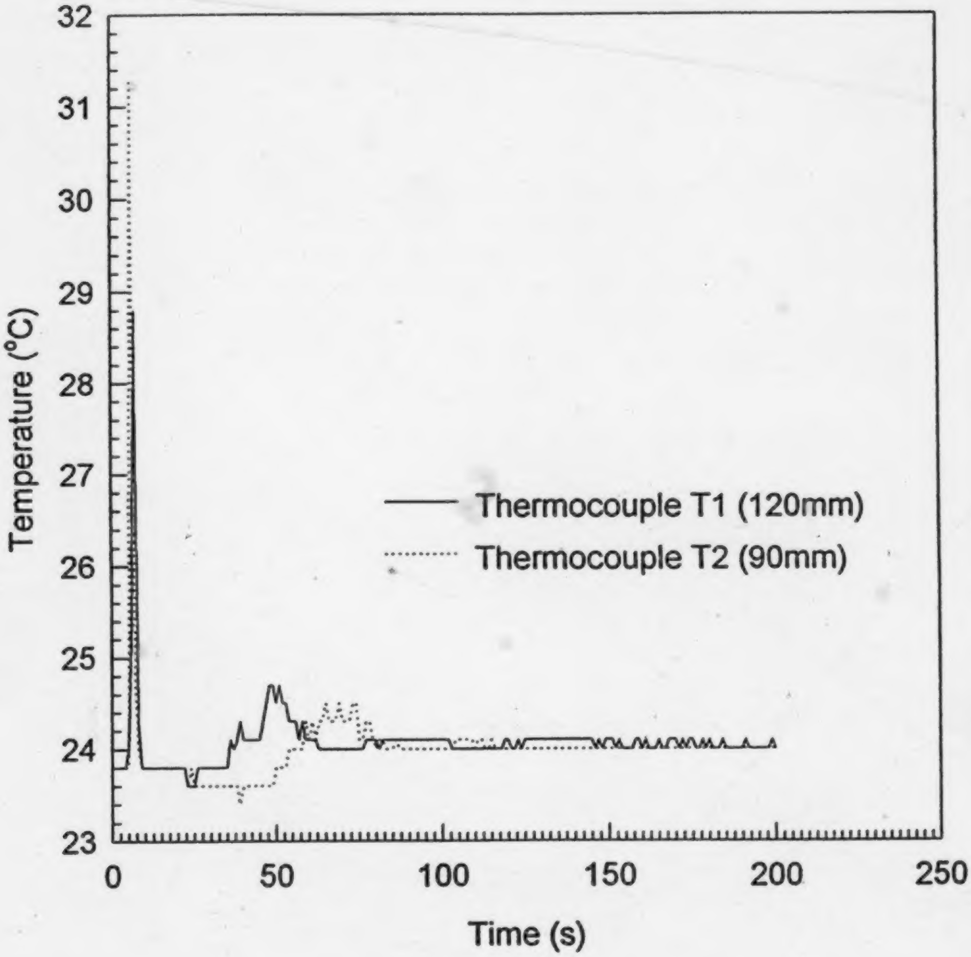

Figure E31 DHR-1 Pumping Upwards; 20rpm
1.48wt% Carbopol; pH 11.5

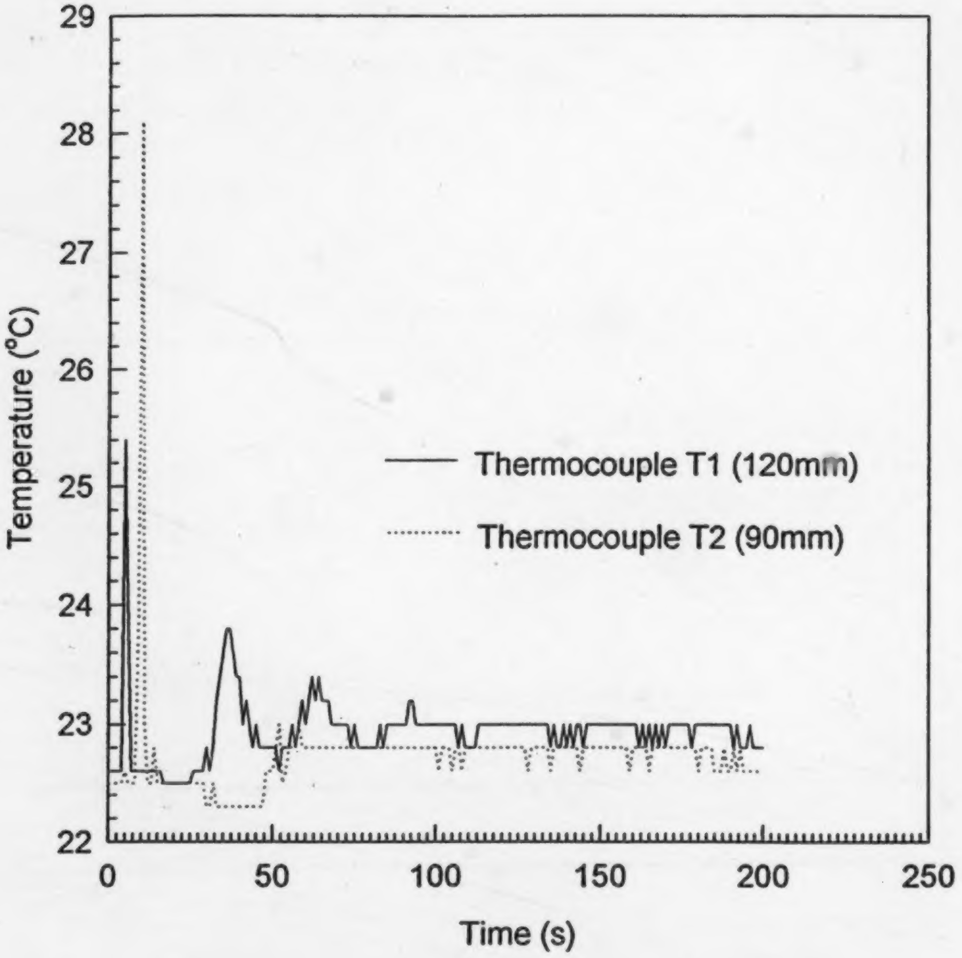

Figure E32 DHR-1 Pumping Downwards; 20rpm
1.48wt% Carbopol; pH 11.5

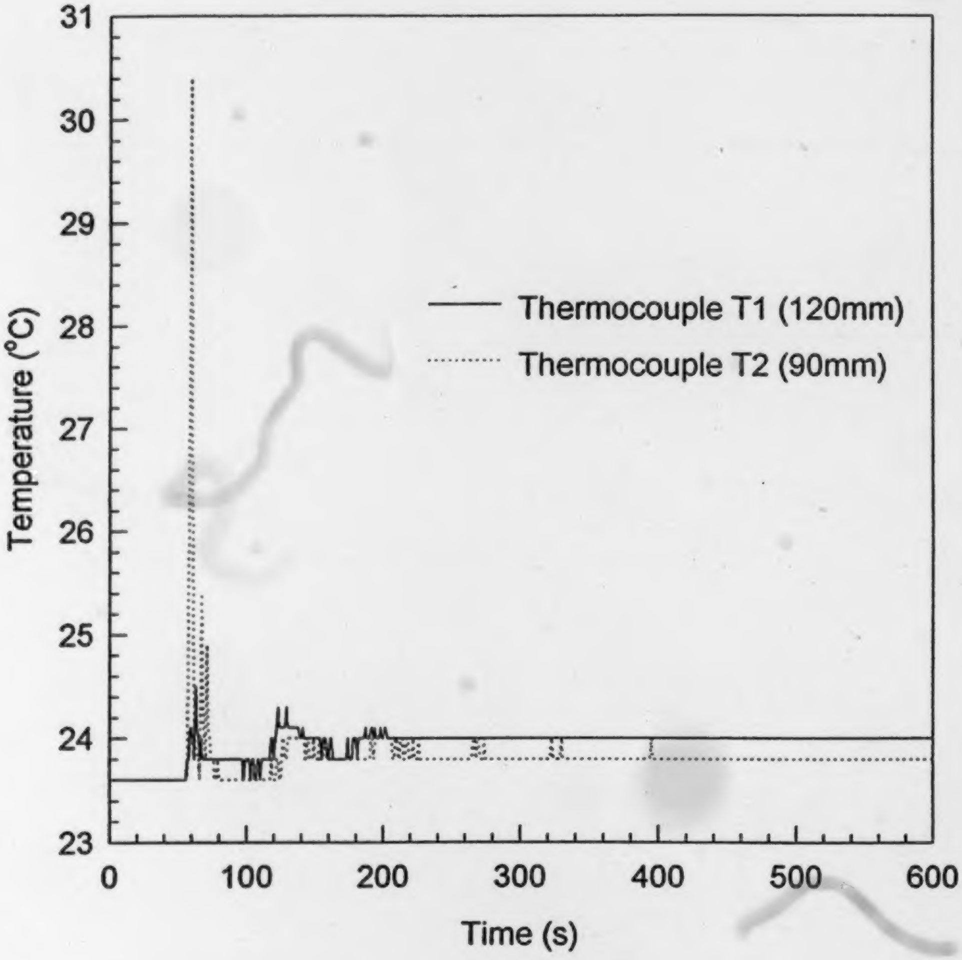

Figure F1 SHR-1 Pumping Upwards; 15rpm
45wt% Polyethylene Glycol Solution

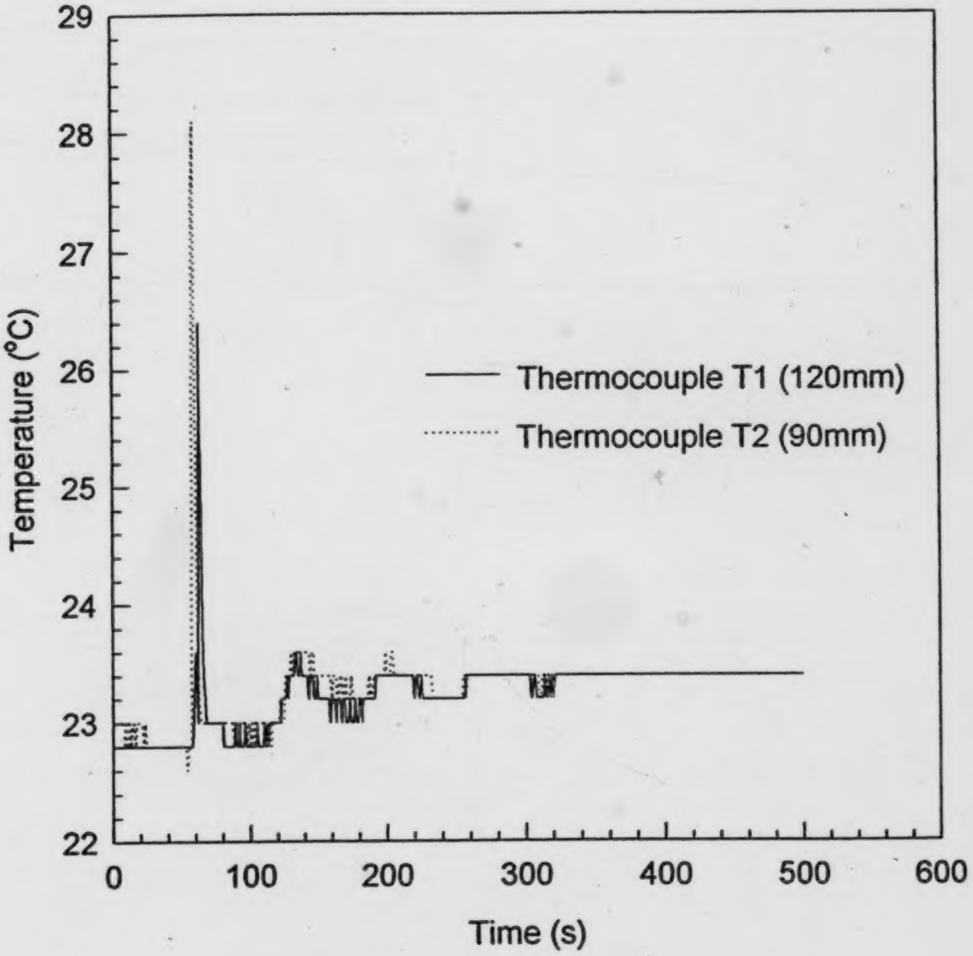

Figure F2 SHR-1 Pumping Upwards; 15rpm
45wt% Polyethylene Glycol Solution

Appendix G1: Flow Visualisation Experiment

Fluid:	1.48wt% Carbopol; pH 11.5
Dye Injection:	10ml. of 2.0 g/l crystal violet
Impeller:	HR1-B
Speed:	15rpm
Direction:	Upwards Pumping

time = 00 s

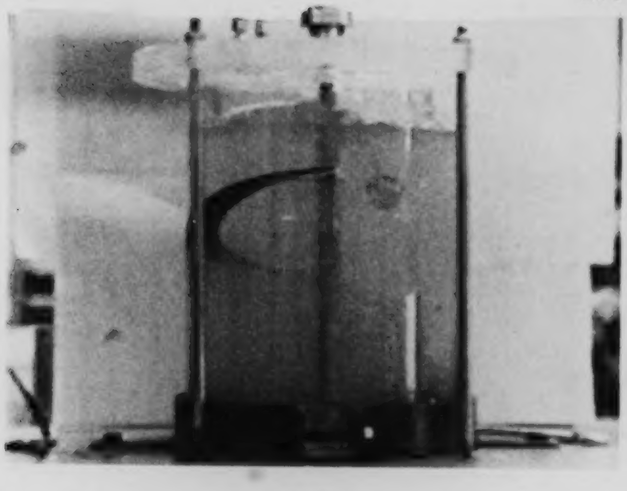

time = 12 s

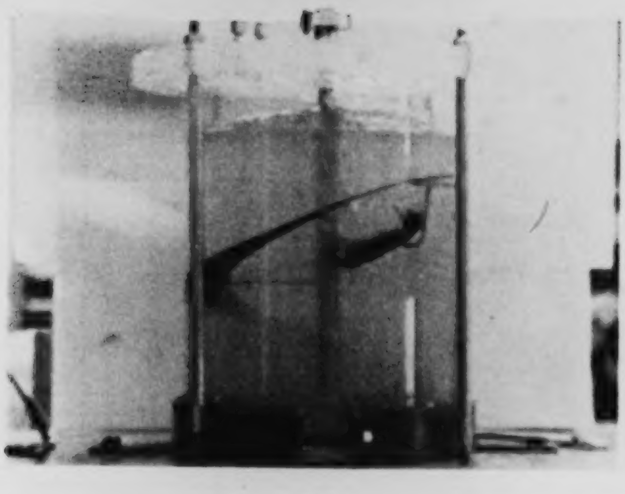

time = 22 s

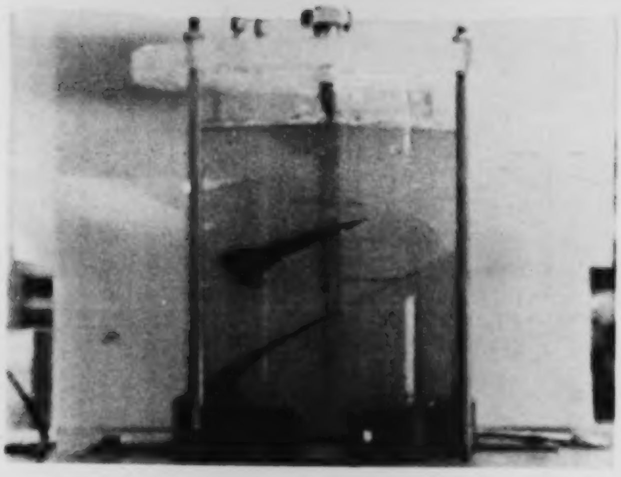

time = 1 m 08 s

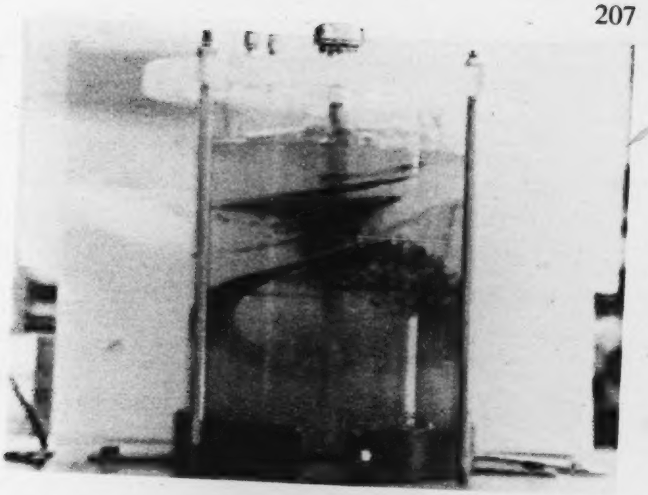

time = 2 m 35 s

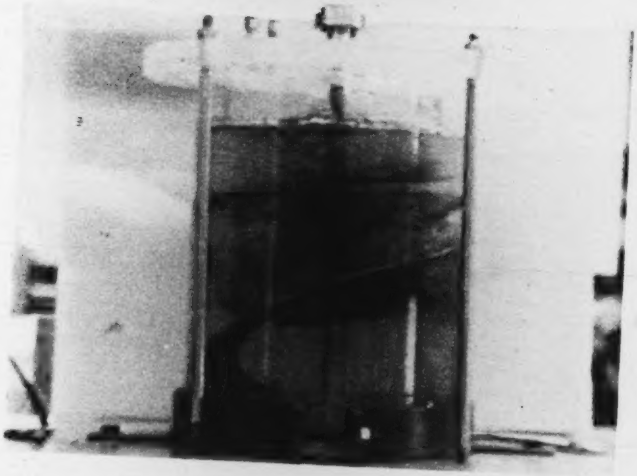

time = 412 s

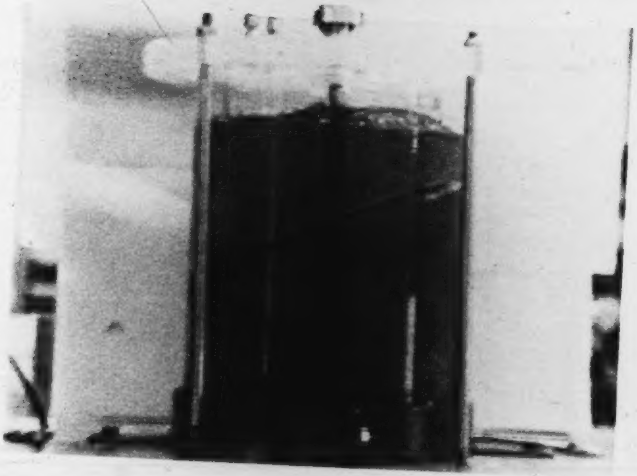

Appendix G2: Flow Visualisation Experiment

Fluid:	1.48wt% Carbopol; pH 11.5
Dye Injection:	10ml. of 2.0 g/l crystal violet
Impeller:	HR1-B
Speed:	15rpm
Direction:	Downwards Pumping

time = 41 s

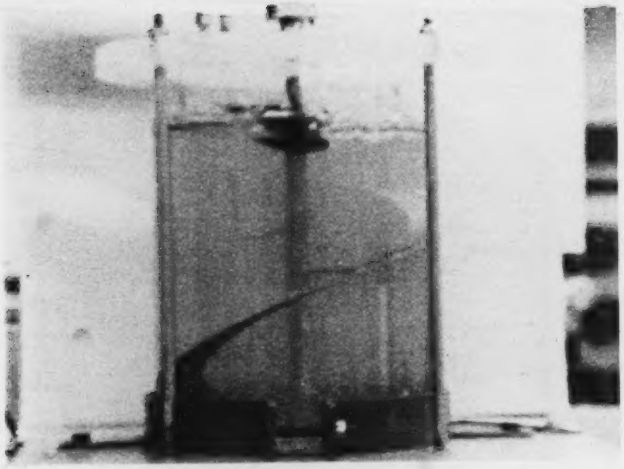

time = 132 s

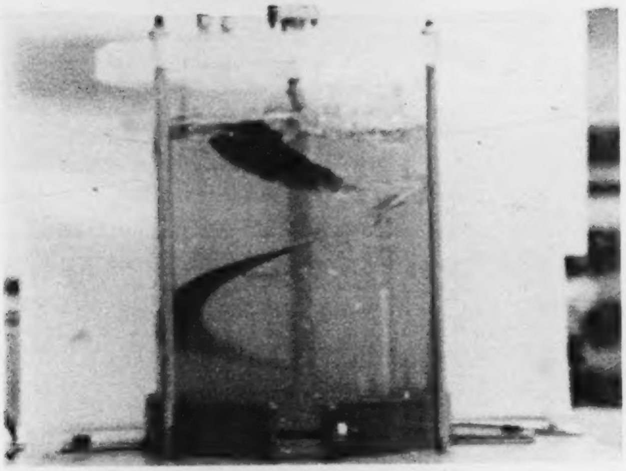

time = 162 s

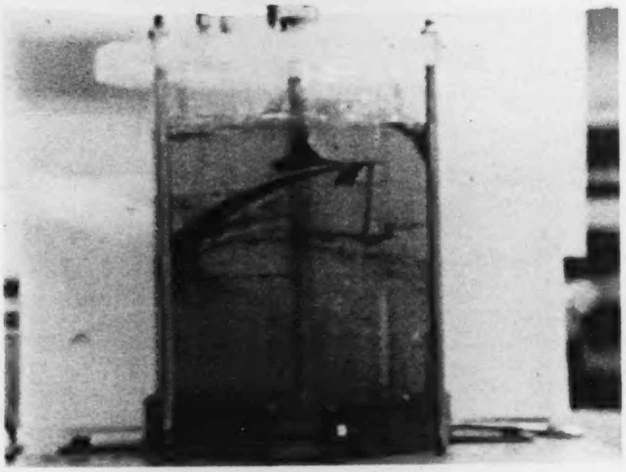

time = 242 s

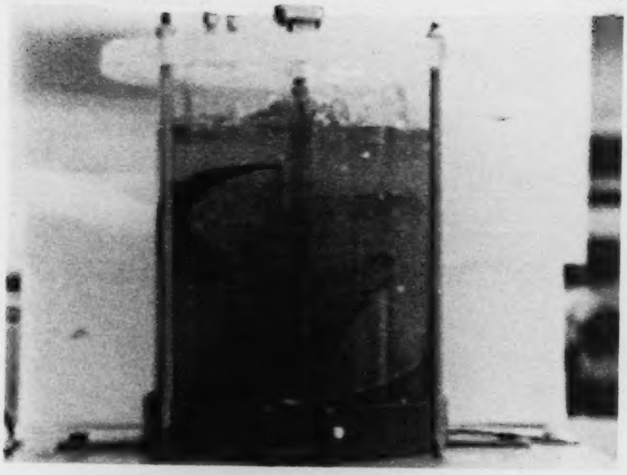

time = 294 s

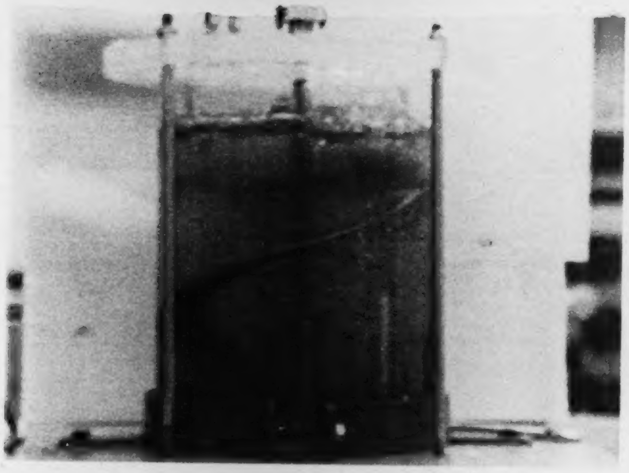

time = 432 s

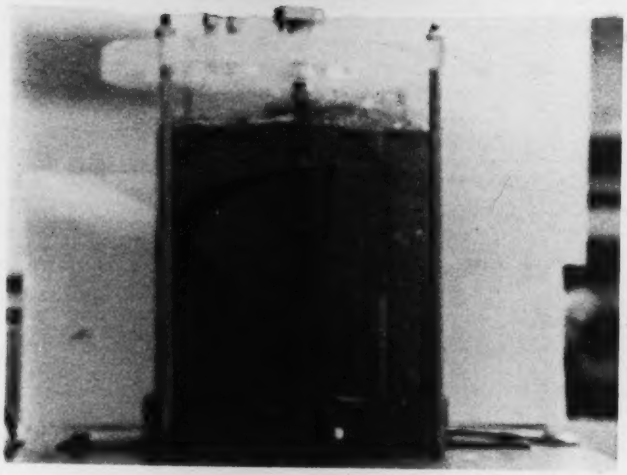

Appendix G3: Flow Visualisation Experiment

Fluid:	1.48wt% Carbopol; pH 11.5
Dye Injection:	10ml. of 2.0 g/l crystal violet
Impeller:	DHR-1
Speed:	15rpm
Direction:	Upwards Pumping

time = 05 s

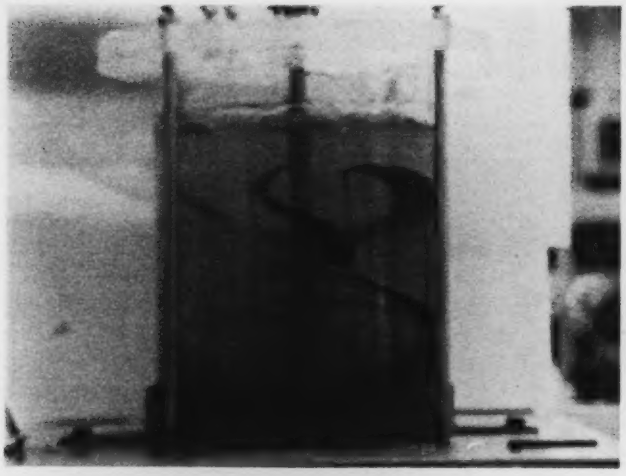

time = 11 s

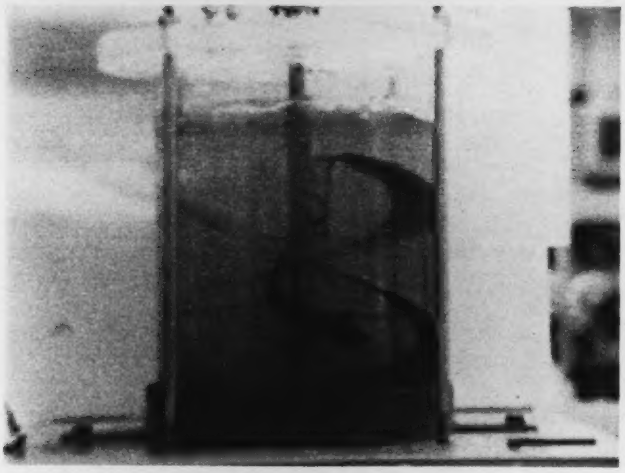

time = 25 s

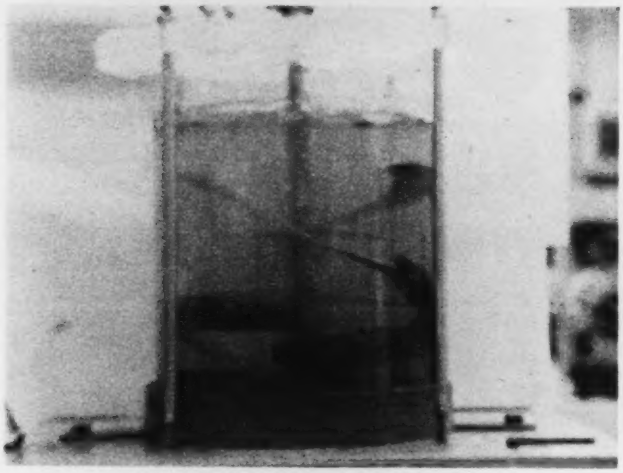

time = 30 s

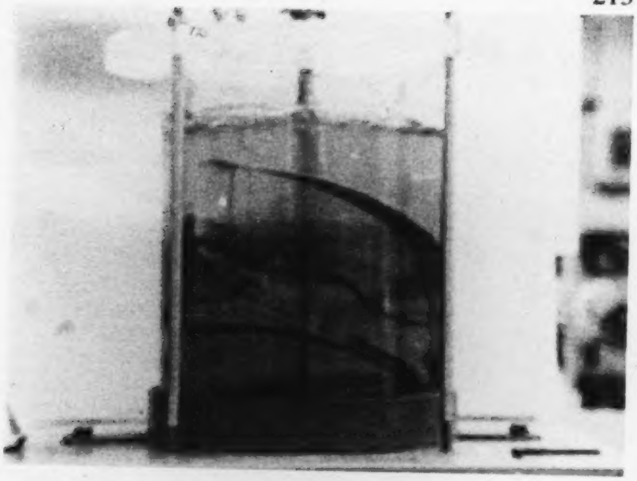

time = 46 s

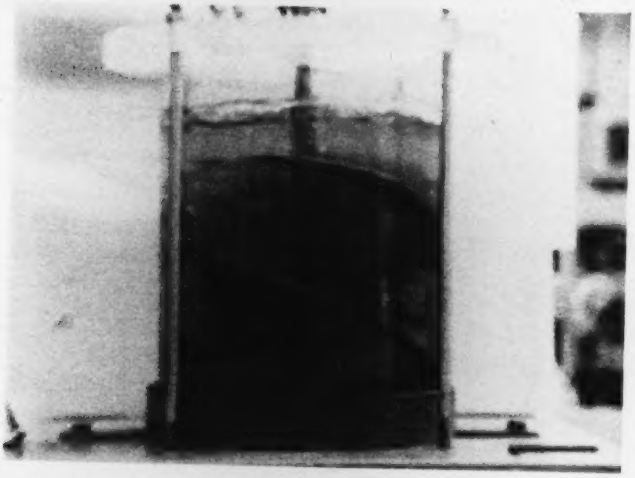

time = 77 s

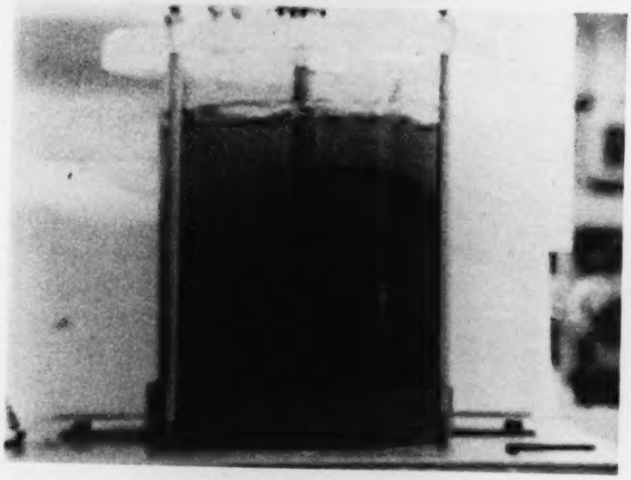

Appendix G4: Flow Visualisation Experiment

Fluid:	45wt% Polyethylene Glycol
Dye Injection:	10ml. of 2.0 g/l crystal violet
Impeller:	HR1-B
Speed:	15rpm
Direction:	Upwards Pumping

time = 06 s

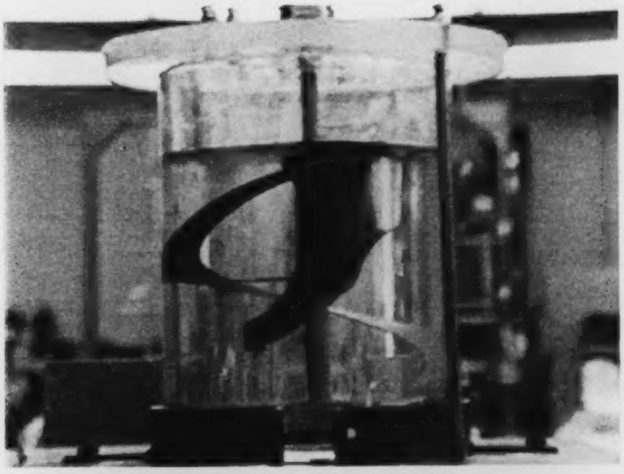

time = 16 s

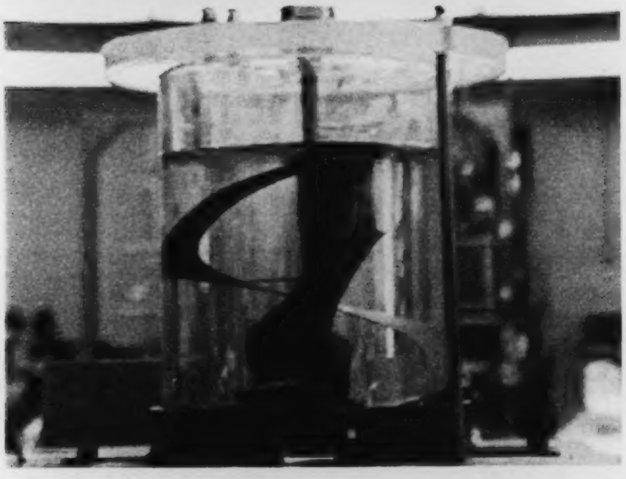

time = 32 s

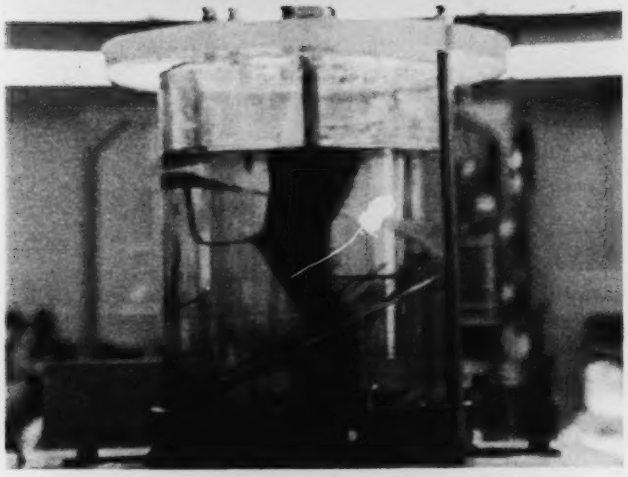

time =50 s

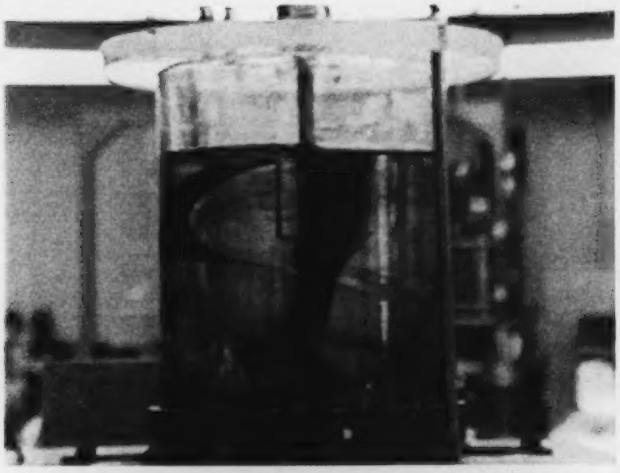

time = 69 s